

Edited by
Oleksij Fomin

ASSESSMENT OF TECHNICAL CONDITION: MEANS OF MEASUREMENT, SAFETY, RISKS

Collective monograph

**UDC 62
A88**

Published in 2024
by TECHNOLOGY CENTER PC®
Shatylova dacha str., 4, Kharkiv, Ukraine, 61165

A88

Authors:

Edited by **Oleksij Fomin**

Oleksij Fomin, Gregori Boyko, Andrii Lytvynenko, Vladyslav Bezlutsky, Pavlo Prokopenko, Maria Miroshnykova, Andriy Klymash, Stanislav Sidnei, Mykola Pelypenko, Mykola Grygorian, Mykhailo Kropyva, Ihor Taran, Serhii Holovchenko, Ievgen Medvediev, Tetiana Sotnikova, Tetiana Yarkho, Tatyana Emelyanova, Dmytro Legeyda

Assessment of technical condition: means of measurement, safety, risks: collective monograph. – Kharkiv: TECHNOLOGY CENTER PC, 2024. – 144 p.

This monograph is a comprehensive work covering the topical issues of operation and modernisation of railway transport in Ukraine. The results of the conducted research and proposed recommendations are aimed at solving the most acute problems facing the industry and contribute to improving its competitiveness at the international level.

The research results presented in the monograph can be used both in practical activities of railway companies and in educational institutions when training railway industry specialists. The proposed methods and approaches will make it possible to optimise the processes of rolling stock operation, improve its reliability and safety, as well as create a scientific basis for further research in the field of railway transport.

The results of scientific research presented in the monograph can be useful for further research, development of new technologies, as well as in the training of railway industry specialists.

Figures 85, Tables 21, References 105 items.

This book contains information obtained from authentic and highly regarded sources. Reasonable efforts have been made to publish reliable data and information, but the author and publisher cannot assume responsibility for the validity of all materials or the consequences of their use. The authors and publishers have attempted to trace the copyright holders of all material reproduced in this publication and apologize to copyright holders if permission to publish in this form has not been obtained. If any copyright material has not been acknowledged please write and let us know so we may rectify in any future reprint.

The publisher, the authors and the editors are safe to assume that the advice and information in this book are believed to be true and accurate at the date of publication. Neither the publisher nor the authors or the editors give a warranty, express or implied, with respect to the material contained herein or for any errors or omissions that may have been made.

Trademark Notice: product or corporate names may be trademarks or registered trademarks, and are used only for identification and explanation without intent to infringe.

DOI: 10.15587/978-617-8360-05-4

ISBN 978-617-8360-05-4 (on-line)

Cite as: Fomin, O. (Ed.) (2024). Assessment of technical condition: means of measurement, safety, risks: collective monograph. Kharkiv: TECHNOLOGY CENTER PC, 144. doi: <http://doi.org/10.15587/978-617-8360-05-4>



Copyright © Author(s) 2024
This is an open access paper under the Creative
Commons Attribution-NonCommercial-NoDerivatives
4.0 International License (CC BY-NC-ND 4.0)

AUTHORS

CHAPTER 1

OLEKSIJ FOMIN

Doctor of Technical Sciences, Professor
Department of Cars and Carriage Facilities
State University of Infrastructure and Technologies
 ORCID: <http://orcid.org/0000-0003-2387-9946>

GREGORI BOYKO

PhD, Associate Professor
Department of Railway, Road Transport and Truck Machines
Volodymyr Dahl East Ukrainian National University
 ORCID: <http://orcid.org/0000-0001-5065-3200>

ANDRII LYTVYENKO

PhD Student
Department of Railway, Road Transport and Truck Machines
Volodymyr Dahl East Ukrainian National University
 ORCID: <http://orcid.org/0000-0002-5182-9607>

VLADYSLAV BEZLUTSKY

PhD Student
Department of Railway, Road Transport and Truck Machines
Volodymyr Dahl East Ukrainian National University
 ORCID: <https://orcid.org/0009-0002-8846-4282>

CHAPTER 2

OLEKSIJ FOMIN

Doctor of Technical Sciences, Profes-sor
Department of Cars and Carriage Fa-cilities
State University of Infrastructure and Technologies
 ORCID: <http://orcid.org/0000-0003-2387-9946>

PAVLO PROKOPENKO

PhD
Branch "Scientific-research and design and technological
institute of railway transport" JSC "Ukrzaliznytsia"
 ORCID: <https://orcid.org/0000-0002-1631-6590>

MARIIA MIROSHNYKOVA

PhD
Department of Logistics management and Transport Safety
Volodymyr Dahl East Ukrainian National University
 ORCID: <https://orcid.org/0000-0002-8370-6724>

GREGORI BOYKO

PhD, Associate Professor
Department of Railway, Road Transport and Truck Machines
Volodymyr Dahl East Ukrainian National University
 ORCID: <http://orcid.org/0000-0001-5065-3200>

ANDRIY KLYMASH

PhD, Associate Professor, Head of Department
Department of Railway, Road Transport and Truck Machines
Volodymyr Dahl East Ukrainian National University
 ORCID: <https://orcid.org/0000-0002-4055-1195>

CHAPTER 3

STANISLAV SIDNEI

PhD, Associate Professor
Department of Safety of Construction and Occupational
Safety
Cherkasy Institute of Fire Safety named after Heroes
of Chernobyl of the National University of Civil Defense
of Ukraine
 ORCID: <http://orcid.org/0000-0002-7664-6620>

MYKOLA PELYPENKO

PhD
Department of Internal Quality Assurance of Education
of the Educational and Methodological Center
Cherkasy Institute of Fire Safety named after Heroes
of Chernobyl of the National University of Civil Defense
of Ukraine
 ORCID: <https://orcid.org/0000-0003-1961-5008>

MYKOLA GRYGORIAN

PhD, Associate Professor
Department of Fire Tactics and Emergency Rescue Works
Cherkasy Institute of Fire Safety named after Heroes
of Chernobyl of the National University of Civil Defense
of Ukraine
 ORCID: <https://orcid.org/0000-0003-0359-5735>

MYKHAILO KROPYVA

PhD, Senior Lecturer
Department of Fire Tactics and Emergency Rescue Works
Cherkasy Institute of Fire Safety named after Heroes
of Chernobyl of the National University of Civil Defense
of Ukraine
 ORCID: <https://orcid.org/0000-0002-1111-8747>

IHOR TARAN

Senior Lecturer
Department of Fire Tactics and Emergency Rescue Works
Cherkasy Institute of Fire Safety named after Heroes
of Chernobyl of the National University of Civil Defense
of Ukraine
 ORCID: <https://orcid.org/0009-0006-1933-570X>

SERHII HOLOVCHENKO

PhD

Department of Automatic Safety Systems and Electrical Installations

Cherkasy Institute of Fire Safety named after Heroes of Chernobyl of the National University of Civil Defense of Ukraine

 ORCID: <https://orcid.org/0000-0002-6782-5221>

CHAPTER 4

OLEKSIJ FOMIN

Doctor of Technical Sciences, Professor

Department of Cars and Carriage Facilities

State University of Infrastructure and Technologies

 ORCID: <http://orcid.org/0000-0003-2387-9946>

IEVGEN MEDVEDIEV

¹ PhD, Researcher

Faculty of Mechanical Engineering and Ship Technology

Department of Ship Design

Gdansk University of Technology

² PhD, Associate Professor

Department of Railway and Road Transport, Lift and Care Systems

Volodymyr Dahl East Ukrainian National University

 ORCID: <http://orcid.org/0000-0001-8566-9624>

TETIANA SOTNIKOVA

PhD, Associate Professor

Department of Computer-integrated Control Systems

Volodymyr Dahl East Ukrainian National University

 ORCID: <http://orcid.org/0000-0001-6929-7672>

TETIANA YARKHO

Doctor of Pedagogical Sciences, Professor

Department of Higher Mathematics

Kharkiv National Automobile and Highway University

 ORCID: <http://orcid.org/0000-0003-2669-5384>

TATYANA EMELYANOVA

PhD, Associate Professor

Department of Higher Mathematics

Kharkiv National Automobile and Highway University

 ORCID: <http://orcid.org/0000-0001-7451-8193>

DMYTRO LEGEYDA

PhD, Researcher

Hub for Biotechnology in the Built Environment

School of Architecture, Planning and Landscape

Newcastle University

 ORCID: <http://orcid.org/0000-0002-8983-0822>

ABSTRACT

Uninterrupted transportation of liquid fuel and lubricant cargoes is one of the key tasks of railway transport in Ukraine. Wide range of liquid cargoes (light and dark oil products, furnace oils) and limited fleet of tank wagons, due to its wear and tear and complexity of renewal in wartime conditions, require constant and qualitative cleaning of tank wagon boilers. Modern technologies of boiler cleaning involve thermal effects associated with washing and steam treatment operations, which affects the stress-strain state of boilers.

In order to achieve the objective, the existing sources were analysed, technical characteristics of modern tank wagons were given and the moment theory of shells was adapted, which allowed to determine the loads in the boiler control points.

The organisation of goods train traffic on the railway transport of Ukraine is an important aspect of its integration into the European transport system. The urgent need for renewal of the freight wagon fleet and speed limitation require the development of modern methods for assessing the technical condition and traffic safety. The proposed methods include strain gauge measurement of mechanical stresses and spectral analysis of dynamic processes to reveal the regularities of interaction of load-bearing structures of freight wagons.

Also, the monograph presents a hierarchical system of methods for calculating the fire resistance of reinforced concrete slabs at the limit state of loss of integrity. Three approaches are proposed: tabular, simplified and refined, allowing designers to choose the optimal method depending on the required accuracy and available data, which contributes to the improvement of fire safety of structures.

In the conditions of multifunctional technical means development, the directions of wagon structural elements integration are considered, including elastic-dissipative, non-split hinge and multi-material concepts. On the basis of theoretical research, promising wagon designs have been developed, such as a covered hopper for cement, a flat wagon made of leaf springs, a universal covered wagon with damping struts and multi-material railway tank car designs. The systematisation of these developments contributes to the extension of rolling stock service life, reduction of material intensity, improvement of maintainability and crack resistance.

The results of scientific research presented in the monograph can be useful for further research, development of new technologies, as well as in the training of railway industry specialists.

KEYWORDS

Transport mechanics, railway transport, temperature influence, stress-strain state, freight cars, running tests, dynamic processes, stability, load-bearing systems, promising structures, fire resistance, limit state, loss of integrity, tabular method, simplified method, refined method.

CIRCLE OF READERS AND SCOPE OF APPLICATION

This monograph will be useful to a wide range of specialists and organisations working in the field of railway transport, rolling stock design and operation, as well as research institutions.

The monograph will provide modern approaches to the maintenance and repair of tank wagons, including boiler cleaning, analysis of temperature effects and ensuring safe operation of rolling stock. Specialists will receive practical recommendations on the application of new techniques for assessing the stress-strain state of boilers during washing and steam treatment, and will be able to optimise the processes of planning and operation of the tank wagon fleet on the basis of the obtained data on ultimate loads and operational reliability.

Designers will receive science-based recommendations for designing new and modernised freight wagon structures taking into account thermal and dynamic loads, and will be able to apply the concepts of multifunctional wagon components to improve the life and efficiency of wagons.

Lecturers of universities and colleges of railway profile can use it in the educational process when training specialists in the specialities 'Rolling Stock', 'Operation of Railway Transport' and 'Mechanical Engineering'.

Production enterprises and repair plants will be able to introduce innovative approaches to diagnostics and maintenance of rolling stock, which will improve the quality of repairs and extend the service life of cars.

CONTENTS

List of Tables	ix
List of Figures	xi
Introduction	1
1 Analysis of the temperature effect on the stress-strain state of the tank car boiler during steaming	3
1.1 Requirements for modern designs of domestic tank cars and their boilers.....	7
1.2 Adoption and use of moment theory of shells for mathematical calculation	11
1.3 Analysis of the temperature effect on the stress-strain state of the tank car boiler during steaming.....	21
Conclusions	25
References.....	26
2 Study of safety indicators and technical condition of rolling stock by mobile systems	29
2.1 Methods and approaches for evaluating indicators of quality, traffic safety and technical condition of cars	33
2.1.1 Measurement of deformations of load-bearing structures. General information	33
2.1.2 Measurement of forces by local deformations of cart frames	36
2.1.3 Measurement of forces of direct interaction of wheels with rails.....	36
2.1.4 Measurement of dynamic indicators of rolling stock.....	40
2.2 Improvement of means and approaches for assessing safety indicators and technical condition of freight cars	41
2.2.1 Mathematical support for determining safety indicators and technical condition of freight cars.....	41
2.2.2 Software for collecting and registering safety indicators and technical condition of cars	45
2.3 Practical aspects of the implementation of improved means and approaches for determining and evaluating safety indicators and the technical condition of cars	48
2.3.1 Mobile system for determining safety indicators and technical condition in operating conditions.....	48
2.3.2 Hardware and primary converters of the mobile system.....	49

2.3.3	Software for collecting and recording measurements.....	53
2.3.4	Practical studies of indicators of the quality and safety of the movement of freight cars in an empty state as part of a train.....	54
2.4	Mobile system for determining the dynamic load of rolling stock under operating conditions	55
2.4.1	General requirements for software and hardware complex	55
2.4.2	Measurement information collection subsystem	56
2.4.3	System for determining movement smoothness	56
2.4.4	System for determining traffic safety indicators.....	58
	Conclusions	60
	References.....	61

3 Hierarchical structure of calculation methods for assessing the fire resistance of enclosure horizontal structures under the limit state of loss of integrity

3.1	Features of the hierarchical structure of calculation methods for assessing the fire resistance of hollow slabs by loss of integrity	65
3.1.1	Improvement of the tabular calculation method for assessing the fire resistance of reinforced concrete hollow slabs	65
3.1.2	Development of a simplified method for assessing fire resistance by loss of integrity for hollow slabs	70
3.2	Features of the hierarchical structure of calculation methods for assessing the fire resistance of ribbed slabs by loss of integrity	80
3.2.1	Improvement of the tabular calculation method for assessing the fire resistance of reinforced concrete ribbed slabs	80
3.2.2	Hierarchical structure of methods for assessing the fire resistance of reinforced concrete ribbed slabs according to the onset of the limit state of loss of integrity	85
3.2.3	Development of a simplified method for calculating the fire resistance of reinforced concrete ribbed slabs according to the limit state of loss of integrity.....	85
	Conclusions	94
	References.....	95

4 Establishing a high-quality technical condition at the design stage: promising concepts of load-bearing components of car structures

4.1	Analysis of information sources that highlight the issues of the prospects for the development of non-load-bearing component structures of freight cars.....	99
4.2	Mathematical description of the procedure for creating car components with a useful pre-stressed and/or deformed state	100

CONTENTS

4.3	Theoretical aspects of creating useful prestressed and/or deformed load-bearing components of car structures.....	103
4.4	A promising useful prestressed and/or deformed concept of a covered hopper car for cement transportation.....	107
4.5	Promising useful prestressed and/or deformed pellet car concept.....	108
4.6	Promising elastic-dissipative concept of a platform car made of leaf springs.....	109
4.7	Promising elastic-dissipative concept of a hopper car for transporting grain from leaf springs.....	110
4.8	Promising elastic-dissipative concept of a hopper car for transporting mineral fertilizers from leaf springs.....	111
4.9	Promising elastic-dissipative concept of a hollow-bottomed gondola with leaf springs.....	112
4.10	Promising elastic-dissipative concept of a universal covered car with racks with damping properties.....	113
4.11	Promising elastic-dissipative concept of a universal hopper car for transporting grain with racks with damping properties.....	114
4.12	Promising concept of a railway tank with supports in the form of leaf springs.....	114
4.13	Promising concept of a railway tank with supports in the form of disc springs.....	115
4.14	Promising articulated concept of a 4-axle dump car.....	116
4.15	Promising articulated concept of a hopper car for grain transportation.....	116
4.16	Promising articulated concept of a hopper car for transporting mineral fertilizers.....	117
4.17	Promising articulated concept of a universal platform car.....	118
4.18	Promising articulated concept of a universal covered car.....	119
4.19	Promising articulated concept of a hollow-bottomed gondola.....	120
4.20	Promising articulated railway tank concept.....	122
4.21	Promising multi-material concept of a covered car.....	122
4.22	A promising multi-material concept of a railway tank car.....	123
4.23	A promising railway tank with a multi-material concept of supports.....	125
	Conclusions.....	125
	References.....	126

LIST OF TABLES

1.1	Characteristics of a typical tank car	7
1.2	The values of the coefficients	16
1.3	The values of the convection coefficient	23
2.1	Results of running dynamic tests in an empty state	55
2.2	Evaluation of the car's running qualities based on the Wz movement smoothness indicator	57
3.1	Planning matrix of a full factorial experiment for building a regression	66
3.2	Intervals of variation of factors in a full factorial experiment	66
3.3	Technical data for reinforced concrete hollow slab	67
3.4	Parameters of fires in model rooms during a full factorial experiment according to the adopted planning matrix	67
3.5	Regression coefficients for determining the limit of fire resistance of reinforced concrete hollow slabs according to the onset of the limit state of loss of integrity	68
3.6	Adequacy of the results of assessing the fire resistance limit of reinforced concrete hollow slabs, determined by regression dependence	69
3.7	Minimum dimensions and axial distances for reinforced concrete hollow slabs	70
3.8	A set of initial data for the implementation of a simplified method of assessing the fire resistance of reinforced concrete hollow slabs according to the limit state of loss of integrity	71
3.9	Basic methods of numerical investigation of the integrity of reinforced concrete hollow slabs in case of fire	77
3.10	Basic methods of numerical investigation of the integrity of reinforced concrete hollow slabs in case of fire	79
3.11	Intervals of variation of factors in a full factorial experiment	81
3.12	Technical data on reinforced concrete ribbed slab	81
3.13	Parameters of fires in model rooms during a full factorial experiment according to the adopted planning matrix	82
3.14	Regression coefficients for determining the limit of fire resistance of reinforced concrete hollow slabs by the onset of the limit state of loss of integrity	82
3.15	Adequacy of the results of assessing the fire resistance limit of reinforced concrete ribbed slabs, determined by regression dependence	84
3.16	Minimum dimensions and axial distances for reinforced concrete ribbed slabs	84

LIST OF FIGURES

1.1	Tank car boiler with elliptical bottoms	8
1.2	Calculation scheme of the shell and its element	11
1.3	Cross section of the boiler shell	19
1.4	Calculated computer model of a tank car boiler	22
1.5	Computational finite-element model of a tank car boiler	22
1.6	Section of the calculation model of the tank car boiler with applied loads from the action of hot steam	23
1.7	Calculation model of a tank car boiler with applied loads from external temperature	24
1.8	Chart of temperature loads of a tank car boiler	24
1.9	Schematic of fixing the tank car boiler	24
1.10	Picture of the stress state of the calculation model of the tank car boiler under the influence of temperature loads	25
2.1	Strain gauge diagram	33
2.2	Connection diagram of the Wheatstone bridge with balancing	34
2.3	Chart of equivalent stresses arising in a pair of wheels under vertical load	37
2.4	The chart of equivalent stresses arising in a pair of wheels (in cross-section)	38
2.5	The chart of equivalent stresses arising in a pair of wheels when loaded with a tare device	38
2.6	The chart of equivalent stresses arising in a pair of wheels when loaded with vertical and lateral loads	39
2.7	Schematic of strain gauge placement on the wheel of the measuring wheelset	40
2.8	UM-type low-frequency experimental accelerometer	41
2.9	An example of an oscillogram of the resulting file from the measurement of the cart accelerations	42
2.10	Characteristics of the Butterworth filter	44
2.11	Example of filter operation: a – before filtering; b – after filtering	44
2.12	General scheme of the system of collection and registration of measured parameters	45
2.13	NI 9237 module	49
2.14	NI 9205 module	50
2.15	NI 9012 controller	50
2.16	NI 9104 chassis	51
2.17	Real-time mobile system	52
2.18	Autonomous mobile system	52
2.19	Block diagram of the mobile system	52
2.20	UM-type accelerometer	53

2.21	Indicators of movement smoothness in the vertical direction: W_zl – indicator of movement smoothness in the pivot section; W_zk – indicator of movement smoothness in the car body	58
2.22	Root mean square deviations of horizontal lateral accelerations of the cart frame measured during the test road	59
3.1	The surface corresponding to the dependence of the fire resistance limit of a reinforced concrete hollow slab upon the onset of the limit state of loss of integrity on its thickness and the axial distance of the reinforcing bars	68
3.2	Nomograms of the dependence of the fire resistance limit of a reinforced concrete hollow slab upon the onset of the limit state of loss of integrity on its thickness and the axial distance of the reinforcing bars	69
3.3	Scheme of the mechanism of the formation of a through crack, which is associated with the onset of the limit state of loss of integrity	71
3.4	Scheme of the mechanism of the formation of a transverse through crack, which is associated with the onset of the limit state of loss of integrity	72
3.5	Scheme of the mechanism of the formation of a transverse through crack, which is associated with the onset of the limit state of loss of integrity	73
3.6	Nomogram for determining the temperature distribution in a reinforced concrete hollow slab	74
3.7	Scheme of the algorithm for the implementation of the method for calculating the fire resistance of a reinforced concrete hollow slab based on the limit state of the loss of integrity when transverse cracks appear	76
3.8	Scheme of the algorithm for the implementation of the method for calculating the fire resistance of a reinforced concrete hollow slab based on the limit state of the loss of integrity when longitudinal cracks appear	77
3.9	Scheme of the algorithm for the implementation of the refined method of fire resistance with implicit integration for a reinforced concrete hollow slab under the limit state of loss of integrity with the appearance of transverse cracks	78
3.10	Hierarchical system of methods for assessing the fire resistance of reinforced concrete hollow and ribbed slabs according to the onset of the limit state of loss of integrity	79
3.11	The surface corresponding to the dependence of the fire resistance limit of a reinforced concrete ribbed slab upon the onset of the limit state of loss of integrity on the slab thickness in the cells between the ribs and the axial distance of the reinforcing rods in the panel	83
3.12	Nomograms of the dependence of the fire resistance limit of a reinforced concrete ribbed slab upon the onset of the limit state of loss of integrity on the slab thickness in the cells between the ribs and the axial distance of the reinforcing rods in the panel	83

LIST OF FIGURES

3.13	Distribution of vertical movements (m) in the studied reinforced concrete ribbed slab at the time of failure at different levels of the applied active load: <i>a</i> – 30 % of the maximum load; <i>b</i> – 50 % of the maximum load; <i>c</i> – 70 % of the maximum load	86
3.14	The nature of the destruction of the panel of the ribbed reinforced concrete slab during its fire tests: <i>a</i> – during the fire tests; <i>b</i> – after the fire tests	87
3.15	The destruction mechanism of the formation of defects associated with the onset of the limit state of loss of integrity of a reinforced concrete ribbed slab during exposure to the standard fire temperature regime	88
3.16	The calculation scheme for the approximation of the lines of plastic hinges, along which the slab destruction in the cell between the ribs of a reinforced concrete ribbed slab occurs	89
3.17	Geometric scheme of the algorithm for constructing Bezier lines	89
3.18	Scheme for determining possible movements when determining the work of internal forces in the panel failure zone in the cell between the ribs of a reinforced concrete ribbed slab	90
3.19	Scheme for determining possible movements when determining the work of external forces in the panel failure zone in the cell between the ribs of a reinforced concrete ribbed slab	92
3.20	Scheme of the algorithm for the implementation of the method for the calculated assessment of the fire resistance of the reinforced concrete ribbed slab according to the limit state of the loss of integrity according to the energy criterion	93
4.1	Expanded scheme of applying loads to car structures in various design cases of the life cycle: <i>a</i> – longitudinal quasi-static compression force; <i>b</i> – longitudinal quasi-static tensile force; <i>c</i> – vertical force due to eccentricity between the axles of the auto couplers; <i>d</i> – transverse forces in curves under quasi-static compression; <i>e</i> – transverse forces in curves under quasi-static tensile force; <i>f</i> – vertical load from the mass of the cargo and its own mass; <i>g</i> – oblique symmetrical loading (for cars with a base of more than 16 m); <i>h</i> – hitting the auto-coupler; <i>i</i> – spurt; <i>j</i> – expansion (pressure) forces of loose and bulk cargo; <i>k</i> – pressure forces of liquids and gases and water hammer forces in tank boilers, reservoirs, tanks; <i>l</i> – forces for creating a deformed state (vertical bending) during assembly and welding work	106
4.2	Cross-section of a half-pipe with cables tensioned in the middle	107
4.3	Side view of a useful pre-deformed backbone beam of a covered hopper car concept for transporting cement	108
4.4	Top view of a useful pre-deformed side wall of a covered hopper car concept for transporting cement and pellet car	108
4.5	Top view of a useful pre-deformed end wall of a covered hopper car concept for transporting cement and pellet car	108
4.6	Concept of a leaf spring platform car frame	109

4.7	Cross-section of the concept of transverse beams of a leaf spring frame	109
4.8	Concept of a frame of a hopper car for transporting grain from leaf springs	110
4.9	Concept of an end wall of a hopper car for transporting grain from leaf springs	110
4.10	Hopper car frame concept for transporting mineral fertilizers from leaf springs	111
4.11	Hopper car end wall concept for transporting mineral fertilizers from leaf springs	112
4.12	Leaf spring gondola frame concept	112
4.13	Leaf spring gondola body concept	113
4.14	Cross-section of a stamped rack with damping properties	114
4.15	Concept of a railway tank with supports of the boiler on the frame in the form of leaf springs	115
4.16	Concept of a railway tank with supports in the form of disc springs	115
4.17	Multifunctional articulated concept of the frame of a 4-axle dump car	116
4.18	Concept of articulated joint of beams of the frame of a 4-axle dump car	116
4.19	Multifunctional articulated concept of the frame of a hopper car for grain transportation	117
4.20	Concept of articulated joint of beams of the frame of a hopper car for grain transportation	117
4.21	Multifunctional articulated concept of a hopper car frame for transporting mineral fertilizers	118
4.22	Multifunctional articulated concept of the frame of a universal platform car	118
4.23	Multifunctional articulated concept of a universal covered car body	119
4.24	Cross-section of the multifunctional articulated concept of the body of a universal covered car	120
4.25	Multifunctional articulated concept of a hollow-bottomed gondola frame	120
4.26	Cross-section of a multifunctional articulated concept of a hollow-bottomed gondola body	121
4.27	Multifunctional articulated concept of a hollow-bottomed gondola body	121
4.28	Multifunctional articulated concept of a railway tank frame	122
4.29	Multi-material concept of a covered car	123
4.30	Multi-material concept of a covered car body	123
4.31	Multi-material concept of a railway tank	124
4.32	Multi-material concept of a railway tank boiler	124
4.33	Cross-section of a railway tank with a multi-material support concept	125

INTRODUCTION

Modern railway transport plays a key role in ensuring economic stability and development of Ukraine, being the main link in the transport and logistics system of the country. In the context of a dynamically changing freight transport market and a difficult economic situation, aggravated by military operations, railway transport faces new challenges related to ensuring reliability, safety and efficiency of transport. One of the most important areas requiring close attention is the transport of liquid fuel and lubricant cargoes, such as light and dark oil products, heating oils and other chemicals.

One of the main problems arising in the process of operation of the fleet of tank wagons is the need for their regular and quality cleaning. Due to significant wear of the rolling stock and impossibility of its operative renewal in conditions of limited resources, special attention is paid to the issues of extending the service life of existing tank wagons by improving the methods of maintenance and diagnostics. Cleaning of tank wagon boilers, including washing and steam treatment operations, has a significant impact on their stress-strain state, which requires detailed scientific substantiation and application of modern calculation methods.

The present monograph is devoted to the topical issues of analysing the temperature impact on the tank wagon structure in the process of cleaning, as well as to the methods of assessing their technical condition and operational safety. In the course of the research, the scientific and applied tasks aimed at determining the optimal operating modes, developing methods for assessing the stress-strain state of boilers and improving the efficiency of the tank car fleet have been solved.

In addition, the monograph considers a wider range of tasks related to the modernisation of freight rolling stock in Ukraine. Modern trends in the railway industry require the introduction of innovative technologies and methods to improve the performance of wagons, reduce maintenance and repair costs, and ensure the integration of Ukrainian railway transport into the European system. In this context, special attention is paid to the issues of increasing the speed of freight trains, improving the safety and comfort of operation.

A separate part of the paper is devoted to the development of new methodological approaches and tools for assessing the dynamic load and reliability of freight wagons. In particular, methods of measuring mechanical stresses in structural elements using modern strain gauge technologies, as well as methods of measuring contact forces and spectral analysis of oscillation processes are proposed, which allow to identify critical operating modes. The developed methods and tools make it possible to test wagons without involving expensive laboratory wagons, which significantly reduces time and financial costs.

An important area of research presented in this paper is the assessment of fire resistance of reinforced concrete structures used in railway construction. The monograph proposes a hierarchical system for calculating the fire resistance of reinforced concrete slabs, including three levels

of analysis: tabular, simplified and refined. These methods allow designers to choose the optimal approach depending on specific operating conditions and safety requirements.

Special attention is paid to the development of multifunctional structural solutions for freight wagons, including elastic-dissipative, multi-material and non-split hinge structures. The paper presents promising designs such as covered hoppers, leaf spring platforms, universal wagons with damping struts and multi-material railway tank wagons. The implementation of these solutions will allow to improve the performance characteristics of wagons, increase their service life and reduce material intensity.

The research results presented in the monograph can be used both in practical activities of railway companies and in educational institutions when training railway industry specialists. The proposed methods and approaches will make it possible to optimise the processes of rolling stock operation, improve its reliability and safety, as well as create a scientific basis for further research in the field of railway transport.

Thus, this monograph is a comprehensive work covering the topical issues of operation and modernisation of railway transport in Ukraine. The results of the conducted research and proposed recommendations are aimed at solving the most acute problems facing the industry and contribute to improving its competitiveness at the international level.

CHAPTER 1**ANALYSIS OF THE TEMPERATURE EFFECT ON THE STRESS-STRAIN STATE OF THE TANK CAR BOILER DURING STEAMING****ABSTRACT**

Uninterrupted transportation of bulk fuel and lubricant cargoes is one of the main tasks facing the railway transport of Ukraine. At the same time, the nomenclature (light and dark petroleum products, fuel oils) of bulk cargoes and the limited number (due to the obsolescence of the existing fleet of tank cars and the inability to renew them in military conditions) of the corresponding rolling stock require constant and high-quality cleaning of tank car boilers. This is due to the need for prompt use of tank cars for the transportation of various types of cargo. Modern boiler cleaning technologies are associated with the application of temperature loads to their boilers, namely with washing and steaming operations. This directly affects the stress-deformed state of tank car boilers. Which, in turn, determines the need for scientific research to determine the temperature effect on the stressed-deformed state of the tank car boiler during washing and steaming operations. It was the solution of such a scientific and applied task that became the goal of research, the results of which are presented in this section of the monograph.

To achieve the set goal, the following scientific and applied tasks were defined and solved. The existing information sources on the relevant topic were analyzed. Next, the technical description and requirements for modern designs of tank cars and their boilers are presented. Then, the used and adapted moment theory of shells is presented. On the basis of this mathematical theory, the load values at the control points of the tank car boiler are determined. Based on these results, the calculation model built in a modern computer computing and software complex was adjusted. Which was calculated using the finite element method and brought to an adequate level. The developed adequate finite element model includes the optimal number of finite elements and nodes: 10 182 768 elements and 18 655 084 nodes. Tetrahedrons and triangles are used as finite elements. With the use of the developed adequate finite-element model, temperature load calculations and simulation of the application of hot steam were carried out. At the same time, the temperature of hot steam is 160 °C, and the calculation period is 20 minutes. As a result of the calculations, it was found that the maximum heating temperature of the boiler is 71.3 °C when the temperature is loaded with steam. On the basis of the obtained results of temperature simulations, the input data for determining the stress-strain state of the tank car boiler were formed. The results of the

calculations made it possible to establish that the maximum stress values are 173 MPa and do not exceed the permissible values. That is, when washing and steaming operations are carried out, the strength condition is fulfilled.

The obtained results of simulations of temperature loads and the stress-strain states corresponding to them will be useful in conducting further research and development works on the selected topic. In addition, the obtained results and achievements can be used in educational activities in the preparation of students of various levels of education.

KEYWORDS

Transport mechanics, railway transport, temperature influence, stress-strain state, cars, tank cars.

Today, one of the priority areas of railway transport is the need for stable transportation of bulk fuel and lubricant cargoes. At the same time, the nomenclature of bulk cargoes is wide and the demand for transportation of specific cargo is constantly changing. That is, there is a constantly changing need to transport: light and dark petroleum products, lubricants, fuel oils, and others. The above determines the need for particularly careful technical maintenance of the fleet of tank cars. Including washing and steaming operations in accordance with the technical regulations.

In general, the temperature of the steam used for washing and steaming works is 160 °C. A thorough scientific research analysis of the stress-deformed state of the tank car boiler during washing and steaming operations was not carried out. And this is exactly the goal set in this study.

The purpose of the manuscript is to highlight the results obtained from the study and analysis of the temperature effect on the stressed-deformed state of the tank car boiler during washing and steaming operations. At the same time, the operating temperature of the hot steam was considered to be 160 °C, which corresponds to the existing operating value.

To achieve the set goal, a number of the following scientific and technical problems were defined and solved:

- 1) analysis of information sources in which issues of temperature influence on machine-building structures, features of relevant mathematical and computer modeling, simulations are covered;
- 2) technical description and requirements for modern designs of domestic tank cars and their boilers. Such descriptions are determined in order to take into account the relevant features when creating a calculation model and conducting computational computer simulations;
- 3) adaptation and application of moment theory of shells for mathematical determination of load values at control points of tank car boiler construction;
- 4) creation of a spatial calculation computer model of a tank car boiler in a modern software complex. Adjusting the adequacy of the developed finite-element calculation model;
- 5) determination of features and implementation of computer simulations. Namely, the determination of the features of applying temperature loads, fixing the calculation model, setting the external

and initial temperatures, etc. At the same time, temperature loads arising from the action of hot steam of 160 °C are considered. Obtaining and analyzing the obtained results of temperature loads;

6) calculation of the stress-strain state of the tank car boiler according to the calculated case of temperature loads. Analysis of the obtained pictures of stress-strain states and comparison of calculated results with permissible values, which are taken in accordance with the characteristics of the material;

7) analysis of the obtained results and formulation of general conclusions.

The search for information sources was aimed at finding works that are devoted to highlighting the achievements and results of research on: determination of temperature effects on mechanical engineering structures, mathematical and computer modeling of processes in mechanical systems, analysis of stress-strain states in transport structures and, in particular, in freight cars.

In work [1], it was found that a specific factor in the production of cellular aggregate for transport structures made of polymer materials is multi-stage impregnation with the composition of the dressing and then the binder in the final operations, followed by drying and heat treatment of the cellular blocks. Which leads to uneven heat transfer of the binder from the central part of the panel to its peripheral end zones. The regularities of this non-uniform heat migration of the binder along the length of the cellular channel have been created and analyzed. It was found that these phenomena are caused by the hydrodynamic movement of the binder, which is mainly caused by temperature gradients. Taking this into account, a method of determining the thickness of the binder layer along the channels of the honeycombs was created with the given input data of the change in density and surface tension along the length of the honeycomb aggregate cell.

In the scientific work [2], the approach to mass optimization of shell transport structures was further developed. Which includes significantly improved components of fragments of known analogues, as well as new fragments that were not taken into account before. This approach made it possible to solve the complex multi-parameter problem of optimal design of the considered class of shell transport structures with almost no loss of accuracy. For this, the optimization process was divided into several stages according to the justified significance levels of the parameters included in the objective function - minimum mass. The analysis of the effectiveness of the reinforcement structure of the load-bearing skins and the preliminary optimization of the properties of the cellular aggregate were carried out, which significantly simplified the choice of their optimal parameters. It is shown that with a minimal gain in mass due to the optimal reinforcement scheme, which is approximately 5 % compared to a quasi-homogeneous shell, there is a real risk of doubling the mass of the shell when choosing a significantly suboptimal shell structure.

Article [3] is devoted to highlighting the results of the analysis and substantiating the fields of tolerances for the relevant types of technological defects in transport engineering structures. The tolerances for the deviation of the thickness of the formed product from the design value were determined. It was found that the input control determines the deviation of the thickness from the nominal value for a single-layer semi-finished product realized in the prepreg. Deviation in thickness from the nominal value includes components that arise during its formation. These components are associated with integral deviations of the technological mode of formation (including temperature)

from that regulated by the relevant documentation. Analytical dependences on the reasonable assignment of tolerance fields for the physical and mechanical characteristics of the material with deviations in thickness, in the presence of local integrity violations in the form of voids, were obtained. In contrast to the existing models, the obtained dependencies made it possible to assess the quality of technological processes of forming semi-finished products and products from polymer composite materials according to the level of defects of the considered class.

The authors of the study [4] proposed a new approach to diagnosing the technical condition of structures that transmit mechanical energy. At the same time, the impact on their stress-strain state was considered. And dependencies were developed accordingly, the publication is devoted to highlighting the features of which.

The work [5] presents the design calculation of the automatic electro-hydraulic drive for the rotary movement of technological equipment. At the same time, special attention was paid to the influence of temperatures on the corresponding properties. However, such studies did not consider the possibility of using the developed method for non-load-bearing transport metal structures.

Research [6] is devoted to the modeling of the dynamics of a node of an element of a general design by the method of spectral analysis. At the same time, the influence of various factors on the stress state of the general structure was investigated. However, special attention was not paid to the issue of temperature influence, which is initially explained by the lack of such a task.

The authors of the article [7] studied, among other things, the temperature effect on the driving components of the power plants of transport. For this purpose, appropriate mathematical and computer models were developed and researched. However, their decisive component is compliance with the tasks of electrical equipment research.

In the scientific and applied work [8], the main attention is also paid to the tasks of researching the electrical equipment of vehicles. At the same time, the results of the conducted simulations, on the diagnosis of thermal effects, will be useful in solving similar problems for other structural components.

The article [9] presents the results of an analysis of the influence of the existing stress-deformed state of freight cars and the possibility of extending their service life. However, the possibility of their accident-free operational temperature loads was not considered.

The scientific study [10] is devoted to the analysis of the influence of the bending deformations of the car body on the indicators of interaction with the railway track. However, not enough attention has been paid to temperature deformations.

Article [11] highlights the results of research into the possibility of extending the service life of the bodies of universal semi-cars that have exhausted their regulatory resource. However, it is not specified how their stressed-strained state will be formed from possible temperature loads from the corresponding load.

The authors of the scientific publication [12] presented the results of computational modeling of the dynamic load of containers placed on a platform car during railway ferry transportation. Which corresponds to the second calculation mode. However, another case of specific perception of loads, namely from temperature influence, was not considered.

Modeling and simulation of the decision support system structure of an intelligent locomotive and evaluation of the quality of operation are given in [14]. It presents complex mathematical models and a proposed computer method for solving them. However, the issue of the possibility of applying appropriate approaches to calculated mathematical strength cases is not given.

Article [15] is devoted to the issues of theoretical and practical determination of the parameters of the on-board capacitive energy storage of metro rolling stock. However, the direction of their influence on the carrying capacity of the car body, or their temperature factors, were not investigated.

In works [17–19], the issue of safety of sea cargo transportation is comprehensively investigated. At the same time, the article [17] proposed an integrated approach to assessing the vulnerability of critical ship equipment and systems. And the work [18] gives the results of the study of the environmental efficiency of the operation of ships from the point of view of ensuring the efficiency of cargo transportation. And finally, in article [19], the issue of environmental efficiency of ship operation from the point of view of ensuring the efficiency of cargo transportation is considered. However, the considered models of stress-deformed vessels did not include the modes of temperature loads on their cases.

Summarizing the above, it can be noted that in all the above-mentioned scientific works, the peculiarities of the temperature effect on the stress-strain state of load-bearing systems of vehicles, and in particular the tank car boiler during steaming, were not investigated.

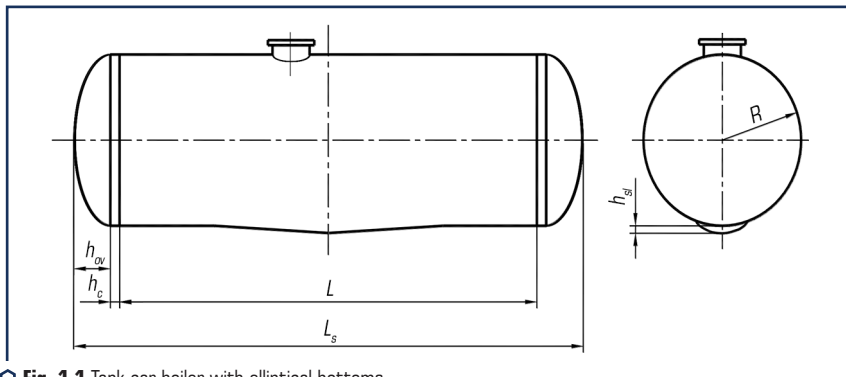
1.1 REQUIREMENTS FOR MODERN DESIGNS OF DOMESTIC TANK CARS AND THEIR BOILERS

One of the common models of tank cars was chosen for the study. It has the characteristics listed in **Table 1.1**.

◆ **Table 1.1** Characteristics of a typical tank car

Parameter name	Designation	Value
Inner radius of the boiler, m	R	1.60
Length of the cylindrical shell, m	L	9.775
Elliptical bottoms:		
– internal height of the oval part, m	H_{ov}	0.64
– height of the cylindrical part, m	H_c	0.06
Length of the car along the coupling axes of auto couplings, m	$2L_c$	12.02
Slope depth, m	H_{sl}	0.03
Slope volume, m ³	V_{sl}	0.02
Number of axles in the cart	n	2
Carrying capacity, t	Q_{tp}	70.5
Container mass and container tolerance, t	$T \pm \Delta T$	23.3
Acceleration of free fall, m/s ²	g	9.81

The image of the tank car boiler under study is shown in **Fig. 1.1**.



○ **Fig. 1.1** Tank car boiler with elliptical bottoms

The tank car is intended for the transportation of petroleum products. Tank cars should be used as intended in accordance with the rules of technical operation of railways and operational documentation. The use of tanks for the transportation of other dangerous goods must be agreed with the manufacturing plant, the main organization of the product being transported, and the bodies that control traffic safety and operation at the discharge-filling points. Operational loads should not exceed those established by current regulatory documents. It is not allowed to replace elements of the tank car with others, which differ in design or materials from those provided in the manufacturer's drawings, during operation, without its consent.

Sampling from tanks containing a dangerous petroleum product must be carried out without releasing the product into the atmosphere, unless it is stipulated by the standard for the transported product.

Tank cars containing dangerous goods must have markings that characterize the transport danger of the goods. The marking should contain: danger sign, UN serial number, emergency card number.

The manufacturer guarantees compliance of tank cars with the requirements of the standard, subject to compliance with the rules of operation, maintenance and repair. The warranty period of operation of tank cars is established in the technical conditions for specific models of tank cars, but not less than 18 months from the day of commissioning. The warranty period for replaceable components, parts and accessories for tank cars is established by relevant regulatory documents for specific products.

Tests of tank cars should be performed under the values of climatic factors of the external performance environment "U" in accordance with the current regulatory documents.

Components of tank cars and tank cars as a whole that are manufactured must be checked for compliance with the requirements of regulatory and technical documentation during technical control.

During the control of tank cars, measuring devices should be used in accordance with the requirements of the technical documentation.

Fitting into the overall dimensions is checked by passing the tank cars through the overall frame.

Assembly and installation of the boiler, frame, carts, ladders, platforms, pouring and pouring fittings, safety devices, performance of the self-clutch mechanism, braking and other equipment of tank cars, tightness of the boiler with pouring and pouring fittings and safety devices, marking, color and quality of painting are controlled visually and by measurements during tests of tank cars in accordance with the design documentation and technical conditions.

The quality control of the welded joints of the boiler is carried out in accordance with the current regulatory documents. Mechanical tests of welded joints of boilers of tank cars are performed in accordance with current regulatory documents.

The quality of welded joints of boilers of tank cars operating under excessive pressure over 0.07 MPa should be tested in accordance with current requirements.

Reliability requirements are monitored based on the results of reliability tests according to a specially developed and agreed program and methodology.

The capacity of the safety valves must be selected according to the calculation in accordance with the current regulatory documents.

Incoming control of materials and component products, which are received for the manufacture of tank cars, must be carried out in the order established by the manufacturer in accordance with the current requirements.

Production, testing and acceptance of the boiler of tank cars must comply with the requirements of current regulatory documents.

The boiler should consist of a shell, two bottoms, a hatch, a hatch for installing a safety inlet valve, and a drain device. The material used for the production of the main elements of the boiler is in accordance with the current regulatory documents.

The boiler must be equipped with a fence, external stairs with a platform that allow for maintenance, repair and control of tank car draining and filling operations, as well as internal stairs fixed to the manhole shell for inspection and repair inside the boiler.

The deviation of the internal diameter of the shell of the tank car boiler from the nominal should be within the tolerance of ± 6 mm.

Bumps, scratches and other defects (pits, sinks, etc.) are not allowed on the surface of the tank car boiler, if their depth exceeds the minus limit deviations provided by the relevant standards or technical conditions for the supply of metal.

The deviation from the straightness of the generator tank car boiler should not exceed 2 mm per 1 m of length, but not more than 20 mm over the entire length of the shell, without taking into account the local deviation from straightness in the welds.

Local dents and convexities with a height of no more than 5 mm per 1 m of length are allowed on the body of the tank car boiler, but no more than 2 units on each side of the shell.

The displacement of the edges of the sheets in the butt joints, the accuracy of the docking of the ends of the shells with the bottoms must be ensured within the tolerances for the displacement and removal of the edges provided by the current regulatory documents.

Welding of the tank car boiler and its elements, as well as welding of parts to the boiler, must be carried out by welders certified in accordance with current regulatory documents.

In the butt welds of the tank car boiler, a joint removal of the edges (inside and outside) is allowed within 10 % of the sheet thickness plus 3 mm, but not more than 5 mm, while the removal of the edges in the longitudinal seams is determined by the template, the length of which (by chord) is equal to 1/3 of the shell radius. The clumsiness of ring seams is determined by a ruler 300 mm long.

The tank car boiler must be symmetrically located on the pivot beams. Permissible displacement of the longitudinal axis of the boiler relative to the longitudinal axes of the backbone beams in the horizontal plane is no more than 5 mm.

The tank car boiler must be equipped with a drain-filling and safety valve.

Draining and filling fittings must include: a draining device, which must ensure the draining and filling of the product at the draining-filling points, the preservation of the product during the transportation of the tank car and include three sequentially installed locking devices:

- internal (main) locking device to ensure complete merging of the cargo and sealing of the tank car boiler during movement;
- additional locking device – disk valve for sealing the tank car boiler in the event of a malfunction of the main locking device;
- external shut-off device for sealing the tank car boiler in the event of a malfunction of the internal (main) and additional shut-off devices.

The distance from the surface of the drain device to the level of the rail head must comply with the current regulatory documents.

The body of the draining device before welding to the tank car boiler shell must be inserted inside flush with the internal surface of the boiler. Then it should be ensured that the joint is fully welded over the entire thickness of the tank car boiler shell.

Draining the product from the tank car boiler must be provided with a slope to the drain device with a height difference of 25...30 mm.

The cover of the hatch of the tank car boiler must ensure the density of the boiler (taking into account water hammer and steam pressure) at a pressure of at least 0.25 MPa (2.5 kgf/cm²). A sealing ring must be installed on the cover.

There should be a device for installing a locking and sealing device on the cover of the tank car's boiler hatch.

The hatch cover of the tank car must be equipped with a device for detonating the cover in the event of its freezing or the presence of a vacuum in the boiler, as well as to ensure safe opening of the cover in the presence of excess pressure in the boiler.

Safety fittings must include a safety inlet valve.

The safety-inlet valve must be installed in the upper part of the boiler and serves to exclude a possible increase in pressure inside the boiler beyond the permissible level, as well as to prevent the formation of a vacuum. The safety-inlet valve cannot act to eliminate the vacuum after steaming operations.

The design of the safety inlet valve and its placement on the boiler should exclude the possibility of accidental release or theft of the product from the tank. The safety valve must be sealed after adjustment.

1.2 ADOPTION AND USE OF MOMENT THEORY OF SHELLS FOR MATHEMATICAL CALCULATION

When calculating for all types of loads, except for the calculation of bottoms from internal pressure, the tank car boiler is considered as a closed cylindrical shell, freely supported at the ends on diaphragms that are absolutely rigid in their plane and absolutely flexible perpendicular to this plane. Such diaphragms are the bottoms of the tank car boiler. To calculate the bottom and the adjacent zone of the cylindrical part of the boiler, the actual shape and elasticity of the tank car may be taken into account.

Let's highlight an infinitesimally small element of the middle surface of the shell with two longitudinal and two transverse sections $ABCD$ (Fig. 1.2, a). This element has the dimensions $dx = R_1 d\alpha$ and $ds = R_1 d\beta$, where α and β are the dimensionless coordinates of the cylindrical system. The coordinate $\alpha = x/R_1$ coincides with the generator x , and $\beta = s/R_1$ with the arc s of the cross section of the cylindrical part of the boiler.

Instead of the removed parts of the shell, it is possible to apply force factors to the longitudinal and transverse sections of the element $ABCD$ (Fig. 1.2, b): normal $T_1(\alpha, \beta)$ and $T_2(\alpha, \beta)$, transverse $Q_1(\alpha, \beta)$ and $Q_2(\alpha, \beta)$, shear $S_1(\alpha, \beta)$ and $S_2(\alpha, \beta)$ forces, bending $M_1(\alpha, \beta)$ and $M_2(\alpha, \beta)$ and torsional $M_{T1}(\alpha, \beta)$ and $M_{T2}(\alpha, \beta)$ moments.

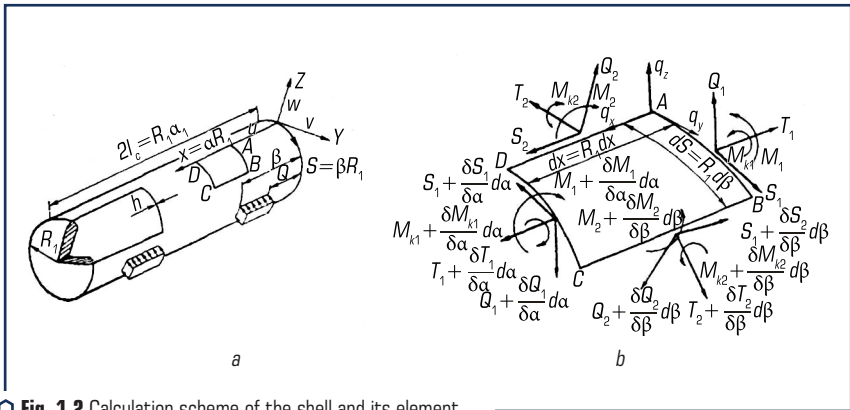


Fig. 1.2 Calculation scheme of the shell and its element

All these force factors, which determine the stress state of the shell, are related to the length unit of the corresponding side of the analyzed element:

$$S_1(\alpha, \beta) = S_2(\alpha, \beta) = S(\alpha, \beta), \quad (1.1)$$

$$M_{T_1}(\alpha, \beta) = M_{T_2}(\alpha, \beta) = M_T(\alpha, \beta). \quad (1.2)$$

Let's take the positive reference direction of the coordinates as shown in **Fig. 1.2, a**. Along these three mutually perpendicular directions, let's decompose the complete displacement of the point, marking its components: longitudinal (along the generator) through $u(\alpha, \beta)$, tangential (along the tangent to the arc of the circle) – $v(\alpha, \beta)$ and radial (along the internal normal) – $w(\alpha, \beta)$.

These movements of the middle surface determine the deformed state of the shell. In addition, the angles of rotation of the longitudinal $\theta_2(\alpha, \beta)$ and $\theta_1(\alpha, \beta)$ transverse planes of sections are considered.

The external load can also be distributed along these three directions. The components of surface loading of the boiler shell have the following designations: longitudinal through $q_x(\alpha, \beta)$, tangential $q_y(\alpha, \beta)$ and radial $q_z(\alpha, \beta)$. The parentheses (α, β) indicate that the considered parameters are, in the general case, functions of two variables α and β , and are omitted in the future to shorten the record. Equilibrium equations are formulated to determine the unknown force factors acting on an infinitesimal element of the shell. Since these equations are not sufficient to solve the statically indeterminate problem under consideration, the conditions of non-discontinuity of deformations are used, i.e. connections between components of movements and deformations (geometric relations) and connections of deformations with force factors (physical relations).

The complete system of equations, consisting of equilibrium equations and strain continuity equations, is equivalent to the following equation in partial derivatives of the eighth order:

$$\nabla^2 \nabla^2 \nabla^2 \nabla^2 \Phi + 4k^4 \frac{\partial^4 \Phi}{\partial \alpha^4} = 0, \quad (1.3)$$

where $\nabla^2 = \partial^2 / \partial \alpha^2 + \partial^2 / \partial \beta^2$ – Laplace differential operator; $\Phi(\alpha, \beta)$ – enabling function.

The part of the expression of equation (1.3) containing $4k^4$ is calculated by the formula:

$$4k^4 = \frac{12(1-\mu^2)R_1^2}{h_1^2}, \quad (1.4)$$

where μ – Poisson's ratio; h_1 – thickness of the wall of the cylindrical part of the boiler.

Through the enabling function Φ , all power factors and displacements of the boiler shell can be determined. However, the calculation of the boiler based on the given equations of the moment theory of shells for all types of loading, especially taking into account the different thicknesses of the sheets that make up the boiler, is a rather difficult and time-consuming task. Therefore, it is advisable to use electronic computing machines to solve it. The machine calculation algorithm in matrix form can be constructed as follows.

Equation (1.3) by substitution is reduced to the form:

$$\Phi = \sum_{m=1}^{\infty} f_m(\beta) \sin \lambda \alpha, \text{ then}$$

$$\sum_{m=1}^{\infty} \left[\frac{d^8 f_m(\beta)}{d\beta^8} - 4\lambda_m^2 \frac{d^6 f_m(\beta)}{d\beta^6} + 6\lambda_m^4 \frac{d^4 f_m(\beta)}{d\beta^4} + \lambda_m^4 (\lambda_m^4 + 4k^4) f_m(\beta) \right] \sin \lambda_m \alpha = 0, \quad (1.5)$$

where m – row member number; $2l_c$ – length of the cylindrical part of the boiler; $f_m(\beta)$ – coefficient of the number of the series of the function, which depends on the coordinate β .

Condition (1.5) is fulfilled for any values α only if for each number the expression in square brackets is equal to zero.

Using this condition, it is possible to obtain a system of independent differential equations of the eighth order with respect to the coefficients $f_m(\beta)$ of the function series Φ . In the future, the index m is lowered, but it should be borne in mind that all calculated dependencies refer to the same number m of the member of the series.

The given expression of the function Φ has an important property: the forces and movements calculated based on it satisfy the boundary conditions adopted above, i.e. the resting of the ends of the boiler on the indicated diaphragms. These conditions mean that when $\alpha = 0$ and $\alpha = \alpha_1 = 2l_c/R_1$, $M_1 = T_1 = w = v = 0$.

To solve ordinary differential equations (1.5), let's formulate a characteristic equation of the form:

$$(\gamma^2 + \lambda^2)^2 + 4k^4 \lambda^4 = 0. \quad (1.6)$$

The roots of equation (1.6) are of the complex form:

$$\gamma_j = \pm c_l \pm id_l, \quad (1.7)$$

where $j = 1, 2, 3, \dots, 8$; $l = 1, 2$.

Real parts c_l and d_l complex roots are calculated according to the formulas obtained from expression (1.6) after transferring its second term to the right part, extracting from the right and left parts the roots of the fourth and then the second degree, taking into account the rules used when performing these operations on complex numbers:

$$c_l^2 = \frac{\lambda}{2} \left\{ (\lambda \pm k) + [(\lambda \pm k)^2 + k^2]^{\frac{1}{2}} \right\}, \quad (1.8)$$

$$d_l = \frac{\lambda k}{2c_l}. \quad (1.9)$$

In formula (1.8), the plus sign corresponds to the index $l=1$, and the minus sign corresponds to $l=2$.

The general integral of each of the homogeneous equations (1.5) has the form:

$$f(\beta) = C_1\varphi_1(\beta) + C_2\varphi_2(\beta) + C_3\varphi_3(\beta) + C_4\varphi_4(\beta) + C_5\varphi_5(\beta) + C_6\varphi_6(\beta) + C_7\varphi_7(\beta) + C_8\varphi_8(\beta), \quad (1.10)$$

where $\varphi_j(\beta)$ – partial integrals of the homogeneous equation.

It is advisable to present them in the form of:

$$\left. \begin{aligned} \varphi_{1,5}(\beta) &= e^{c_{1,2}(\beta-\beta_0)} \cos d_{1,2}(\beta-\beta_0); \\ \varphi_{2,6}(\beta) &= e^{c_{1,2}(\beta-\beta_0)} \sin d_{1,2}(\beta-\beta_0); \\ \varphi_{3,7}(\beta) &= e^{-c_{1,2}(\beta+\beta_0)} \cos d_{1,2}(\beta+\beta_0); \\ \varphi_{4,8}(\beta) &= e^{-c_{1,2}(\beta+\beta_0)} \sin d_{1,2}(\beta+\beta_0). \end{aligned} \right\} \quad (1.11)$$

In formula (1.11), β_0 means half of the central angle corresponding to the arc of the panel from which the cylindrical part of the boiler can be assembled.

Representing force factors M_1, M_2, T_1, T_2, Q_2 and displacements v, w, θ_2 in series by $\sin \lambda \alpha$, and S, M_k, Q_1, u and θ_1 series by $\cos \lambda \alpha$ using the formulas of V. Vlasov [20], through the known coefficients $f(\beta)$, it is possible to obtain the coefficients of the series of the listed force factors and displacements.

It is advisable to present the coefficient formulas in matrix form. Then, if to denote the vector of coefficients of force factors on the longitudinal edges $-\beta_0$ and β_0 the panel through the expression:

$$\vec{S} = \|S(-\beta_0)T_2(-\beta_0)Q_2(-\beta_0)M_2(-\beta_0)S(\beta_0)T_2(\beta_0)Q_2(\beta_0)M_2(\beta_0)\|, \quad (1.12)$$

and the vector of arbitrary integrations by \vec{C}_j , then it is possible to write:

$$\vec{S} = \|A\|\vec{C}_j. \quad (1.13)$$

Similarly, if the vector of displacement coefficients of the longitudinal edges:

$$\vec{u} = \|u(-\beta_0)v(-\beta_0)w(-\beta_0)\theta_2(-\beta_0)u(\beta_0)v(\beta_0)w(\beta_0)\theta_2(\beta_0)\|, \quad (1.14)$$

then it can be represented as:

$$\vec{u} = \|B\|\vec{C}_j. \quad (1.15)$$

In formulas (1.13) and (1.15) $\|A\|$ and $\|B\|$ are matrices of transformation of the vector of arbitrary integrations into vectors of forces and displacements. At the same time:

$$\left. \begin{aligned} \|A\| &= \|A_d\| \|A_{sq}\|; \\ \|B\| &= \|B_d\| \|B_{sq}\|; \end{aligned} \right\} \quad (1.16)$$

where $\|A_d\|$ and $\|B_d\|$ – diagonal matrices of the eighth order; $\|A_{sq}\|$ and $\|B_{sq}\|$ – square matrices of the eighth order.

In diagonal matrices, the non-zero elements are, respectively:

$$\left. \begin{aligned} \frac{Eh_1}{R_1} \lambda^3, \frac{Eh_1}{R_1} \lambda^4, -2 \frac{D}{R_1^3} \lambda^2 k^2, 2 \frac{D}{R_1^2} \lambda^2 k^2, \\ \frac{Eh_1}{R_1} \lambda^3, \frac{Eh_1}{R_1} \lambda^4, -2 \frac{D}{R_1^3} \lambda^2 k^2, 2 \frac{D}{R_1^2} \lambda^2 k^2, \\ \lambda, 1, 2 \lambda^2 k^2, 2 \frac{\lambda^2 k^2}{R_1}, 1, 2 \lambda^2 k^2, 2 \frac{\lambda^2 k^2}{R_1}, \end{aligned} \right\} \quad (1.17)$$

where $D = \frac{Eh_1^3}{12(1-\mu^2)}$ – cylindrical stiffness of the shell; E – modulus of elasticity of the boiler material; μ , h_1 and R_1 have the previous values.

Denote by $\beta = -\beta_0$ the function $\varphi_j = p_j$, and by $\beta = \beta_0$ the function $\varphi_j = \delta_j$. Taking this into account, square matrices can be represented in the form:

$$\|A_{sq}\| = \left\| \begin{array}{cccc} (\alpha_s p_1 - \beta_s p_2)(\alpha_s p_2 + \beta_s p_1) - (\alpha_s p_3 + \beta_s p_4) - (\alpha_s p_4 - \beta_s p_3) & \dots & & \\ \vdots & \vdots & \vdots & \vdots \\ (\alpha_s \delta_1 - \beta_s \delta_2)(\alpha_s \delta_2 + \beta_s \delta_1) - (\alpha_s \delta_3 + \beta_s \delta_4) - (\alpha_s \delta_4 - \beta_s \delta_3) & \dots & & \\ \vdots & \vdots & \vdots & \vdots \end{array} \right\} \quad (1.18)$$

$$\|B_{sq}\| = \left\| \begin{array}{cccc} (\alpha_u p_1 - \beta_u p_2)(\alpha_u p_2 + \beta_u p_1) - (\alpha_u p_3 + \beta_u p_4) - (\alpha_u p_4 - \beta_u p_3) & \dots & & \\ \vdots & \vdots & \vdots & \vdots \\ (\alpha_u \delta_1 - \beta_u \delta_2)(\alpha_u \delta_2 + \beta_u \delta_1) - (\alpha_u \delta_3 + \beta_u \delta_4) - (\alpha_u \delta_4 - \beta_u \delta_3) & \dots & & \\ \vdots & \vdots & \vdots & \vdots \end{array} \right\} \quad (1.19)$$

In matrices (1.18) and (1.19) to shorten the record, only the first halves of the two terms corresponding to the effort S and displacement u at the edges of the panel $-\beta_0$ and β_0 . The next four elements are the same as the first, but in them the coefficients α_s and β_s must be replaced by α_{1s} and α_{2s} and the coefficients α_u and β_u by α_{1u} and β_{1u} . In addition, the functions $p_{1, 2, 3, 4}$ and $\delta_{1, 2, 3, 4}$ are replaced by $p_{5, 6, 7, 8}$ and $\delta_{5, 6, 7, 8}$, respectively. The other six terms, marked in the

matrices with dots, correspond to the written terms if the coefficients and with indices are replaced by coefficients α and β with indices S , on the coefficients with indices T , Q and M , and coefficients with indices u are replaced by coefficients with indices v , w and θ .

The values of the coefficients are given in **Table 1.2**. In addition, in the matrices $\|A_{sq}\|$ and $\|B_{sq}\|$, the third, fourth, seventh and eighth elements of the terms with the coefficients having indices T , M , v and θ , must have signs reversed to the signs of these elements in the terms with indices S and u .

● **Table 1.2** The values of the coefficients

Index	Coefficients			
	α	β	α_1	β_1
S	c_1	d_1	c_2	d_2
T	1	0	1	0
Q	$(d_1^3 - 3c_1^2 d_1) +$ $+(2 - \mu)\lambda^2 d_1$	$(c_1^3 - 3c_1 d_1^2) -$ $-(2 - \mu)\lambda^2 c_1$	$-(d_2^3 - 3c_2 d_2^2) -$ $-(2 - \mu)\lambda^2 d_2$	$-(c_2^3 - 3c_2 d_2^2) +$ $+(2 - \mu)\lambda^2 c_2$
M	$-2c_1 d_1$	$(c_1^2 - d_1^2) - \mu\lambda^2$	$2c_2 d_2$	$-(c_2^2 - d_2^2) + \mu\lambda^2$
u	$(c_1^2 - d_1^2) + \mu\lambda^2$	$2c_1 d_1$	$(c_2^2 - d_2^2) + \mu\lambda^2$	$2c_2 d_2$
v	$-(c_1^3 - 3c_1 d_1^2) +$ $+(2 + \mu)\lambda^2 c_1$	$(d_1^3 - 3d_1 c_1^2) +$ $+(2 + \mu)\lambda^2 d_1$	$-(c_2^3 - 3c_2 d_2^2) +$ $+(2 + \mu)\lambda^2 c_2$	$(d_2^3 - 3d_2 c_2^2) +$ $+(2 + \mu)\lambda^2 d_2$
w	0	1	0	1
θ	$-d_1$	c_1	d_2	$-c_2$

Let's use the displacement method to calculate the tank car boiler. Let's present the cylindrical part of the tank car boiler divided into separate panels, which are the main elements of the calculation scheme. As the boundaries of these elements, it is expedient to take the lines of transition from one thickness of the sheet to another, intersections of sudden changes in load, generating lines along which concentrated forces are applied. For the hydrostatic pressure of the liquid, which is variable along the arc of the section of the cylindrical part of the tank car boiler, it is advisable to choose the width of the panels in such a way that it is possible to accept the load on it as constant.

Let's apply bonds to the longitudinal edges $-\beta_0$ and β_0 of selected panels, and then one by one, let's assign to these bonds forced displacements u , v , w and θ_2 , which change along the generating line according to the law $\cos \lambda \alpha$ or $\sin \lambda \alpha$ with a unit amplitude. These movements will be single.

For each main element from equation (1.15) let's find the vectors:

$$\vec{C}_j = \|B\|^{-1} \vec{u}, \quad (1.20)$$

where $\|B\|^{-1}$ – inverse matrix $\|B\|$.

In a vector \bar{u} , one of the components in sequence is equal to one, and all others are equal to zero.

The vector of reactions of the longitudinal edges at all considered single displacements according to equations (1.13) and (1.20) is:

$$\bar{S} = \|A\| \|B\|^{-1} \bar{u}. \quad (1.21)$$

So, the reaction matrix of the main element can be presented in the form:

$$\|r\| = \|A\| \|B\|^{-1}. \quad (1.22)$$

Formulas (1.13) and (1.15) are valid for homogeneous equations. In the case of an inhomogeneous equation, when the right-hand side of equation (1.3) is not equal to zero, these formulas will have the form:

$$\left. \begin{aligned} \bar{S} &= \|A\| \bar{C}_j + \bar{S}_{part}, \\ \bar{u} &= \|A\| \bar{C}_j + \bar{u}_{part}, \end{aligned} \right\} \quad (1.23)$$

where \bar{S}_{part} and \bar{u}_{part} are, respectively, the vectors of partial values of force factors and displacements determined by the right-hand side of the inhomogeneous equation, which depends on the nature of the surface external load.

So, if the power element of the boiler shell is loaded with surface radial forces, then the vectors \bar{S}_{part} and \bar{u}_{part} also have non-zero components:

$$\left. \begin{aligned} T_{2,part} &= \frac{Eh_1}{\Delta R_1} Z; \\ M_{2,part} &= -\frac{D\mu\lambda^2}{\Delta R_1} Z; \\ u_{part} &= \frac{\mu}{\lambda\Delta} Z; \\ w_{part} &= \frac{1}{\Delta} Z, \end{aligned} \right\} \quad (1.24)$$

where Z – coefficient of expansion in a series along $\sin\lambda\alpha$ the radial load, which is transmitted to the main element of the shell of the tank car boiler:

$$\Delta = \frac{Eh_1 \left[h_1^2 \lambda^4 + 12R_1^2 (1 - \mu^2) \right]}{12R_1^4 (1 - \mu^2)}. \quad (1.25)$$

If the main element is loaded with surface tangential loads, then the non-zero components will be:

$$S_{part} = - \left[1 + \frac{h_1^2}{12(1-\mu^2)R_1^2} \lambda^4 \right] \frac{Eh_1}{\Delta R_1 \lambda} Y, \quad (1.26)$$

$$v_{part} = 2 \left[(1+\mu) + \frac{h_1^2}{12(1-\mu^2)R_1^2} \lambda^4 \right] \frac{1}{\Delta \lambda^2} Y, \quad (1.27)$$

where Y – coefficient of expansion into a series of tangential load transmitted to the main element of the shell of the tank car boiler.

Components of vectors of private solutions for the main element loaded with surface longitudinal forces:

$$\left. \begin{aligned} N_{2\ part} &= - \frac{Eh_1^3 \mu \lambda^3}{12R_1^3 (1-\mu^2) \Delta} X; \\ M_{2\ part} &= - \frac{Eh_1^3 \mu^2 \lambda}{12R_1^2 (1-\mu^2) \Delta} X; \\ u_{part} &= - \frac{1 + \frac{h_1^2}{12R_1^2} \lambda^4}{\Delta \lambda^2} X; \\ w_{part} &= \frac{\mu}{\lambda \Delta} X, \end{aligned} \right\} \quad (1.28)$$

where X – coefficient of expansion in a series by $\cos \lambda \alpha$.

With the known law of load distribution along the coordinate lines α , the calculation of expansion coefficients Z , Y and X is carried out according to the Euler-Fourier formulas [21, 22].

The tank boiler is a symmetrical structure with respect to the average section, symmetrically loaded by external forces – support, hydrostatic and internal pressures, and for frameless tank cars – by longitudinal tensile and compressive forces. Therefore, members of the series with odd numbers are kept in the series, i.e. $m=1, 3, 5$.

For bearing radial and tangential loads, uniformly distributed over the sections of the boiler supports, the series coefficients are determined by the formulas:

$$\left. \begin{aligned} Z &= \frac{4q_{z1}}{m\pi}, \\ Y &= \frac{4q_{y1}}{m\pi}, \end{aligned} \right\} \quad (1.29)$$

where q_{z1} and q_{y1} – the intensities of radial and tangential loads uniformly distributed over the entire length of the main element, respectively.

For an inhomogeneous equation, the vector of arbitrary integrations is found from formula (1.23) taking into account the obtained values \vec{u}_{part} , that is, from the expression:

$$\vec{C}_j = \|B\|^{-1} \vec{u} - \|B\|^{-1} \vec{u}_{part}. \quad (1.30)$$

Therefore, the vector of reactions on the longitudinal edges of the main element subjected to external forces, according to the first formula (1.23) and equation (1.22), will be equal to:

$$\vec{S} = \|A\| \|B\|^{-1} \vec{u} - \|A\| \|B\|^{-1} \vec{u}_{part} + \vec{S}_{part} = \|r\| \vec{u} - \|r\| \vec{u}_{part} + \vec{S}_{part}. \quad (1.31)$$

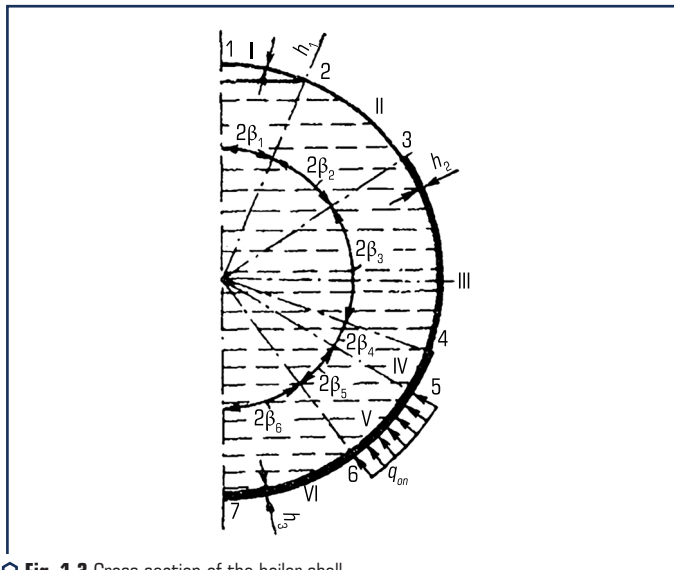
The second and third components of formula (31) at a given load represent an eighth-order vector:

$$\vec{S}_{\Sigma part} = -\|r\| \vec{u}_{part} + \vec{S}_{part}. \quad (1.32)$$

Formula (1.31) is convenient for machine calculations of boiler shells made of panels of the same length, but of different thicknesses.

A boiler composed of panels with different radii of curvature and made of different materials can be calculated in a similar way.

Consider the calculation sequence of a boiler with a symmetrical design and loading, the cylindrical part of which consists of six panels (**Fig. 1.3**).



○ **Fig. 1.3** Cross section of the boiler shell

In **Fig. 1.3**, panel numbers are indicated by Roman numerals. Nodal intersections are indicated by Arabic numerals. The length of the arc of the i -th panel is equal to $2R\beta_i$. Having constructed reaction matrices $\|r\|$ and vectors \vec{S}_{part} for each of the main elements, let's fulfill the condition of conjugation of the panels that make up the shell. These conditions are expressed in the equality of forces along the panel joining lines. For this, it is necessary to equate the last four components of the vector \vec{S} , i.e. $S(\beta_0)$, $T_2(\beta_0)$, $Q_2(\beta_0)$ and $M_2(\beta_0)$ respectively to the first four components of the vector of the next panel, i.e. $S(-\beta_0)$, $T_2(-\beta_0)$, $Q_2(-\beta_0)$ and $M_2(-\beta_0)$. As a result of such superimposition of vectors, let's get a canonical system of equations of the displacement method.

Such a canonical system must satisfy the boundary conditions at the initial edge of the first and the final edge of the last panel.

According to the conditions of symmetry on the generators of the boiler, which coincide with the upper and lower ends of the vertical diameter $v=\theta_2=Q_2=S=0$. Therefore, in the canonical order system n , let's cross out the second, fourth, $n-2$, and n -th columns, as well as the second, fourth, $n-2$, and n -th row. After solving such a system that has an order $n-4$, let's determine the vectors \vec{v} of each panel of the calculation scheme, and based on them and formula (1.31) – the vectors of power factors \vec{S} . Let's multiply the obtained vectors of force factors and displacements by the diagonal matrix $\|\alpha_i\|$ of the eighth order, the elements of which are $\cos\lambda\alpha$, $\sin\lambda\alpha$, $\sin\lambda\alpha$, $\sin\lambda\alpha$, $\cos\lambda\alpha$, $\sin\lambda\alpha$, $\sin\lambda\alpha$, $\sin\lambda\alpha$.

At certain values of the argument α_i , after summing over the number of retained members of the series m , let's determine the force factors and displacements in the cross-sections of the shell of the tank car boiler:

$$\left. \begin{aligned} \vec{S}(\alpha_i) &= \sum_{m=1}^m \|\alpha_i\|_m \vec{S}_m; \\ \vec{u}(\alpha_i) &= \sum_{m=1}^m \|\alpha_i\|_m \vec{u}_m. \end{aligned} \right\} \quad (1.33)$$

In formula (1.33) $\vec{S}(\alpha_i)$ and $\vec{u}(\alpha_i)$ are, respectively, the vectors of force factors and displacements in the intersections α_i , and the indices m emphasize that the matrices and vectors in the right-hand side of the equalities depend on the number of the member of the series.

In addition to the forces that are components of the vector \vec{S} , normal forces $T_1(\alpha_i)$ and bending moments $M_1(\alpha_i)$ on the cross-sections are important for assessing the stress state of the boiler. The coefficients of the series of these power factors are determined from the elasticity ratios using the formulas:

$$\left. \begin{aligned} T_1 &= \mu T_2 - \frac{Eh_1}{R_1} \lambda u; \\ M_1 &= \mu M_2 + \lambda^2 \frac{D}{R_1^2} (1 - \mu^2) w. \end{aligned} \right\} \quad (1.34)$$

So:

$$\left. \begin{aligned} T_1(\alpha_i) &= \sum_{m=1}^m T_{1m} \sin \lambda \alpha_i; \\ M_1(\alpha_i) &= \sum_{m=1}^m M_{1m} \sin \lambda \alpha_i. \end{aligned} \right\} \quad (1.35)$$

The normal stresses on the transverse σ_1 and longitudinal σ_2 surfaces of the sections of the cylindrical part of the boiler are determined by the formulas:

$$\left. \begin{aligned} \sigma_1 &= \frac{T_1}{h_1} \pm \frac{6M_1}{h_1^2}; \\ \sigma_2 &= \frac{T_2}{h_1} \pm \frac{6M_2}{h_1^2}. \end{aligned} \right\} \quad (1.36)$$

The specified mathematical approach to determining the stresses in the control locations of the tank car boiler was implemented with the help of the modern Mathcad computer software complex. Solving the relevant equations made it possible to obtain stress values, which became the basis for adjusting the adequacy of the developed calculated finite-element model.

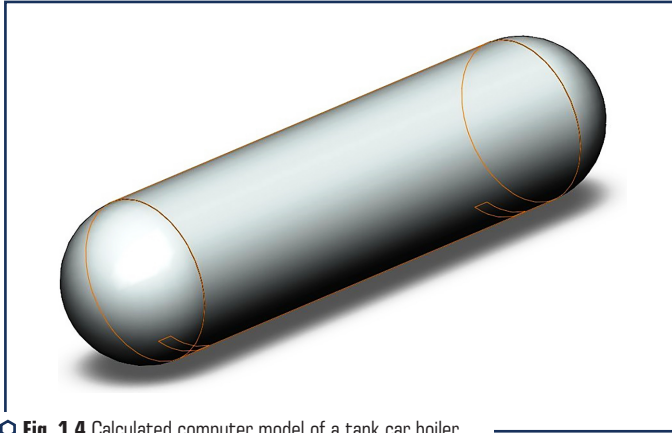
1.3 ANALYSIS OF THE TEMPERATURE EFFECT ON THE STRESS-STRAIN STATE OF THE TANK CAR BOILER DURING STEAMING

Modeling/simulation of the temperature effect of hot steam at a temperature of 160 °C on a tank car boiler. Such a temperature effect is standard during a typical washing-steaming process of tank car boilers. At the same time, the time of the washing-steaming technological operation is from 15 minutes to 1 hour, depending on the external temperature and the initial temperature of the tank car boiler with cargo residues.

In the case under investigation, the following input data are taken into account: steaming time is 20 minutes; the temperature of the supplied steam is 160 °C; the external temperature is equal to 20 °C; the temperature of the tank car boiler with cargo residues is 20 °C.

At the first stage, a calculation model of a tank car boiler was created in a modern software computing environment, in natural size (**Fig. 1.4**).

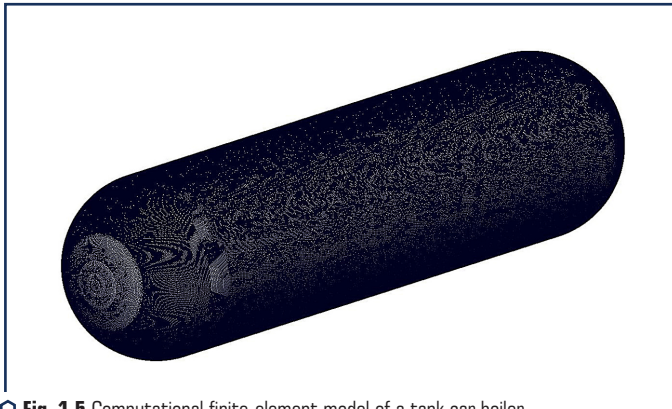
At the same time, the above technical characteristics and requirements for its design are taken into account. Steel O9G2D was chosen as the material. Taking into account the peculiarities of the given task, the loading hatch was not taken into account in the model of the tank car boiler. Fixation of the calculation model is carried out by zonal abutments on the stud nodes, which are given below.



○ Fig. 1.4 Calculated computer model of a tank car boiler

At the second stage, the adequacy of the developed calculation model was adjusted by comparing theoretically (mathematically, based on the method of moment theory of shells) obtained stress values at the control points of the tank car boiler with those determined by computer modeling. Namely, the values were taken in the control locations of the bottoms and the shells. On the basis of the performed tuning, it was found that an adequate calculation model will have the optimal parameters of the finite element mesh presented below. The number of mesh elements was 10 182 768, nodes – 18 655 084. The maximum size of the mesh element is 11 mm, the minimum is 0.55 mm, the maximum aspect ratio of the elements is 41.031, the percentage of elements with an aspect ratio less than three is 99.3, more than ten is 0.0215.

The finite element model of the tank car boiler is shown in **Fig. 1.5**.



○ Fig. 1.5 Computational finite-element model of a tank car boiler

At the next (third) stage of research, temperature analysis was carried out. Temperature loads were applied to all internal faces of the tank car boiler. At the same time, the temperature effect was equal to 160 °C, and the convection coefficient was selected from **Table 1.3**.

● **Table 1.3** The values of the convection coefficient

No.	Average value	Convection coefficient (W/m ² ·K)
1	Air (natural convection)	5–25
2	Air/superheated steam (forced convection)	20–300
3	Steam (condensing)	4 000–20 000

The calculated model with applied temperature loads is shown in **Fig. 1.6**.

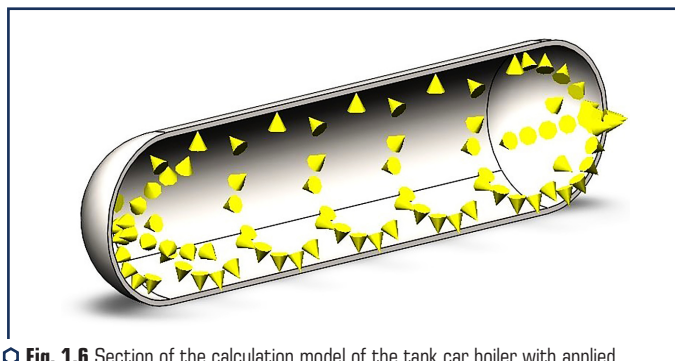
At the fourth stage, the application of loads from the external temperature, which is equal to 20 °C, to the external faces of the calculation model was simulated. At the same time, the convection coefficient was also chosen from **Table 1.3**. The model with applied external temperature loads is shown in **Fig. 1.7**.

Later, the characteristics of the transient process of temperature analysis were specified. Namely, the process time is 20 minutes, and the process step is 1 minute.

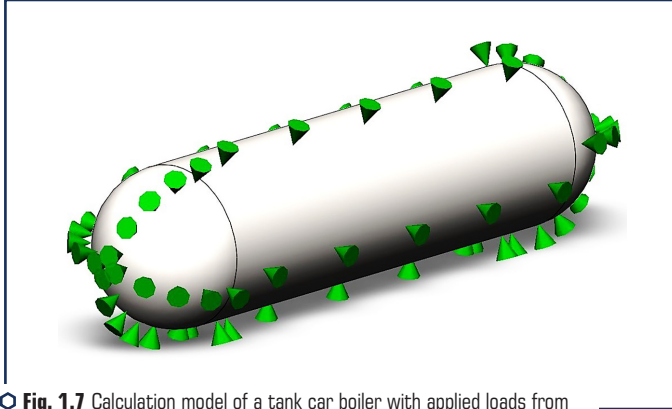
At the fifth stage of the research, the initial temperature of the tank car boiler with cargo remains was set at 20 °C.

The obtained temperature load modeling data made it possible to determine temperature analysis patterns at all 20 calculation steps. At the same time, it was found out that the construction undergoes the greatest temperature effect in the fifth step (**Fig. 1.8**) and is 71.3 °C.

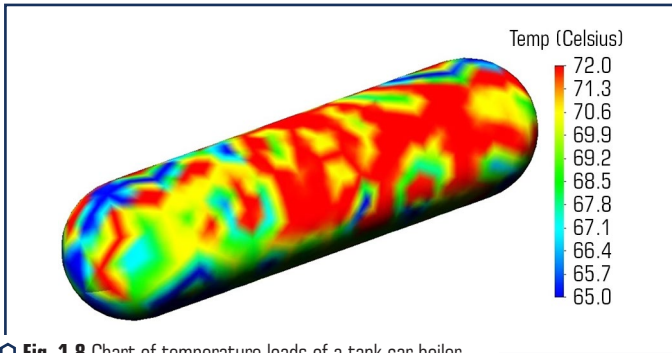
At the sixth stage of research, in order to find out the stress-deformed state of the tank car boiler due to temperature effects, a new study was performed. This is how the calculation model was first attached (**Fig. 1.9**).



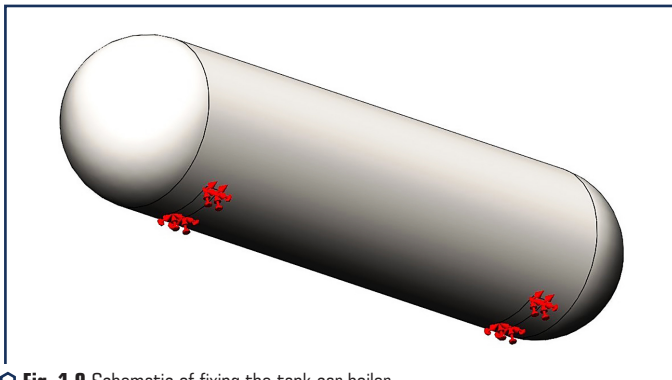
○ **Fig. 1.6** Section of the calculation model of the tank car boiler with applied loads from the action of hot steam



○ Fig. 1.7 Calculation model of a tank car boiler with applied loads from external temperature



○ Fig. 1.8 Chart of temperature loads of a tank car boiler



○ Fig. 1.9 Schematic of fixing the tank car boiler

After that, the previously obtained temperature loads were transferred to be taken into account in static studies. Temperature loads corresponding to the fifth calculation step were chosen as the calculation case. As a result of the calculations, the picture of the stress state due to the action of temperature loads is presented in **Fig. 1.10**.

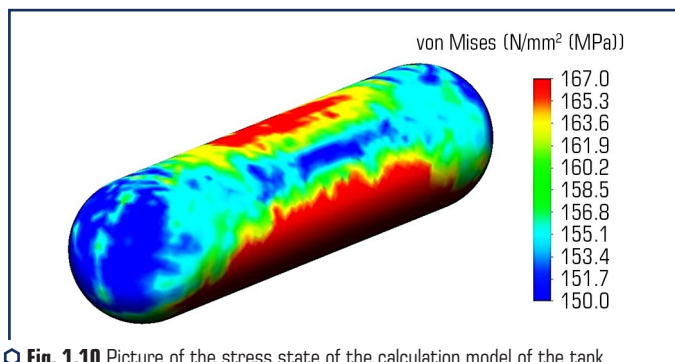


Fig. 1.10 Picture of the stress state of the calculation model of the tank car boiler under the influence of temperature loads

It was found that the maximum stress value is 173 MPa and does not exceed the permissible values.

CONCLUSIONS

The article presents the results of a scientific and applied research on determining the temperature effect on the stressed-deformed state of the tank car boiler during washing and steaming operations.

During the creation of the estimated finite-element model of the tank car boiler, the following basic requirements for its design were taken into account. The quality of welded joints of boilers of tank cars operating under excessive pressure over 0.07 MPa should be tested in accordance with current requirements. The boiler should consist of a shell, two bottoms, a hatch, a hatch for installing a safety inlet valve, and a drain device. The material used for the production of the main elements of the boiler is in accordance with the current regulatory documents. The deviation of the internal diameter of the bottom of the tank car boiler from the nominal should be within the tolerance of ± 6 mm. Bumps, scratches and other defects (pits, sinks, etc.) are not allowed on the surface of the tank car boiler, if their depth exceeds the minus limit deviations provided by the relevant standards or technical conditions for the supply of metal. The deviation from the straightness of the generator tank car boiler should not exceed 2 mm per 1 m of length, but not more than 20 mm over the entire length of the shell, without taking into account the local deviation from straightness in the welds. Local dents and convexities with a height of no more than 5 mm per 1 m

of length are allowed on the body of the tank car boiler, but no more than 2 units on each side of the shell. In the butt welds of the tank car boiler, a joint removal of the edges (inside and outside) is allowed within 10 % of the sheet thickness plus 3 mm, but not more than 5 mm, while the removal of the edges in the longitudinal seams is determined by the template, the length of which (by chord) is equal to 1/3 of the shell radius. The clumsiness of ring seams is determined by a ruler 300 mm long. Longitudinal welds of adjacent shells and bottom welds must be offset relative to each other by at least 100 mm. The main dimensions of tank car boiler bottoms must comply with current regulatory documents, while the reduction in sheet thickness in the bottoms after stamping should not exceed 15 % of the nominal sheet thickness.

The moment theory of shells used and adapted to the given tasks is presented. On the basis of this mathematical theory, the load values at the control points of the tank car boiler are determined. Based on these results, the calculation model built in a modern computer computing and software complex was adjusted. It was calculated using the finite element method and brought to an adequate level.

The developed finite element model includes the optimal number of finite elements and nodes. Tetrahedrons and triangles are used as finite elements. The optimal number of finite elements includes 10 182 768 elements and 18 655 084 nodes.

As a result of the calculations, it was found that with a steam temperature load of 160 °C, the highest stress temperatures in the boiler are 71.3 °C.

The results of the calculations made it possible to establish that the maximum stress values are 173 MPa and do not exceed the permissible values. That is, when washing and steaming operations are carried out, the strength condition is fulfilled.

The obtained results of simulations of temperature loads and the stress-strain states corresponding to them will be useful in conducting further research and development works on the selected topic. In addition, the obtained results and achievements can be used in educational activities in the preparation of students of various levels of education.

REFERENCES

1. Kondratiev, A., Slivinsky, M. (2018). Method for determining the thickness of a binder layer at its non-uniform mass transfer inside the channel of a honeycomb filler made from polymeric paper. *Eastern-European Journal of Enterprise Technologies*, 6 (5 (96)), 42–48. <https://doi.org/10.15587/1729-4061.2018.150387>
2. Kondratiev, A. (2019). Improving the mass efficiency of a composite launch vehicle head fairing with a sandwich structure. *Eastern-European Journal of Enterprise Technologies*, 6 (7 (102)), 6–18. <https://doi.org/10.15587/1729-4061.2019.184551>
3. Kondratiev, A., Gaidachuk, V., Nabokina, T., Kovalenko, V. (2019). Determination of the influence of deflections in the thickness of a composite material on its physical and mechanical

- properties with a local damage to its wholeness. *Eastern-European Journal of Enterprise Technologies*, 4 (1 (100)), 6–13. <https://doi.org/10.15587/1729-4061.2019.174025>
4. Krol, O., Sokolov, V. (2020). Research of toothed belt transmission with arched teeth. *Diagnostyka*, 21 (4), 15–22. <https://doi.org/10.29354/diag/127193>
 5. Sokolov, V., Porkuian, O., Krol, O., Stepanova, O. (2021). Design Calculation of Automatic Rotary Motion Electrohydraulic Drive for Technological Equipment. *Advances in Design, Simulation and Manufacturing IV*. Cham: Springer, 133–142. https://doi.org/10.1007/978-3-030-77719-7_14
 6. Krol, O., Sokolov, V. (2020). Modeling of Spindle Node Dynamics Using the Spectral Analysis Method. *Advances in Design, Simulation and Manufacturing III*. Cham: Springer, 35–44. https://doi.org/10.1007/978-3-030-50794-7_4
 7. Gubarevych, O., Goolak, S., Daki, E., Tryshyn, V. (2021). Investigation of Turn-To-Turn Closures of Stator Windings to Improve the Diagnostics System for Induction Motors. *Problems of the Regional Energetics*, 2 (50), 10–24. <https://doi.org/10.52254/1857-0070.2021.2-50.02>
 8. Gubarevych, O., Goolak, S., Melkonova, I., Yurchenko, M. (2022). Structural diagram of the built-in diagnostic system for electric drives of vehicles. *Diagnostyka*, 23 (4), 1–13. <https://doi.org/10.29354/diag/156382>
 9. Koshel, O., Sapronova, S., Kara, S. (2023). Revealing patterns in the stressed-strained state of load-bearing structures in special rolling stock to further improve them. *Eastern-European Journal of Enterprise Technologies*, 4 (7 (124)), 30–42. <https://doi.org/10.15587/1729-4061.2023.285894>
 10. Muradian, L., Shvets, A., Shvets, A. (2024). Influence of wagon body flexural deformation on the indicators of interaction with the railroad track. *Archive of Applied Mechanics*, 94 (8), 2201–2216. <https://doi.org/10.1007/s00419-024-02633-2>
 11. Okorokov, A., Fomin, O., Lovska, A., Vernigora, R., Zhuravel, I., Fomin, V. (2018). Research into a possibility to prolong the time of operation of universal open top wagon bodies that have exhausted their standard resource. *Eastern-European Journal of Enterprise Technologies*, 3 (7 (93)), 20–26. <https://doi.org/10.15587/1729-4061.2018.131309>
 12. Fomin, O., Lovska, A., Pišták, V., Kučera, P. (2019). Dynamic load computational modelling of containers placed on a flat wagon at railroad ferry transportation. *Vibroengineering Procedia*, 29, 118–123. <https://doi.org/10.21595/vp.2019.21132>
 13. Sagin, S., Kuropyatnyk, O., Sagin, A., Tkachenko, I., Fomin, O., Pišták, V., Kučera, P. (2022). Ensuring the Environmental Friendliness of Drillships during Their Operation in Special Ecological Regions of Northern Europe. *Journal of Marine Science and Engineering*, 10 (9), 1331. <https://doi.org/10.3390/jmse10091331>
 14. Gorobchenko, O., Fomin, O., Gritsuk, I., Saravas, V., Grytsuk, Y., Bulgakov, M. et al. (2018). Intelligent Locomotive Decision Support System Structure Development and Operation Quality Assessment. 2018 IEEE 3rd International Conference on Intelligent Energy and Power Systems (IEPS). Kharkiv, 239–243. <https://doi.org/10.1109/ieps.2018.8559487>
-

15. Sulym, A. O., Fomin, O. V., Khozia, P. O., Mastepan, A. G. (2018). Theoretical and practical determination of parameters of on-board capacitive energy storage of the rolling stock. *Naukovyi Visnyk Natsionalnoho Hirnychoho Universytetu*, 5, 79–87. <https://doi.org/10.29202/nvngu/2018-5/8>
16. Fomin, O., Sulym, A., Kulbovskiy, I., Khozia, P., Ishchenko, V. (2018). Determining rational parameters of the capacitive energy storage system for the underground railway rolling stock. *Eastern-European Journal of Enterprise Technologies*, 2 (1 (92)), 63–71. <https://doi.org/10.15587/1729-4061.2018.126080>
17. Melnyk, O., Onyshchenko, S., Onishchenko, O., Lohinov, O., Ocheretna, V. (2023). Integral Approach to Vulnerability Assessment of Ship's Critical Equipment and Systems. *Transactions on Maritime Science*, 12 (1). <https://doi.org/10.7225/toms.v12.n01.002>
18. Melnyk, O., Onishchenko, O., Onyshchenko, S., Golikov, V., Sapiha, V., Shcherbina, O., Andrievska, V. (2022). Study of Environmental Efficiency of Ship Operation in Terms of Freight Transportation Effectiveness Provision. *TransNav, the International Journal on Marine Navigation and Safety of Sea Transportation*, 16 (4), 723–729. <https://doi.org/10.12716/1001.16.04.14>
19. Melnyk, O., Onyshchenko, S., Onishchenko, O., Shumylo, O., Voloshyn, A., Koskina, Y., Volianska, Y. (2022). Review of Ship Information Security Risks and Safety of Maritime Transportation Issues. *TransNav, the International Journal on Marine Navigation and Safety of Sea Transportation*, 16 (4), 717–722. <https://doi.org/10.12716/1001.16.04.13>
20. Fomin, O., Lovska, A., Pištěk, V., Kučera, P. (2019). Dynamic load effect on the transportation safety of tank containers as part of combined trains on railway ferries. *Vibroengineering Procedia*, 29, 124–129. <https://doi.org/10.21595/vp.2019.21138>
21. Sapronova, S., Tkachenko, V., Fomin, O., Hatchenko, V., Maliuk, S. (2017). Research on the safety factor against derailment of railway vehicleless. *Eastern-European Journal of Enterprise Technologies*, 6 (7 (90)), 19–25. <https://doi.org/10.15587/1729-4061.2017.116194>
22. Lovska, A., Fomin, O., Kučera, P., Pištěk, V. (2020). Calculation of Loads on Carrying Structures of Articulated Circular-Tube Wagons Equipped with New Draft Gear Concepts. *Applied Sciences*, 10 (21), 7441. <https://doi.org/10.3390/app10217441>

Oleksij Fomin, Pavlo Prokopenko, Mariia Miroshnykova, Gregori Boyko, Andriy Klymash
© The Author(s) 2024. This is an Open Access chapter distributed under the terms of the CC BY-NC-ND license

CHAPTER 2

STUDY OF SAFETY INDICATORS AND TECHNICAL CONDITION OF ROLLING STOCK BY MOBILE SYSTEMS

ABSTRACT

The organization of the movement of freight trains in Ukraine is an important factor in the integration of the country's railway transport into the European system. Currently, a situation has arisen that requires a significant renewal of the freight car park with modern cars to meet the requirements of freight transportation. Also, a significant drawback of railway transport of Ukraine is the limitation of the speed of trains, which include freight cars with a reduced container in an empty state, therefore, at the moment, the issue of improving the methodological and software and instrumental testing tools for evaluating the quality and safety indicators of the movement of such cars is relevant at the moment.

Subsection 2.1 offers methods and approaches for assessing quality indicators, traffic safety, and the technical condition of cars. The first method of measuring mechanical stresses in the surface layers of elements of load-bearing structures of rolling stock by the method of tensometry. The second method of measuring contact forces: due to the deformation of the discs of the wheels of the wheel pairs.

Subsection 2.2 proposes a method of in-depth processing of the results of road tests of rolling stock is proposed. The essence is to perform a spectral analysis of dynamic processes for various elements of the load-bearing structures of the freight car, with the aim of identifying the relationships between the oscillatory processes of the load-bearing structures and the frequencies at which the interaction between them occurs.

Subsection 2.3 forms and implements the general requirements for the mobile system for determining the quality and safety indicators of the movement of freight cars with reduced containers in operation were formed and implemented. This mobile system allows running tests without involving the laboratory car, which reduces costs and time for conducting such tests by 25.8 %. A method of in-depth processing of the results of road tests of rolling stock is proposed.

Subsection 2.4 formulates the general requirements for the software and hardware complex for determining the dynamic load of running parts under the conditions of operation of rolling stock. Technical solutions have been implemented regarding the means of running tests of rolling stock to determine the dynamic loading of running parts in operating conditions, which increases the effectiveness of forecasted assessments and increases the efficiency of testing.

A set of software subsystems for collecting measurement information, determining movement smoothness and safety indicators of rolling stock according to simplified schemes has been developed.

KEYWORDS

Freight cars, running tests, traffic quality and safety indicators, dynamic processes, stability, mobile system, dynamics, software.

The organization of the movement of freight trains in Ukraine is a key aspect of the integration of the country's railway transport into the European system. Today, there is a need for a significant renewal of the fleet of freight cars with modern models in order to meet the requirements of freight transportation. One of the serious shortcomings of railway transport in Ukraine is the limitation of the speed of movement of trains containing cargo cars with reduced containers in an empty state. This makes the issue of improving methodological and software, as well as instrumental means for tests that evaluate the indicators of the quality and safety of the movement of such cars, urgent. As a result of their unsatisfactory movement dynamics, certain groups of freight cars, such as platform cars, are limited to a speed of up to 60 km/h, which negatively affects the overall speed of freight transportation by rail.

In recent years, rail transport has been rapidly developing and integrated into the high-speed rail system. The safety of train operation is becoming a more acute issue. To assess the safety quality of the movement of cars, locomotives and other types of rail rolling stock, there are various approaches to assessing safety conditions and solving this problem.

In [1], the results of the study and establishment of the mechanism of interaction between a railway wheel and a rail are given. The modeling is based on the fundamental theory of circular motion kinematics. The proposed method makes it possible to determine the characteristic criteria of the kinematics of the interaction of the cross-section of the tire of the wheel pairs of the rolling stock with the lateral sides of the rail heads. However, the work does not describe the process of interaction between the railway wheel and the rail from the point of view of traffic safety.

The paper [2] presents a theoretical basis for modeling the interaction of a railway car and a track, in which the dynamic equations of motion of car-track systems are built by effectively connecting linear and nonlinear dynamic characteristics. The result of this study is the determination of the critical speed of a railway train and the localization of track irregularities through the effective integration of a dynamic modeling model, a probabilistic model of track irregularities and a time-frequency analysis method. But the work does not consider the possibility of developing a mobile system for determining the indicators of the interaction of a railway car and a track based on the conducted research.

The authors of the paper [3] investigate the longitudinal forces acting on a railway car for different loading conditions of the cars in the train. Three different types of cars are considered

in the work, namely fully loaded, partially loaded and empty cars. The purpose of this work is to determine the best place for their location in a freight train where the smallest longitudinal forces occur, regardless of the car loading scheme. However, the work does not assess the influence of horizontal forces on the railway car, which significantly affect the safety of the movement of railway cars.

The article [4] presents a study of the descent of freight cars in symmetric turnouts No. 6. A dynamic model of a semi-car and a model of a flexible turnout that undergoes derailment when the wheel flange is lifted is presented. In addition, a full-scale wheel-rail interaction test was conducted to verify the dynamic model. As a result of the simulation of derailment when lifting, the wheels are consistent with the research data, and the safety of the cart depends on the condition of both the front and rear wheels.

In the article [5], the authors present the concept of a smart railway car modeled from smart components. This concept can meet the safety requirements of a complex railway system. Adding self-diagnostic features to a rail car reduces the risk of accidents. This paper also presents the concept and functional model of this railway car and illustrates the utility of this concept based on investigated railway accidents.

The study [6] describes the behavior of dynamic derailment caused by the failure of rail connections of a railway switch, as well as the assessment of the impact of such parameters on the safety of train operation. The developed model takes into account the transverse difference between the sections of the rail connection, which directly cause the wheel lift. The conducted research indicates that the proposed derailment model is able to effectively assess operational safety as a result of various wheel and track defects, and thus provide a basis for providing a cost-effective platform for future optimization of railway track and rolling stock parameters.

In [7], the authors study the influence of gaps between the blocks, changes in the wheel-rail friction coefficient, and the radius of the track curve on the nonlinear critical speed of a railway vehicle. The effect of the gaps between the axle boxes on the wear of the wheels and the interaction of the wheels with the railway track was also investigated.

The paper [8] describes the dynamic behavior of the wheel-rail interaction under various surface contaminations of the rail track using the methodology of experimental and numerical modeling. The results of the study showed that the wheel-rail creep force drops sharply when the wheel enters the low adhesion zone, and when the adhesion is restored, there is a sudden increase in the creep force, which negatively affects the dynamics of the railway car.

In the study [9], a refined wheel-rail contact formula was proposed for the analysis of nonlinear train-track interaction, which takes into account the geometry of the wheel and rail. While most of the existing methods consider contact forces as external forces, the work uses modeling of the behavior of the contact surface based on Hertz's theory and Kalker's laws. The proposed refined mathematical model is confirmed by experimental data.

In the article [10] three-dimensional numerical modeling of the moving load of the wheel-rail interaction for high-speed and heavy trains is investigated. Simulations were performed in ANSYS

with a hybrid model involving a flexible wheel pair moving on a pair of rigid rails, which helped in estimating the frictional stresses at the wheel-rail interface during train motion. As a result of the work, it was found that contact pressure and frictional stress increase quadratically with increasing train speed.

In the article [11], the authors proposed a three-dimensional (3-D) model of train-track interaction. As a result of the study of the developed dynamic model, it was found that this model demonstrates high computational stability, accuracy and efficiency in comparison with traditional solutions; in addition to some key parameters such as bridge element length, the length of the track and bridge section in numerical integration can be conveniently refined using this model.

In the paper [12], the authors develop a dynamic model for studying the vertical interaction of the rail track and the car system. The developed model is verified using several test data and other numerical models.

In the article [13], the authors present an analysis of the influence of creep paths on the contact forces of the wheel and rail. The simulation results showed that the maximum normal wheel-rail contact stresses are less than 1600 MPa in the range of typical conditions of normal operation.

The article [14] presents the features and results of the cataloging of the supporting system of semi-cars, the application of this approach for the end wall of one of the basic models of cars.

In work [15], the authors describe the problem of various deformations at all stages of operation of freight cars. The main type of these deformations are residual deformations that occur during welding as a result of thermal exposure.

The authors of the article [16] describe the process of conducting control tests of tank cars for dangerous goods. The testing methodology described in this work was used during the research.

In the article [17], the author highlights the results of work on determining ways to increase the degree of ideality of freight cars and forecasting the evolution of the chassis of new generation cars. Review of examples of application of the idealistic strategy of improving the undercarriage of railway universal freight semi-cars.

In [18], the authors describe a method of increasing the efficiency of the braking system by controlling the cooling of the friction surfaces using adaptive air supply; a mathematical model of air pressure supply to the friction contact of the brake was created in order to obtain the optimal diameter of the holes of the friction linings and the speed of air supply.

In work [19], the authors present the features of mathematical modeling of the dynamic load of containers placed on the platform during a maneuvering collision. Numerical values of accelerations acting on the container are determined. The results are confirmed by computer simulation. The developed models are tested according to the F-criterion.

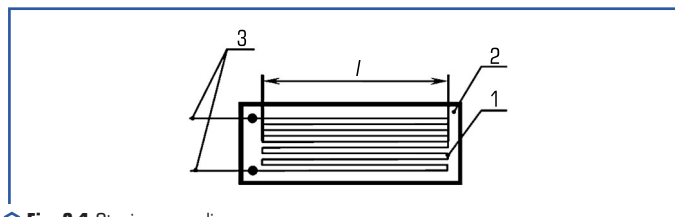
Based on the results of the analysis of literary sources [1–19], it can be concluded that the issue of direct measurement of the forces of interaction of wheel pairs with rails using the measurement of wheel deformations at control points is relevant and requires research.

2.1 METHODS AND APPROACHES FOR EVALUATING INDICATORS OF QUALITY, TRAFFIC SAFETY AND TECHNICAL CONDITION OF CARS

2.1.1 MEASUREMENT OF DEFORMATIONS OF LOAD-BEARING STRUCTURES. GENERAL INFORMATION

To measure the mechanical stresses in the surface layers of the elements of the load-bearing structures of the rolling stock, the methods and means of strain measurement are used, that is, strain gauges and recording equipment. The operation of the strain gauge is based on the tensor effect of the conductor or semiconductor, which is attached to the surface of the supporting element of the structure with a special glue. Thus, deforming together with the metal element when it is loaded, the strain gauge changes its electrical resistance.

Strain gauges are divided into wire, foil and semiconductor tensors by design. The wire strain gauge schematically shown in **Fig. 2.1**, is a wire spiral 1 placed between two layers of thin paper 2. Terminals 3 are soldered to the spiral for connecting strain gauges to each other in an electrical circuit. Constantan (copper and nickel alloy) or nichrome (nickel and chromium alloy) wire is used for strain gauges. The diameter of such a wire is 0.015...0.025 mm.



○ **Fig. 2.1** Strain gauge diagram

Foil strain gauges are made by etching or stamping from Constantan foil fixed on a film or paper base. Semiconductor strain gauges are made of semiconductor materials in the form of thin strips of germanium or silicon with soldered metal terminals. Such strain gauges have a sensitivity 1–2 orders of magnitude higher than wire or foil ones.

The main characteristics of strain gauges are nominal resistance R , base l and sensitivity γ . The sensitivity of the strain gauge is defined as the ratio of the relative change in resistance to its relative elongation:

$$\gamma = \frac{\frac{\Delta R}{R}}{\varepsilon}, \quad (2.1)$$

where ΔR – the change in resistance of the tensor when it is deformed; ε – the relative elongation of the conductor.

The change in resistance of the strain gauge during deformation is very small, usually of the order of several hundreds of Ohms. One of the most convenient means of measuring such changes is the Wheatstone bridge. It includes four resistors connected to a DC power supply, as shown in **Fig. 2.2**.

If $R_1=R_2=R_3=R_4$, this indicates that the bridge is balanced, and the voltmeter connected to the measuring diagonal of the bridge will show 0 V. The principle of operation of the bridge circuit is that the electric current flowing through the resistors in the case unbalanced state of the bridge creates a potential difference in the measuring diagonal, and an electric current will flow through the measuring device.

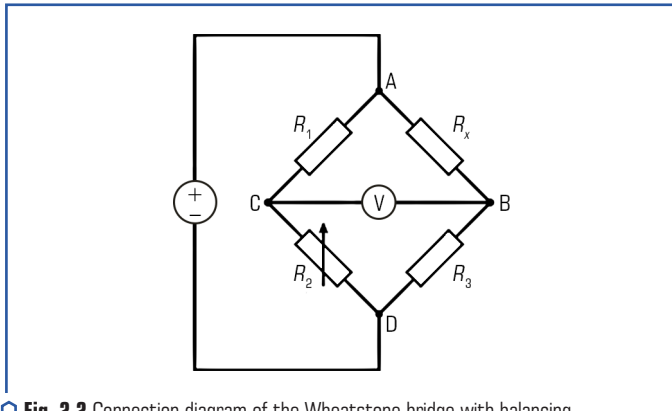


Fig. 2.2 Connection diagram of the Wheatstone bridge with balancing

In order to measure the voltage, the resistors shown in **Fig. 2.2**, are replaced by one or more strain gauges (which are usually variable resistors whose resistance changes with a change in voltage). At the beginning of the test, a balancing potentiometer is used to balance the bridge, setting 0 V on the voltmeter. Applying a test load will change the resistance of the strain gauge and bring the bridge out of balance, producing a voltage proportional to the applied voltage.

The bridge can contain one, two, or four strain gauges according to the schematics, such a configuration is known as one-fourth, half-bridge, and full-bridge, respectively. Of these three schemes, one fourth of the bridge will have the lowest sensitivity. Failure to take precautions can lead to errors because strain gauges are sensitive to thermal effects. In order to prevent this, one of the strain gauges adjacent to the active one can be replaced by a so-called compensation one. This strain gauge is identical to the active one, is in the same ambient conditions, but is not subjected to the load, which is achieved, for example, by installing it on an unstressed part of the object under test. Both strain gauges are subjected to the same temperature changes, and as a result, the effect of any resulting effect on the balance of the bridge due to thermal effects is canceled out.

A half bridge will have a higher sensitivity than a quarter bridge because the additional strain gauge will produce a larger unbalanced voltage across the Wheatstone bridge. The presence of two active strain gauges also excludes any thermal effects as described above. Of the three schemes, the full bridge has the highest sensitivity. In addition, it is self-compensating for temperature changes.

It should be noted that the changes in the output voltage from bridges for measuring mechanical stresses are usually very small and therefore need to be amplified as close to the bridge as possible. Cable lines must be fully enclosed and shielded to prevent distortion of test data.

When measuring the deformation of the surface of the wheel disc, a statistical method was adopted to estimate the measurement error with a probability of $P=0.95$. The deformation ε_i , measured by the device under a unit load is determined by the formula:

$$\varepsilon_i = \frac{\rho \cdot \bar{U}_{out}}{K \cdot U_{sup}}, \quad (2.2)$$

in which

$$\bar{U}_{out} = \frac{1}{n} \sum_{i=1}^n U_{i out},$$

where $\rho=2$ – for a half-bridge circuit; U_{sup} – voltage of the measuring system supply, V; \bar{U}_{out} – average value of the output voltage, mV; K – coefficient of tensile sensitivity (1.9–2.04).

The average arithmetic value of deformations is determined by the formula:

$$\bar{\varepsilon} = \frac{\sum_{i=1}^n (\varepsilon_i)}{m}, \quad (2.3)$$

where m – the number of measurement points.

The mean square deviation of the measurement results $\tilde{\sigma}(\dot{\Delta})$ is determined by the formula:

$$\tilde{\sigma}(\dot{\Delta}) = \sqrt{\frac{\sum_{i=1}^n (\bar{\varepsilon} - \varepsilon_i)^2}{m(m-1)}}. \quad (2.4)$$

The sum of random and non-excluded systematic errors is determined by the formula:

$$\sigma(\Delta) = \sqrt{\tilde{\sigma}(\dot{\Delta})^2 + \tilde{\sigma}_1(\Delta_s)^2 + \tilde{\sigma}_2(\Delta_s)^2}, \quad (2.5)$$

where $\tilde{\sigma}_1(\Delta_s)$ – non-excluded remainder of the systematic error caused by the error of the measuring system; $\tilde{\sigma}_2(\Delta_s)$ – non-excluded remainder of the systematic error due to the error of the strain gauges.

The upper $\tilde{\Delta}_h$ and lower $\tilde{\Delta}_l$ limits of the measurement error are determined by the formula:

$$\tilde{\Delta}_h = \tilde{\Delta}_l = t_p \sigma(\Delta), \quad (2.6)$$

where t_p – the Student coefficient, which depends on the number of measurements and the given probability [20, 21].

2.1.2 MEASUREMENT OF FORCES BY LOCAL DEFORMATIONS OF CART FRAMES

Strain gauge bridges are widely used when conducting static strength and dynamic running tests of rolling stock. For example, the method of determining vertical and horizontal transverse (frame) forces acting on wheel pairs, according to the rules that are currently in force on railways with a gauge of 1520 mm, involves the measurement of deformations of cart frames.

Strain gauges are pasted on the outer and inner sides of the side frames and assembled into schemes that, as a rule, have good sensitivity with sufficient compensation for temperature deformations. This method allows to continuously measure horizontal (frame) and vertical forces when moving along a track section of any length.

The characteristics of the force action measured in this way in the "cart frame – wheelset" system are calculated using the calculation method to estimate the forces of interaction between the wheels and the rails, the ratio of which determines the so-called reserve coefficient of stability of the wheel from leaving the rail [22–24].

2.1.3 MEASUREMENT OF FORCES OF DIRECT INTERACTION OF WHEELS WITH RAILS

One of the important aspects in the system of direct measurement of the forces of the contact interaction between wheels and rails is the determination of the zones of deformation sensitivity on the wheel disks from the action of vertical and lateral forces. From the determined zones, it is important to localize those in which the deformations were the result of the action of forces in one direction.

To carry out calculations of the stress-strain state of the wheel pair using the finite element method, 3D models of individual elements of the wheel pair and P65 type rails were created in the SolidWorks software package, from which a general 3D model of the wheel pair installed on the rails was created.

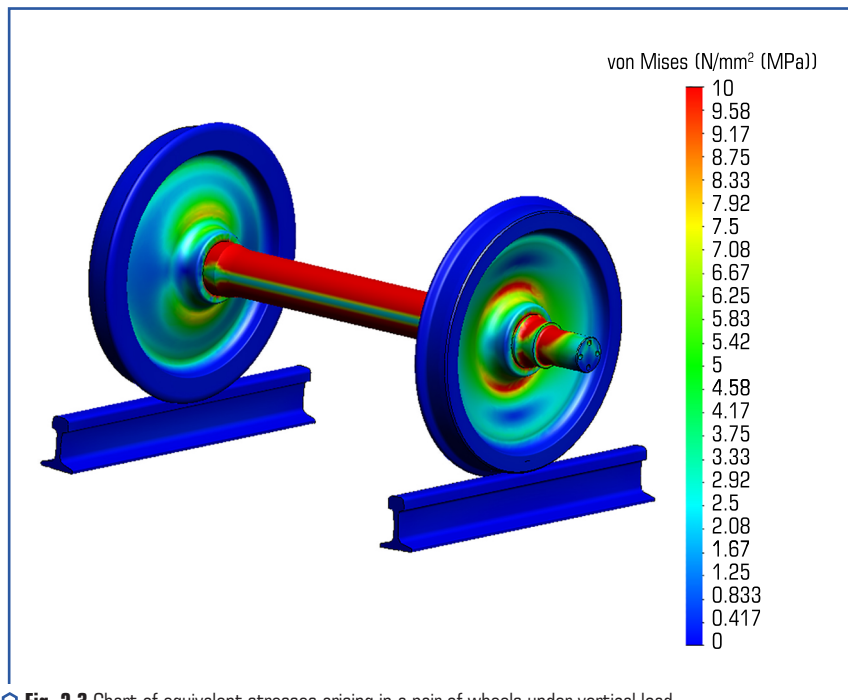
To determine these zones, a finite element calculation was performed for three calculation schemes:

- a) vertical load of the wheel pair;
- b) loading by vertical forces and forces from the action of the tare system;
- c) loading of the wheel pair by vertical and horizontal forces when passing curved sections of the track.

Below are the results of the characteristic calculations for the specified load patterns of the wheel pair.

Vertical load. Based on the task of the research, in order to ensure greater visibility of the results, the maximum value in the chart legend was reduced to 10 MPa, since these are the stresses that occur on the wheel disc.

Fig. 2.3 shows a picture of the distribution of calculated stresses in the elements of a wheel pair under the action of a vertical load. As can be seen, the greatest stresses occur in the wheel disc at the point of transition of the disc to the hub part of the wheel and amount to 7.78 MPa, as well as in the hub transition between the neck and the hub part – 46 MPa.



○ **Fig. 2.3** Chart of equivalent stresses arising in a pair of wheels under vertical load

In the axis of the wheelset, which mainly works in bending, the stresses in the cross sections are unevenly distributed, reaching the largest values in the outer fibers and the smallest in the inner fibers, as shown in **Fig. 2.4**.

Fig. 2.5 presents a chart of equivalent stresses, from which it can be seen that when simulating the action of the tare device, the greatest stresses occur in the places between the hub part and the disk and amount to 10.49 MPa.

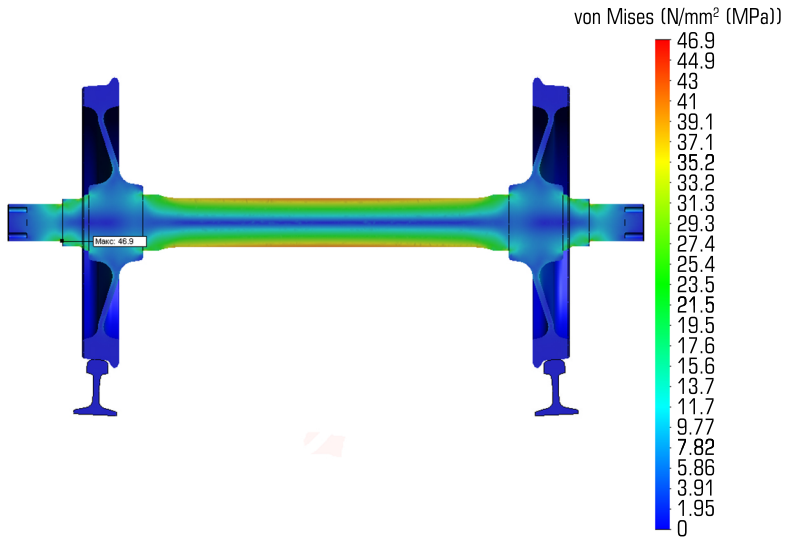


Fig. 2.4 The chart of equivalent stresses arising in a pair of wheels (in cross-section)

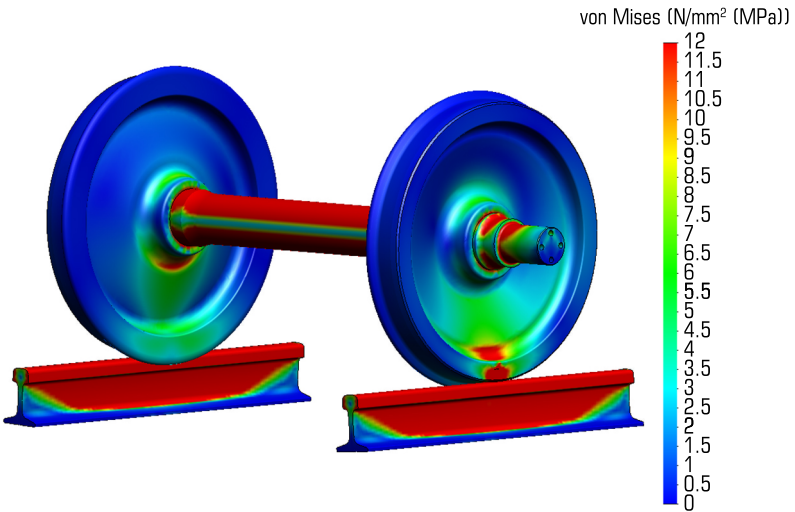


Fig. 2.5 The chart of equivalent stresses arising in a pair of wheels when loaded with a tare device

Fig. 2.6 presents a chart of equivalent stresses, from which it can be seen that when simulating the action of a lateral load, the greatest stresses occur in the places between the hub part and the disk and are equal to 12 MPa.

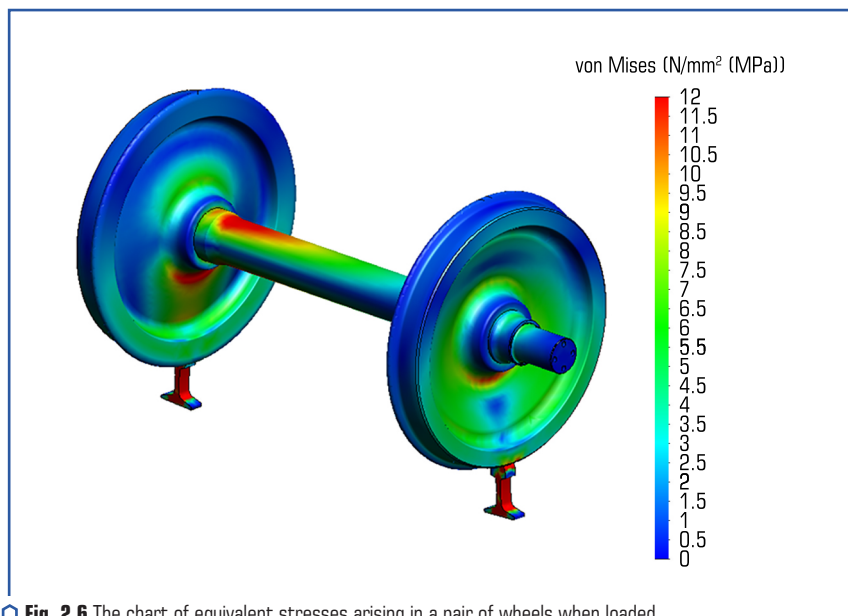


Fig. 2.6 The chart of equivalent stresses arising in a pair of wheels when loaded with vertical and lateral loads

Thus, the most sensitive zone is the zone of the wheel disc at the point of transition of the disc to the hub part of the wheel, but it is also the most sensitive to vertical load. Therefore, to measure the lateral load, it is possible to choose the zone between the hub part and the disk, which is practically sensitive only to lateral forces, and to measure the vertical load, choose the zone in the zone of the rim of the wheel disk [25].

Places of strain gauges on the disc of a wheel pair and methods of their inclusion in the measuring scheme should be such that, with sufficient sensitivity of the scheme to the measured force, influence on the scheme of the force of the other direction is excluded.

Thus, for separate registration of the forces acting on the wheel pair, it is necessary to determine the places of the strain gauges, each of which is sensitive only to the force acting in one direction.

To determine the sensitive zones of action of the vertical and lateral load on the wheel, a diagram of the arrangement of strain gauges (**Fig. 2.7**) and the coordinates of the location of the strain gauges on the wheel of the measuring wheelset was developed. The distance between strain gauges sensitive only to horizontal or only to vertical forces is approximately 55 mm [26].

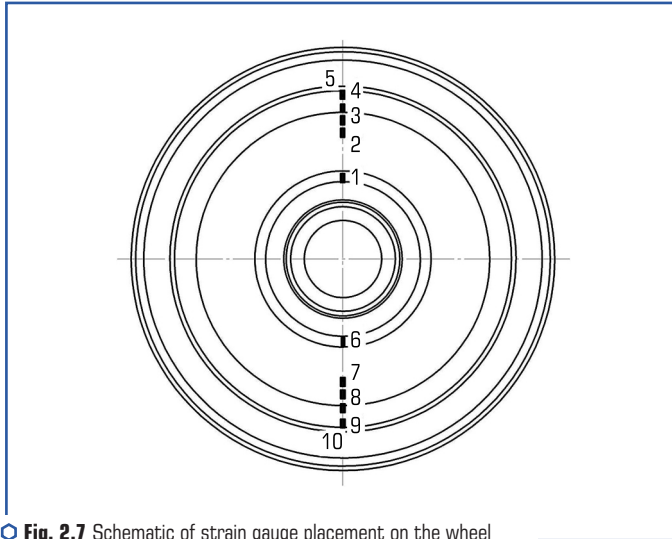


Fig. 2.7 Schematic of strain gauge placement on the wheel of the measuring wheelset

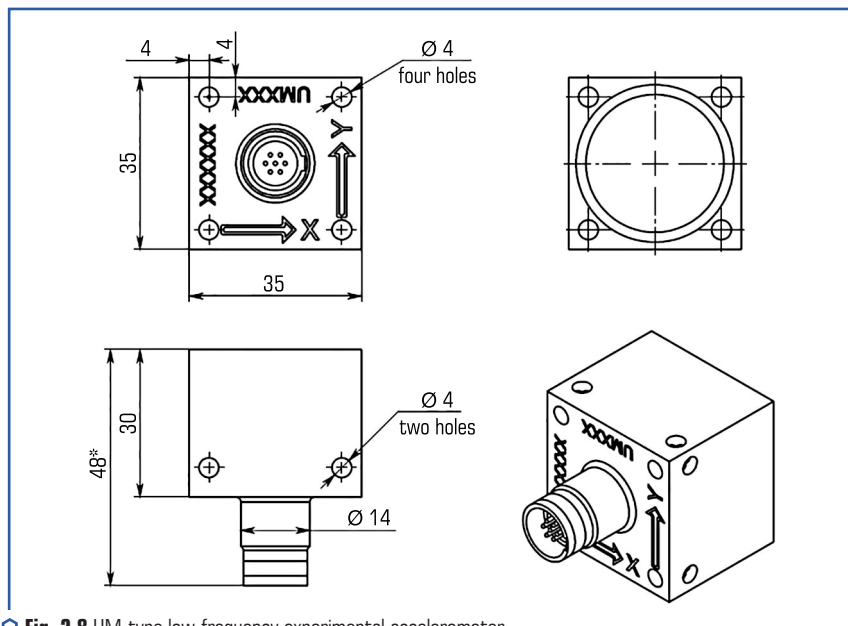
2.1.4 MEASUREMENT OF DYNAMIC INDICATORS OF ROLLING STOCK

In order to measure and evaluate the dynamic load of the crew part of the rolling stock, UM-type low-frequency experimental accelerometer was developed. In order to use this accelerometer for measuring accelerations on rolling stock, a cubic body was developed. The choice of this design of the accelerometer body is determined by its ease of use. It consists of a case, a cover, a circuit board and an electrical connector, as well as fasteners (magnet, bolts, washers, nuts).

The case has a cut-out in which the board with the ADXL 278 microcircuit is placed on one side and the electrical connector is installed on the other. The cover and the electrical connector are filled with epoxy glue. The general view of the accelerometer is shown in **Fig. 2.8**.

The measured accelerations can be used as indicators of the quality of the track geometry and to detect local geometric deviations affecting the dynamic behavior of the rolling stock. These measurements should be used in conjunction with basic parameter measurements.

Measurement of accelerations should be carried out in specified places on the body and carts, depending on the need for a specific assessment. Thus, the vertical accelerations of the boxes are measured to detect defects on the rail surfaces and isolated geometric irregularities. Transverse accelerations of the cart are measured to detect short-wave irregularities. According to the lateral and vertical accelerations of the body, track defects affecting the dynamics of the rolling stock are revealed.



○ **Fig. 2.8** UM-type low-frequency experimental accelerometer

The sampling frequency should be at least 2.5 times higher than the cutoff frequency applied to the signal. Measurements of the accelerations of the carts and the body should be performed in the working range of movement speeds for the line within the tolerance of $\pm 10\%$.

In order to measure displacements and evaluate dynamic qualities, cable displacement sensors are used. Cable sensors measure linear displacement using a steel cable that is connected to a sensing element that converts the cable's displacement into a linear output signal [27, 28].

2.2 IMPROVEMENT OF MEANS AND APPROACHES FOR ASSESSING SAFETY INDICATORS AND TECHNICAL CONDITION OF FREIGHT CARS

2.2.1 MATHEMATICAL SUPPORT FOR DETERMINING SAFETY INDICATORS AND TECHNICAL CONDITION OF FREIGHT CARS

The software for evaluating the received experimental data of movement quality indicators was developed in the LabView software shell.

The LabView software system implements the process of in-depth processing of the results of running dynamic tests to identify relationships between the vibrational processes of load-bearing

structures, estimate the frequencies at which the interaction between them occurs and the levels of interaction.

The above-mentioned processing of the test results consists in performing a correlation and spectral analysis of the processes investigated for various elements of the load-bearing structures. The values measured during the tests are compiled into a multidimensional time series $X(t) = [x_1(t)/x_p(t)]$, in which each line $X_p(t) = [x_{p1} \dots x_{pn} \dots x_{pN}]$ is a one-dimensional series one measuring channel.

Fig. 3.1, a, b shows the block diagram of the developed software for evaluating the received experimental data of traffic quality indicators and consists of 5 main blocks.

In block 1, the input parameters for processing the results are specified and the location of the resulting file creation is specified.

In block 2, primary data of binary form is read from primary files. Data conversion from binary to text and numeric.

In block 3, the array of data used in further work is defined (so many values of strain gauges, accelerometers, GPS are obtained). The number of received GPS values is determined in relation to the number of values received from tensors and accelerometers, an array of values is formed that come to one GPS value.

In block 4, the array of data is filled that meets the previous requirements for processing in block 1: speed ranges, the number of values per range, etc.

In block 5, the resulting file based on the accumulated array of data in block 4 is written in text form and represents an oscillogram (**Fig. 2.9**).

Next, the resulting file must be filtered with a linear digital filter.

A specialized software module in the LABVIEW software shell is used to estimate the smoothness index of rolling stock.

The software module is a finished application, the input data of which are the digitized oscillograms received from the acceleration sensors and registered by the software hardware recorder based on the programmable controller after initial processing.

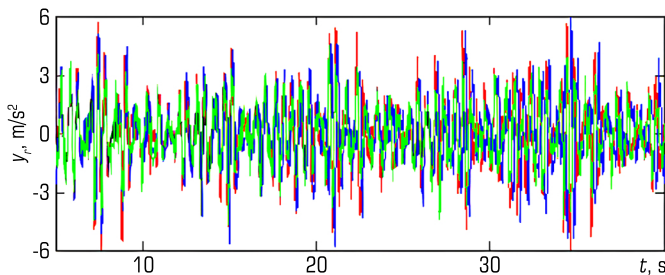


Fig. 2.9 An example of an oscillogram of the resulting file from the measurement of the cart accelerations

The result is the smoothness index value W for the input registration.

The algorithm of the application is as follows.

The size of the input block for calculations is determined. The size of the input block is determined by the base number.

Using the built-in function of LABVIEW, the Fourier transform is performed to construct the power spectrum.

On the basis of the Fourier transformation, frequency arrays and a data array are built in a given frequency range from 0.5 Hz to 20 Hz.

The values of the normalized amplitude-frequency characteristic of the correction filter $q_n(f)$ are calculated according to the formula:

$$q_n(f) = 1.15f \sqrt{\frac{(1 + 0.1f^2)}{(1 + 4.04f^2)((1 + 0.0364f^2)^2 + 0.045f)}} \quad (2.7)$$

The final smoothness index W_j for the input array is calculated according to the formula [29]:

$$W_j = \alpha \cdot \tilde{a}_{kj}^{0.3}, \quad (2.8)$$

where $\tilde{a}_{kj}^{0.3}$ – the mean square value of vibration accelerations at the output of the correcting filter, m/s^2 ; $\alpha = 4.346$ for vertical oscillations [29]; $\alpha = 4.676$ for horizontal (transverse) oscillations [29].

The Butterworth digital filter function of the LABVIEW software shell is used to evaluate safety indicators and quality of rolling stock movement.

The transfer function of the Butterworth filter is given below:

$$K(\omega) = \frac{1}{\sqrt{1 + \left(\frac{\omega}{\omega_0}\right)^{2n}}}, \quad (1.9)$$

where ω_0 – the cutoff frequency (it is 1 rad/s); n – the filter order.

The transmission coefficient at 0 is often 1, at the cutoff frequency, regardless of the order of the filter, it is $1/\sqrt{2} = 3$ dB. At ω , which approaches ∞ , the amplitude-frequency characteristic approaches zero. The amplitude-frequency characteristic of the Butterworth filter is maximally flat at $\omega = 0$ and $\omega = \infty$. In general, the amplitude-frequency characteristic decreases from 1 to 0 when the frequency changes from 0 to ∞ (**Fig. 2.10**) [30–32].

Fig. 2.11 shows the results of filtering a signal using a Butterworth filter, obtained from an accelerometer located on the shouldered part of a car that was moving at a speed of 70 km/h.

Filtering the recorded accelerometer signal with a Butterworth filter provides a filtered signal that is used for the movement smoothness metric.

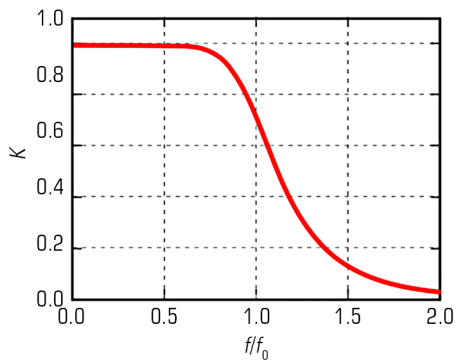


Fig. 2.10 Characteristics of the Butterworth filter

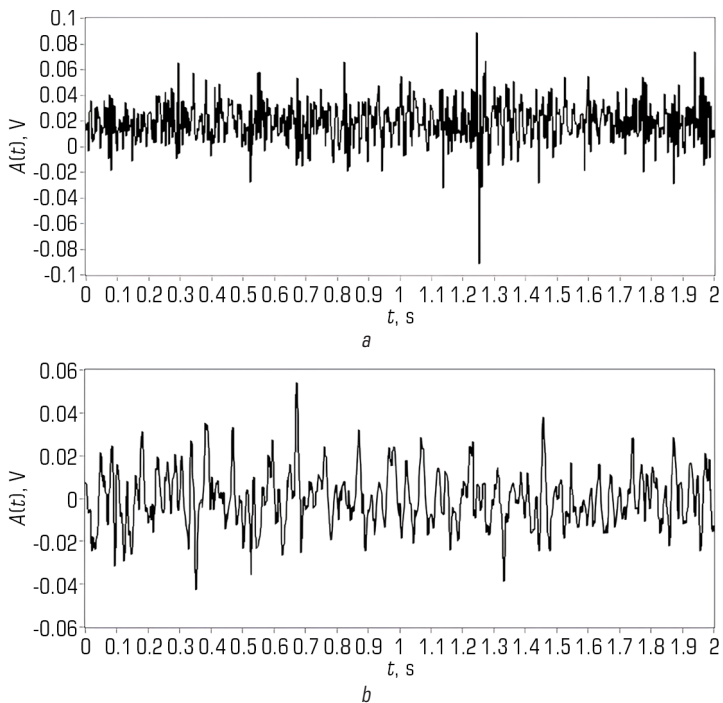


Fig. 2.11 Example of filter operation: *a* – before filtering; *b* – after filtering

2.2.2 SOFTWARE FOR COLLECTING AND REGISTERING SAFETY INDICATORS AND TECHNICAL CONDITION OF CARS

The software of the data collection and registration system performs registration, storage and visualization of changes in information channels (accelerometers, strain gauges). GPS module readings are used to analyze the influence of movement speed on the change of research parameters.

Fig. 2.12 shows a block diagram of the system for collecting and registering measured parameters.

A chassis for 8 modules with a built-in programmable logic device (PLD) and two universal 9205 ADC modules with a maximum sampling frequency of 250 kHz and five 9237 strain gauge modules with a maximum frequency of 50 kHz per channel, a GPS signal receiver module.

Thanks to the built-in PLD, CompactRIO has the ability to implement measurement data processing algorithms at the hardware level with a deterministic execution time of 25 ns without transferring the load to the central processor of the controller. A typical CompactRIO setup includes a controller with a PharLab or VxWorks real-time operating system, a chassis, and I/O modules. The chassis carries the PLD core, is directly connected to universal or specialized input-output modules that have built-in means of matching and processing information signals. There are different chassis models that have different numbers of module slots and differ in the characteristics of the PLD chips.

The developed collection subsystem ensures the operation of the CompactRIO controller.

Thanks to its autonomy, hardware and mass-dimensional characteristics, as well as the ability to work in adverse conditions, CompactRIO can be used to solve a wide range of tasks related to the collection of measurement information and process management.

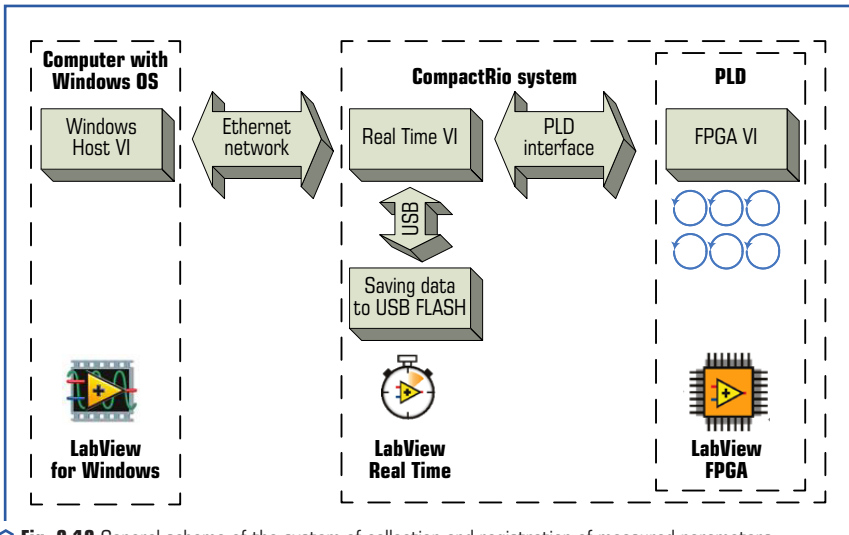


Fig. 2.12 General scheme of the system of collection and registration of measured parameters

Most of the software for CompactRIO is developed according to a scheme that provides for its conditional separation into three levels: a virtual instrument HOST VI on a control PC with a Windows OS, an RT VI on a controller with a real-time OS, and an FPGA VI on a PLD that does not have its own OS, since the logic of the program was implemented directly at the hardware level. Each of the presented levels has its own specific functionality and implements individual functions of the system as a whole.

Typical tasks performed using the HOST VI on a Windows computer are:

- saving data on a computer and accessing databases;
- integration with external information systems;
- organization of the interface.

Typical tasks performed in RT VI on a real-time controller:

- data processing;
- management;
- saving data in the built-in memory of the controller and on external media.

Typical tasks performed in FPGA VI on PLD:

- input-output operations;
- hardware interpretation and management of the process of interaction with the equipment;
- low-level processing of measurement signals.

PLD is a microcircuit whose functionality is determined by programming or "configuration", which is the more common term when working with this class of integrated circuits. The LabView FPGA Module package is an addition to the LabView software environment, which allows to specify the logic operations of the PLD in the form of a regular virtual device instead of programming it using a specialized VHDL language. This package allows to create programs with synchronous and asynchronous parallel loops that are executed at the hardware level and provides time-deterministic data collection and analysis.

The LabVIEW FPGA Module software package completely takes over the multi-step process of converting a virtual device into binary PLD code. At the first stage, the virtual device is converted into text code in VHDL language, which is then compiled by the standard Xilinx ISE industrial compiler into binary form. During the compilation process, the code is optimized according to the speed of execution and the number of logic gates involved.

The result of compilation is a binary file (bitstream file), which completely defines the PLD configuration. When the program starts, the binary file is loaded on the chassis, that is, the PLD configuration process takes place. The binary file can be written to the built-in flash memory and automatically loaded when the system is turned on. When the power is turned off, the configuration is not saved, so the binary must be downloaded again after a power-up. With the appropriate configuration, it can be loaded automatically from the flash memory of the PLD device or by the program, using the controller.

FPGA VI virtual instruments can run completely independently of other system components and remain functional even when the controller fails. Moreover, a buffer can be organized on the PLD, which prevents data loss in a similar situation.

PLD is primarily intended for interpretation, synchronization, control, data collection and preliminary digital processing of information signals, control of each input-output module.

A virtual device for a CompactRIO controller usually includes two or more loops: a loop with critical priority, in which the control and data processing algorithms are implemented, and a loop with normal priority, which is responsible for saving data, a remote web interface, and communication over an Ethernet network or RS-232 bus.

To raise the data received from the modules to the level of the real-time controller, the CompactRIO platform provides three ways: through the elements of the front panel, using the mechanism known in LabView as local variables (Local Variables), and through the DMA FIFO buffer. The first two approaches are relatively simple from the point of view of implementation, but suboptimal from the point of view of efficiency. At the same time, the DMA FIFO method allows to receive data obtained at high sampling rates from a large number of modules without delay. One of the advantages of DMA mode is that data transfer occurs independently of the central processor.

PLD devices that support DMA FIFO buffers have direct access to memory, unlike other methods that require the mandatory participation of the processor. Direct memory access is implemented by capturing the PCI bus (bus mastering) by the PLD device, in which it gets access to bus management, and therefore, access to memory, bypassing the processor.

The DMA FIFO buffer consists of two parts: one part is in the PLD memory, the other part is in the memory of the controller. PLD can be written to or read from the buffer element by element using the FIFO Read and FIFO Write methods, and the controller can be written to or read from samples of elements. Communication between the two parts of the buffer is carried out using the software-hardware DMA controller. Thus, from a software perspective, look like a single FIFO buffer.

The virtual device FPGA VI on the PLD implements the functionality of initialization, clocking, polling of data collection modules and subsequent loading of the received readings into the DMA FIFO buffer. To ensure a deterministic sequence of command execution, the structure of the programming language in LabView "Flat Sequence Structure" is used, in which the elements of polling modules and writing to the buffer are located.

The DMA FIFO buffer is polled cyclically at a time interval set by a timer at the real-time controller level, after which the readings obtained as integers according to the dynamic range and bit rate of the acquisition module are normalized by the values of accelerations and deformations. The received data is sent to a virtual device, which ensures their processing and storage on an external drive connected via a USB bus.

CompactRIO controllers have a built-in USB 2.0 controller, but not all storage devices support this standard, which can lead to significant recording delays, which, in turn, lead to overflow of the DMA FIFO buffer and incorrect operation of the system as a whole.

In the presented system, there is no virtual control device placed on a personal computer, and the LabView Remote Panel mechanism is used instead. This function implements the so-called Client-Server model, where the server is the controller, and the client is any computer with LabView installed. By default, CompactRIO is licensed for one external connection, but the number can

be expanded. To activate the Remote Panel on the controller, it is necessary to activate the Web server in the project settings and select those virtual devices to which remote access must be allowed. This function allows to significantly reduce the time required for the development of HOST VI, but it can create a load on the data transmission network.

In addition to the collection modules, for time synchronization and acquisition of current speed and coordinates, a GPS receiver is also connected to the controller, which is installed on the chassis in the same way as standard modules. Because the receiver is manufactured by a third-party company, the LabView Real Time Module does not have a standard means of acquiring GPS data, so it uses a set of closed virtual devices that are installed separately to interact with it. In addition, to ensure the correct functioning of the module as part of the project, it is also possible to add the SubVIs supplied with the module to the FPGA VI. If the initialization is successful, the GPS data is presented as a cluster or directly in a text format that can be used to debug the software or perform other tasks [33].

Therefore, the proposed scheme of the system for collecting and registering measured parameters registers the following indicators: vertical and horizontal transverse accelerations of the cart frames and the car body, dynamic stresses in the body and cart frames at different driving modes. In the future, the registered parameters are used to determine the safety indicators and the technical condition of the cars, namely: stress in the structural elements, indicators of vertical and horizontal dynamics, the coefficient of stability of the wheel from derailment, frame forces and acceleration of the body.

2.3 PRACTICAL ASPECTS OF THE IMPLEMENTATION OF IMPROVED MEANS AND APPROACHES FOR DETERMINING AND EVALUATING SAFETY INDICATORS AND THE TECHNICAL CONDITION OF CARS

2.3.1 MOBILE SYSTEM FOR DETERMINING SAFETY INDICATORS AND TECHNICAL CONDITION IN OPERATING CONDITIONS

Operation of rolling stock and complex technical hardware and software systems are usually subject to failures. The reasons for such failures can be: non-compliance with the manufacturing technology, difficult conditions of use, non-compliance with the requirements for the operation of such systems and rolling stock, aging and wear of nodes. Therefore, the implementation of periodic tests and diagnostics of rolling stock during their life cycle on the railways of Ukraine is an urgent and important task.

Currently, the development of measuring equipment and systems provides an opportunity for the implementation of advanced instrumental approaches for evaluating the quality and safety indicators of train traffic and taking measures to prevent emergency situations. The successful experience of implementing diagnostic systems for locomotives and passenger cars substantiates the feasibility of further improvement of methods and means of experimental evaluation of dynamic qualities and indicators of traffic quality and safety during the entire period of rolling stock operation.

The mobile system for determining the quality and safety indicators of the movement of rolling stock in operation should include: sensors primary converters; GPS receiver; cables for signal transmission; system of collection and registration of measurement indicators; transfer of data about the location and status of the system to the server; determination and assessment of traffic quality and safety indicators in the express processing mode.

Sensors are primary transducers – strain gauges and accelerometers. Cables are intended for connecting sensors with recording devices, the working voltage of which is ± 10 V. The cables are shielded 6-core, resistant to the influence of external factors with an operating temperature from -40 to $+80$ °C.

The mobile system should provide autonomous dynamic testing of the rolling stock to determine the coefficient of stability of the wheel from derailment, vertical and lateral forces and acceleration of sprung and non-sprung parts of the rolling stock, as a basis for assessing the quality of scheduled repairs and determining traffic quality and safety indicators in operating conditions.

During running dynamic tests, the following indicators are recorded: vertical and horizontal transverse accelerations of the cart frames and the car body, dynamic stresses in the body and cart frames at different driving modes [34].

2.3.2 HARDWARE AND PRIMARY CONVERTERS OF THE MOBILE SYSTEM

The mobile system for running dynamic tests and evaluation of movement quality and safety indicators based on National Instruments CompactRIO solves a wide range of tasks aimed at monitoring the technical condition of rolling stock during tests and in normal operation.

Strain gauges are connected to the strain gauge module NI 9237 (**Fig. 2.13**), and accelerometers are connected to the ADC module NI 9205 (**Fig. 2.14**), they perform scaling of the instantaneous values of the input voltage and analog-digital conversion into a digital code.



Fig. 2.13 NI 9237 module



○ Fig. 2.14 NI 9205 module

Digital signals via the internal bus are transmitted from the NI 9237 and NI 9205 modules to the NI 9012 controller (Fig. 2.15), from the output of which they are sent to the computer via the Ethernet interface bus, where the measurement information is processed, displayed and stored.

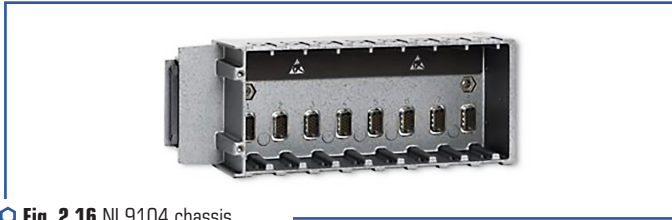


○ Fig. 2.15 NI 9012 controller

The software performs the functions of managing the recording process, initial setting of the mode of registration of signals from measurement channels, modes of operation of the automatic

recorder, mathematical functions of processing, presentation and storage of measurement information. It consists of the following blocks:

- software for flashing programmable logic;
- integrated microcircuit (PLD) located in the NI 9104 chassis (**Fig. 2.16**);
- application software of the NI 9012 controller;
- client part of the application software of the registrar of the host computer.



○ **Fig. 2.16** NI 9104 chassis

The software of the software-hardware logger is developed in the LabView FPGA software shell.

The application software is designed to read measurement data from channels selected by the user at the hardware level with a given sampling frequency, select the type of connection of the outputs of the primary measuring transducers, and set the voltage measurement limits.

The NI 9012 controller application software consists of two parts. The first part reads data from NI 9237 and NI 9205 ADC modules, performs data processing and writes to the non-volatile memory of the controller. The second part transmits data using the Transmission Control Protocol (TCP) to an external computer.

The computer software, through the user interface, performs general control functions and displays the current measurements on the monitor screen.

The mobile system can work in two functional modes: assessment of quality indicators, traffic safety and strength indicators in real time (**Fig. 2.17**) and measurement of acceleration and deformation in autonomous mode on rolling stock with further processing (**Fig. 2.18**). During the processing of the obtained values, the data obtained with the help of a GPS receiver are used to assess the impact of the change in the speed of movement on the controlled parameters.

The general block diagram of the mobile diagnostic system is shown in **Fig. 2.19**.

Low-frequency accelerometers of the UM type are used to measure and evaluate dynamic indicators of rolling stock. It consists of a shock-resistant and waterproof case, a board with an ADXL 278 microcircuit, a detachable UZNTS 05-7/12VP11 and fastening elements. The general view of the accelerometer is shown in **Fig. 2.20**.

The resulting vibration accelerations can be used to evaluate track quality indicators to identify point geometric deviations that affect the indicators of rolling stock movement dynamics. Measurement data must be used with GPS data and basic measurement parameters.



Fig. 2.17 Real-time mobile system



Fig. 2.18 Autonomous mobile system

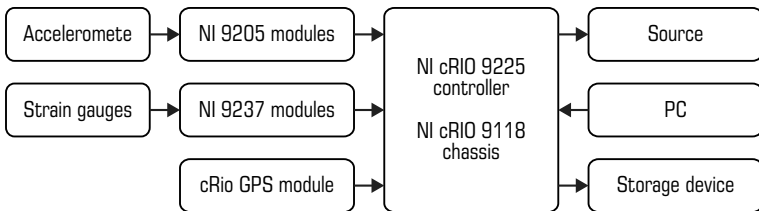


Fig. 2.19 Block diagram of the mobile system



○ Fig. 2.20 UM-type accelerometer

Vibration acceleration must be measured in certain places of the body and cart, the places are chosen depending on which indicator needs to be evaluated. Vertical accelerations on the axles are measured to evaluate the surface roughness of the track. Transverse accelerations of the cart are measured to evaluate track deviations in the form of short waves. Measurement of transverse and vertical accelerations of the body makes it possible to evaluate dynamic indicators of the quality of movement of rolling stock. The speed at which acceleration measurements of bodies and carts are carried out must be carried out in the established working range.

The measured accelerations can be used as indicators of the quality of the track geometry and to detect local geometric deviations affecting the dynamic behavior of the rolling stock. These measurements should be used in conjunction with basic parameter measurements.

Measurement of accelerations should be carried out in specified places on the body and carts, depending on the need for a specific assessment. Thus, the vertical accelerations of the boxes are measured to detect defects on the rail surfaces and isolated geometric irregularities. Transverse accelerations of the cart are used to detect irregularities with short waves. According to the lateral and vertical accelerations of the body, track defects affecting the dynamic performance of the rolling stock are revealed.

The sampling frequency should be at least 2.5 times higher than the cutoff frequency applied to the signal. Measurements of the accelerations of the carts and the body should be performed in the working speed range for the line within the tolerance of $\pm 10\%$ [35, 36].

2.3.3 SOFTWARE FOR COLLECTING AND RECORDING MEASUREMENTS

The measurement information collection subsystem collects, stores, and visualizes changes in the information signals of displacement sensors, vibration accelerations, and mechanical deformations.

In addition, data from the GPS receiver is used to analyze the influence of movement speed on changes in controlled parameters, receive accurate time signals, and determine current coordinates. The developed acquisition subsystem provides the operation of a CompactRIO controller with a chassis of 8 modules with a built-in programmable logic devices (PLD) and two universal 9205 ADC modules with a maximum sampling frequency of 250 kHz and five 9237 strain gauge modules with a maximum frequency of 50 kHz per channel, module – GPS signal receiver.

Thanks to the built-in PLD, CompactRIO has the ability to implement measurement data processing algorithms at the hardware level with a deterministic execution time of 25 ns without transferring the load to the central processor of the controller. A typical CompactRIO setup includes a controller with a PharLab or VxWorks real-time operating system, a chassis, and I/O modules. The chassis carries the PLD core, is directly connected to universal or specialized input-output modules that have built-in means of matching and processing information signals. There are different chassis models that have different numbers of module slots and differ in the characteristics of the PLD chips.

Thanks to its autonomy, hardware and mass-dimensional characteristics, as well as the ability to work in adverse conditions, CompactRIO can be used to solve a wide range of tasks related to the collection of measurement information and process management.

Most of the software for CompactRIO is developed according to a scheme that provides for its conditional separation into three levels: a virtual instrument HOST VI on a control PC with a Windows OS, an RT VI on a controller with a real-time OS, and an FPGA VI on a PLD that does not have its own OS, since the logic of the program was implemented directly at the hardware level. Each of the presented levels has its own specific functionality and implements individual functions of the system as a whole.

2.3.4 PRACTICAL STUDIES OF INDICATORS OF THE QUALITY AND SAFETY OF THE MOVEMENT OF FREIGHT CARS IN AN EMPTY STATE AS PART OF A TRAIN

The objects of research were a universal model platform car, a tank car and a hopper car for cement with the roof removed in an empty state.

The mass of the platform car is 20.4 tons, the mass of the hopper car is 22.15 tons, and the mass of the cement hopper car with the roof removed is 18.15 tons.

Tests as part of the train were carried out in 3 options:

- option 1 locomotive – 6 empty semi-cars – experimental coupling – 30 loaded semi-cars;
- option 2 locomotive – 15 loaded semi-cars – experimental coupling – 6 empty semi-cars – 15 loaded semi-cars;
- option 3 – locomotive – 30 loaded semi-cars – experimental coupling – 6 empty semi-cars.

Registration of processes was carried out with the use of strain gauges, which were installed on the structural elements of the carts.

To determine the longitudinal forces acting on the tested car, a coupling dynamometer was used, equipped with strain gauges and a pre-calibrated static load on the stand with a force of up to 3.5 MN.

After installing the measuring equipment on the test cars, the carts were calibrated against vertical and horizontal forces.

To register readings of strain gauges and vibration transducers, a software-hardware complex is used, which consists of a cRIO NI 9012 controller with NI 9237 ADC strain gauge modules, NI 9205 ADC modules and specialized software developed in the LabVIEW software package.

Data processing under static loads was performed using automated experimental data processing complexes.

The results of running dynamic tests were determined on the basis of data (measurements, calculations, control, visual inspection) recorded during the measurements (**Table 2.1**).

● **Table 2.1** Results of running dynamic tests in an empty state

Car	Permissible value of the stability margin factor	The actual value of the stability margin factor at speed				
		40±5 km/h	50±5 km/h	60±5 km/h	70±5 km/h	80±5 km/h
Platform car	At least 1.3	1.46	1.41	1.31	1.29	1.24
Tank car		1.5	1.47	1.38	1.35	1.33
Hopper car		1.48	1.45	1.38	1.32	1.3

The stability of the wheel from the wheel coming off the rail was determined for the most dangerous cases of a combination of a large transverse force of the interaction of the oncoming wheel with the rail and a small vertical load on this wheel. With the simultaneous action of such a combination of extreme forces over a period of time, it is possible for the crest of the approaching wheel to roll onto the head of the rail and further departure of the car from the rail.

2.4 MOBILE SYSTEM FOR DETERMINING THE DYNAMIC LOAD OF ROLLING STOCK UNDER OPERATING CONDITIONS

2.4.1 GENERAL REQUIREMENTS FOR SOFTWARE AND HARDWARE COMPLEX

A mobile system for determining the dynamic load of running parts of rolling stock in operation should consist of primary converters, a global positioning system receiver, analog signal transmission lines, measuring information collection subsystems, determination of movement safety indicators in the express processing mode, determination of the level of movement smoothness, determination of dynamic tensions.

The primary transducers should be strain gauges, low-frequency accelerometers, and displacement sensors. Analog signal transmission lines are cables that connect primary converters with recording devices with an operating voltage of up to 10 V and are components of the measuring system. Cables must be shielded, resistant to lubricants, have at least six cores, the flexibility of the cable must correspond to class 1 or 2 and not change its properties at temperatures from minus 40 °C to plus 80 °C.

The mobile system should provide the possibility of autonomously conducting control tests of dynamic diagnostics of rolling stock units in order to determine the load of running parts, as the main component of checking the quality of capital repairs, assessing the residual resource of load-bearing structures, performing control tests as part of works to extend the designated service life and determining loads of running parts under conditions of rolling stock operation.

2.4.2 MEASUREMENT INFORMATION COLLECTION SUBSYSTEM

The measurement information collection subsystem collects, stores, and visualizes changes in the information signals of displacement sensors, vibration accelerations, and mechanical deformations. In addition, data from the GPS receiver is used to analyze the influence of movement speed on changes in controlled parameters, receive accurate time signals, and determine current coordinates.

The developed acquisition subsystem provides the operation of a CompactRIO controller with a chassis of 8 modules with a built-in programmable logic devices (PLD) and two universal 9205 ADC modules with a maximum sampling frequency of 250 kHz and five 9237 strain gauge modules with a maximum frequency of 50 kHz per channel, module – GPS signal receiver.

In addition to the collection modules, for time synchronization and acquisition of current speed and coordinates, a GPS receiver is also connected to the controller, which is installed on the chassis in the same way as standard modules. Because the receiver is manufactured by a third-party company, the LabView Real Time Module does not have a standard means of acquiring GPS data, so it uses a set of closed virtual devices that are installed separately to interact with it. In addition, to ensure the correct functioning of the module as part of the project, it is also possible to add the SubVIs supplied with the module to the FPGA VI. If the initialization is successful, the GPS data is presented as a cluster or directly in a text format that can be used to debug the software or perform other tasks [37].

2.4.3 SYSTEM FOR DETERMINING MOVEMENT SMOOTHNESS

The subsystem for determining movement smoothness is based on the requirements of the standard on requirements for the movement smoothness of railway rolling stock [29]. The specified standard is intended to check the conformity of the smoothness indicator of the car W_z with the

norms stipulated in the technical documentation for the cars. The smoothness indicator depends on the intensity and spectral composition of the accelerations of the car body.

According to the accepted methodology, the indicators of the movement smoothness W_z are calculated from the acceleration of the body over the pivot nodes at the output of the "physiological filter". According to this, smoothness indicators are calculated in the vertical (W_{zv}) and horizontal (W_{zh}) directions. Data in **Table 2.2** characterize the assessment of movement smoothness.

● **Table 2.2** Evaluation of the car's running qualities based on the W_z movement smoothness indicator

Parameter	Value, m/s ²
Perfectly	2
Good	2–2.5
Sufficient for passenger cars	2.5–3
Limit for passenger cars	3–3.25
Sufficient for freight cars	3.6–4
Limit for freight cars	4–4.25
Limit for a person from a physiological point of view	4.5
Dangerous from the point of view of derailment of rolling stock	5

The calculation of movement smoothness indicators is implemented according to the following algorithm: the size of the block for calculations is determined; the size of the input block is determined by the logarithm to the base two, and with the help of the built-in function of LABVIEW, the Fourier transform is performed to construct the power spectrum; on the basis of the Fourier transformation, frequency arrays and data arrays are formed in the specified frequency range from 0.5 Hz to 20 Hz; the value of the normalized amplitude-frequency characteristic of the correcting filter is calculated.

The final movement smoothness indicator W_z for the data array is calculated according to the formula [29]:

$$W_j = \alpha \cdot \tilde{a}_{kj}^{0.3}, \quad (2.10)$$

where $\tilde{a}_{kj}^{0.3}$ – the average square value of vibration accelerations at the output of the correcting filter, m/s²; $\alpha=4.346$ for vertical oscillations; $\alpha=4.676$ for horizontal (transverse) oscillations.

An example of the results of the assessment of the movement smoothness is shown in **Fig. 2.21**. It is possible to compare the obtained values of movement smoothness indicators with the permissible limit value $[W_z]=3.75$.

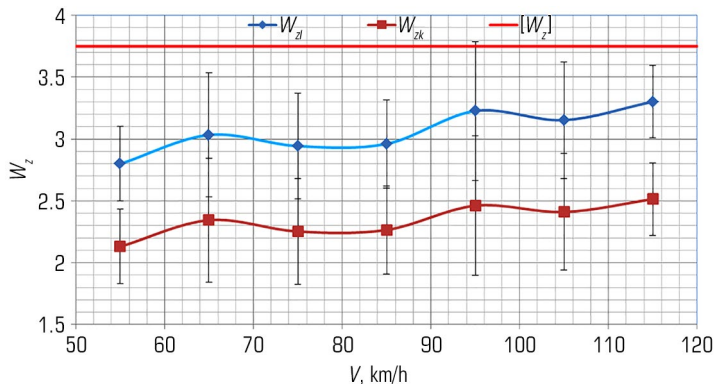


Fig. 2.21 Indicators of movement smoothness in the vertical direction: W_{dl} – indicator of movement smoothness in the pivot section; W_{zk} – indicator of movement smoothness in the car body

2.4.4 SYSTEM FOR DETERMINING TRAFFIC SAFETY INDICATORS

The subsystem for determining security indicators is designed to work in the express processing mode. This subsystem is a set of software installed on a PC and realizes the determination and display of safety indicators in real time with the interval of updating the result once every two seconds or once every 100 meters of the traveled path.

According to the current methods of field tests on railways with a gauge of 1520 mm, it is envisaged to determine traffic safety indicators based on the so-called "frame forces" that act on the wheel pairs from the frame structures of the running parts. However, due to the fact that these characteristics do not give a direct picture of the force interaction of the wheels with the rails, this leads to a decrease in the reliability of the results obtained in the process of running studies.

On the railways of the EU countries, the assessment of safety indicators of the movement of high-speed rolling stock is regulated by standards that establish the following test methods:

- normal method: measurement of contact interaction forces in the horizontal transverse (Y) and vertical (Q) directions;
- simplified method: measurement of lateral force (H) and body accelerations in transverse (\ddot{y}^*) and vertical (\ddot{z}^*) directions;
- simplified method: measurement of lateral accelerations of the cart frame (\dot{y}^+) and body accelerations in the transverse (\dot{y}^*) and vertical (\dot{z}^*) directions.

In order to introduce modern approaches to the evaluation of traffic safety indicators, work was carried out on the technical implementation of a simplified test method based on the measurement of accelerations (\dot{y}^+ , \dot{y}^* , \dot{z}^*).

After filtering, the mathematical expectation (\bar{x}) and standard deviation (s) are calculated to further determine the maximum possible acceleration values (X_{\max}) according to the following formula:

$$X_{\max} = \bar{x} + k \cdot s, \tag{2.11}$$

where k – coefficient that depends on the given confidence level (to determine the security indicators $k=3$).

The values determined in this way are compared with the maximum permissible values specified by the UIC 518 standard as follows: for vertical accelerations of the body $(\ddot{z}_s^*)_{\lim} = 3 \text{ m/s}^2$; for lateral accelerations of the body – $\left\| \left(\ddot{y}_s^* \right)_{\lim} = 3 \text{ m/s}^2 \right\|$ when moving straight and in curves with a large radius; $(\ddot{y}_s^*)_{\lim} = 2.8 \text{ m/s}^2$ – in curves with a radius of $400 \leq R \leq 600 \text{ m}$; $(\ddot{y}_s^*)_{\lim} = 2.6 \text{ m/s}^2$ – in curves with a radius of $250 \leq R \leq 400 \text{ m}$. For transverse accelerations of the cart frame, the maximum permissible accelerations are determined as follows:

$$\left(\left(\ddot{y}_s^+ \right)_{\lim} \right)_{\lim} = 12 - M_b / 5, \tag{2.12}$$

where M_b – the cart mass in tons.

Experimental implementation of the subsystem was carried out on the basis of the results of road tests.

Fig. 2.22 presents the root-mean-square deviations of the horizontal transverse accelerations of the cart frame recorded during the movement of the experimental train. Based on the fact that the mass of the cart is 6.68 tons, the value $\left(\ddot{y}_s^+ \right)_{\lim} = 5.33 \text{ m/s}^2$.

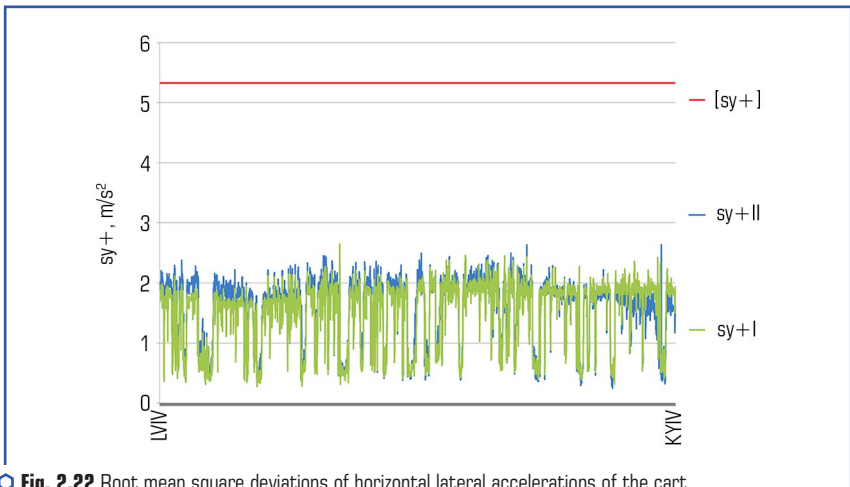


Fig. 2.22 Root mean square deviations of horizontal lateral accelerations of the cart frame measured during the test road

As can be seen from the presented results, the largest rms deviations of accelerations are at least two times lower than the maximum permissible value, which indicates a significant margin of stability of the car from derailment.

CONCLUSIONS

Subsection 2.1 offers three methods and approaches for assessing quality indicators, traffic safety and technical condition of railway rolling stock. The method of measuring mechanical stresses in the surface layers of the elements of the load-bearing structures of the rolling stock by the tensometry method makes it possible to assess the indicators of the technical condition and safety of the movement of the railway rolling stock in its defined dangerous zones. For example, this method allows to determine the vertical and horizontal transverse (frame) forces acting on wheel pairs, according to the rules that are currently in force on railways with a gauge of 1520 mm. The method of measuring contact forces: due to the deformation of the discs of the wheels of the wheel pairs. The proposed method of measuring contact forces makes it possible to directly measure contact forces, thereby evaluating the real traffic safety indicators for this experimental rolling stock, in contrast to the existing method: measurement by deformations of cart frames, which gives only an indirect assessment and does not apply to the conditions of passenger train traffic above 140 km/h.

In subsection 2.2, a method of in-depth processing of the results of road tests of rolling stock is proposed. The essence is to perform a spectral analysis of dynamic processes for various elements of the load-bearing structures of the freight car, with the aim of identifying the relationships between the oscillatory processes of the load-bearing structures and the frequencies at which the interaction between them occurs. A software algorithm for in-depth assessment of experimental indicators of the quality of the movement of freight cars with reduced containers is developed.

In subsection 2.3, the general requirements for the mobile system for determining the quality and safety indicators of the movement of freight cars with reduced containers in operation are formed and implemented. This mobile system allows running tests without involving the laboratory car, which reduces costs and time for conducting such tests by 25.8 %. Based on the results of the practical research, it is established that a decrease in the tare mass index by more than 10 % negatively affects the quality indicators of the movement of such cars, and a speed range of 60–70 km/h was found, during which a sharp deterioration of the movement dynamics indicators was recorded in a number of experimental cars. A safe scheme for the formation of trains, which include freight cars with reduced containers, is proposed. The compression force values obtained during running dynamic tests, which act on autocoupling devices of cars and reach or exceed critical values in the main and middle parts of the train according to the following schemes. It is advisable to place empty cars in the last third of the train.

In subsection 2.4, the general requirements for the software and hardware complex for determining the dynamic load of running parts in the conditions of operation of the rolling stock are

formulated. Technical solutions are implemented regarding the means of running tests of rolling stock to determine the dynamic loading of running parts in operating conditions, which increases the effectiveness of forecasted assessments and increases the efficiency of testing. A set of software subsystems for collecting measurement information, determining movement smoothness and safety indicators of rolling stock according to simplified schemes is developed.

REFERENCES

1. Novachuk, Y., Koblov, R., Teplyakov, A., Egorov, P. (2016). Innovative Method of Determination of Speed of Interaction of Wheels with Rails. *Procedia Engineering*, 165, 1503–1511. <https://doi.org/10.1016/j.proeng.2016.11.886>
2. Xu, L., Chen, X., Li, X., He, X. (2018). Development of a railway wagon-track interaction model: Case studies on excited tracks. *Mechanical Systems and Signal Processing*, 100, 877–898. <https://doi.org/10.1016/j.ymssp.2017.08.008>
3. Rakshit, U., Malakar, B., Roy, B. K. (2018). Study on Longitudinal Forces of a Freight Train for Different Types of Wagon Connectors. *IFAC-PapersOnLine*, 51 (1), 283–288. <https://doi.org/10.1016/j.ifacol.2018.05.074>
4. Lai, J., Xu, J., Wang, P., Yan, Z., Wang, S., Chen, R., Sun, J. (2021). Numerical investigation of dynamic derailment behavior of railway vehicle when passing through a turnout. *Engineering Failure Analysis*, 121, 105132. <https://doi.org/10.1016/j.engfailanal.2020.105132>
5. Clarhaut, J., Hayat, S., Conrard, B., Coquempot, V. (2010). The concept of the smart wagon for improving the safety of a railroad transportation system. *IFAC Proceedings Volumes*, 43 (8), 638–643. <https://doi.org/10.3182/20100712-3-fr-2020.00102>
6. Lai, J., Xu, J., Liao, T., Zheng, Z., Chen, R., Wang, P. (2022). Investigation on train dynamic derailment in railway turnouts caused by track failure. *Engineering Failure Analysis*, 134, 106050. <https://doi.org/10.1016/j.engfailanal.2022.106050>
7. Rezvani, M. A., Mazraeh, A. (2017). Dynamics and stability analysis of a freight wagon subjective to the railway track and wheelset operational conditions. *European Journal of Mechanics – A/Solids*, 61, 22–34. <https://doi.org/10.1016/j.euromechsol.2016.08.011>
8. Wu, B., Xiao, G., An, B., Wu, T., Shen, Q. (2022). Numerical study of wheel/rail dynamic interactions for high-speed rail vehicles under low adhesion conditions during traction. *Engineering Failure Analysis*, 137, 106266. <https://doi.org/10.1016/j.engfailanal.2022.106266>
9. Fomin, O., Lovska, A., Pišták, V., Kučera, P. (2019). Dynamic load computational modelling of containers placed on a flat wagon at railroad ferry transportation. *Vibroengineering Procedia*, 29, 118–123. <https://doi.org/10.21595/vp.2019.21132>
10. Khan, M. R., Dasaka, S. M. (2018). Wheel-rail Interactions in High Speed Railway Networks during Rapid Train Transit. *Materials Today: Proceedings*, 5 (11), 25450–25457. <https://doi.org/10.1016/j.matpr.2018.10.350>

11. Xu, L., Zhai, W. (2019). A three-dimensional model for train-track-bridge dynamic interactions with hypothesis of wheel-rail rigid contact. *Mechanical Systems and Signal Processing*, 132, 471–489. <https://doi.org/10.1016/j.ymssp.2019.04.025>
12. Sun, Y. Q., Dhanasekar, M. (2002). A dynamic model for the vertical interaction of the rail track and wagon system. *International Journal of Solids and Structures*, 39 (5), 1337–1359. [https://doi.org/10.1016/s0020-7683\(01\)00224-4](https://doi.org/10.1016/s0020-7683(01)00224-4)
13. Xia, F., Cole, C., Wolfs, P. (2008). The dynamic wheel-rail contact stresses for wagon on various tracks. *Wear*, 265 (9-10), 1549–1555. <https://doi.org/10.1016/j.wear.2008.01.035>
14. Okorokov, A., Fomin, O., Lovska, A., Vernigora, R., Zhuravel, I., Fomin, V. (2018). Research into a possibility to prolong the time of operation of universal open top wagon bodies that have exhausted their standard resource. *Eastern-European Journal of Enterprise Technologies*, 3 (7 (93)), 20–26. <https://doi.org/10.15587/1729-4061.2018.131309>
15. Gorobchenko, O., Fomin, O., Gritsuk, I., Saravas, V., Grytsuk, Y., Bulgakov, M. et al. (2018). Intelligent Locomotive Decision Support System Structure Development and Operation Quality Assessment. 2018 IEEE 3rd International Conference on Intelligent Energy and Power Systems (IEPS). Kharkiv, 239–243. <https://doi.org/10.1109/ieps.2018.8559487>
16. Fomin, O., Sulym, A., Kulbovskiy, I., Khozia, P., Ishchenko, V. (2018). Determining rational parameters of the capacitive energy storage system for the underground railway rolling stock. *Eastern-European Journal of Enterprise Technologies*, 2 (1 (92)), 63–71. <https://doi.org/10.15587/1729-4061.2018.126080>
17. Sulym, A. O., Fomin, O. V., Khozia, P. O., Mastepan, A. G. (2018). Theoretical and practical determination of parameters of on-board capacitive energy storage of the rolling stock. *Naukovyi Visnyk Natsionalnoho Hirnychoho Universytetu*, 5, 79–87. <https://doi.org/10.29202/nvngu/2018-5/8>
18. Gorbunov, M. I., Fomin, O. V., Prosvirova, O. V., Prokopenko, P. M. (2019). Conceptual basis of thermo-controllability in railway braking tribo pairs. *Naukovyi Visnyk Natsionalnoho Hirnychoho Universytetu*, 2, 58–66. <https://doi.org/10.29202/nvngu/2019-2/5>
19. Fomin, O., Lovska, A., Radkevych, V., Horban, A., Skliarenko, I., Gurenkova, O. (2019). The dynamic loading analysis of containers placed on a flat wagon during shunting collisions. *ARNP Journal of Engineering and Applied Sciences*, 14 (21), 3747–3752. Available at: http://www.arnpjournals.org/jeas/research_papers/rp_2019/jeas_1119_7989.pdf
20. Marye, G. (1933). *Vzaimodeistvie puti i podvizhnogo sostava*. Moscow: Goszheldorizdat, 338.
21. Nadal, M. (1908). *Locomotives a Vapeur Collection Encyclopedia Scientifique Biblioteque de Mecanique Applique et Genie*, Paris, 186.
22. Mishchenko, K. (1950). *Sovremennoe sostoianie voprosa o vspolzanii koleasa na rels*. *Trudy DIIT*, XX, 53–67.
23. Saponova, S., Tkachenko, V., Fomin, O., Hatchenko, V., Maliuk, S. (2017). Research on the safety factor against derailment of railway vehicleless. *Eastern-European Journal of Enterprise Technologies*, 6 (7 (90)), 19–25. <https://doi.org/10.15587/1729-4061.2017.116194>

24. Krol, O., Sokolov, V. (2020). Research of toothed belt transmission with arched teeth. *Diagnostyka*, 21 (4), 15–22. <https://doi.org/10.29354/diag/127193>
25. Melnyk, O., Onyshchenko, O., Onyshchenko, S., Golikov, V., Sapiha, V., Shcherbina, O., Andrievska, V. (2022). Study of Environmental Efficiency of Ship Operation in Terms of Freight Transportation Effectiveness Provision. *TransNav, the International Journal on Marine Navigation and Safety of Sea Transportation*, 16 (4), 723–729. <https://doi.org/10.12716/1001.16.04.14>
26. Melnyk, O., Onyshchenko, S., Onyshchenko, O., Shumylo, O., Voloshyn, A., Koskina, Y., Volianska, Y. (2022). Review of Ship Information Security Risks and Safety of Maritime Transportation Issues. *TransNav, the International Journal on Marine Navigation and Safety of Sea Transportation*, 16 (4), 717–722. <https://doi.org/10.12716/1001.16.04.13>
27. Masliev, V. (2002) Dinamika lokomotiva s ustroystvom dlia radialnoi ustanovki kolesnykh par v krivyykh. *Visnyk Skhidnoukr. nats. un-tu. Tekhnichni nauky. Seriiia Transport.*, 6 (52), 69–74.
28. Sagin, S., Kuropyatnyk, O., Sagin, A., Tkachenko, I., Fomin, O., Pištěk, V., Kučera, P. (2022). Ensuring the Environmental Friendliness of Drillships during Their Operation in Special Ecological Regions of Northern Europe. *Journal of Marine Science and Engineering*, 10 (9), 1331. <https://doi.org/10.3390/jmse10091331>
29. SOU MPP 45.060-204:2007. Vahony pasazhyrski. Plavnist rukhu. *Metody vyznachenia* (2007). Kyiv: Minprompolityky Ukrainy, 12.
30. Kondratiev, A., Slivinsky, M. (2018). Method for determining the thickness of a binder layer at its non-uniform mass transfer inside the channel of a honeycomb filler made from polymeric paper. *Eastern-European Journal of Enterprise Technologies*, 6 (5 (96)), 42–48. <https://doi.org/10.15587/1729-4061.2018.150387>
31. Kondratiev, A. (2019). Improving the mass efficiency of a composite launch vehicle head fairing with a sandwich structure. *Eastern-European Journal of Enterprise Technologies*, 6 (7 (102)), 6–18. <https://doi.org/10.15587/1729-4061.2019.184551>
32. Pogorelov, D., Simonov, V. (2010). An indicator for assessing the danger of rolling stock derailing by rolling a wheel onto the rail head. *Newsletter of the Eastern Ukrainian National University named after V. Dahl*, 5 (147), I, 64–70.
33. Dyomin, Yu. V., Chernyak, G. Yu. (2003). *Osnovy dynamiky vahoniv*. Kyiv: KUETT, 270.
34. Chernyak, A. Yu., Diomin, Yu. V., Zakhovaiiko, O. P., Shevchuk, P. A. (2014). Computer modeling of the dynamics of rack transport vehicles. *News of the National News. tech. University of Ukraine "Kiev Polytechnic Institute". Machine-building series*, 94–98.
35. Chernyak, A. Yu. (2009). *Primenenie kompiuternogo modelirovaniia dlia opredeleniia veroiatnykh prichin skhoda s relsov gruzovykh vagonov*. *Zalozhnykh transport Ukraini*, 3, 49–52.
36. Chernyak, A. Yu. (2010). Computer model for prompt determination of the probable causes of derailment of freight cars. *News of Skhidnoukrain National University im. V. Dahl*, 5 (147), 1, 40–46.
37. Samsonkin, V. M., Chernyak, G. Yu. (2012). Before assessing the risks of building a dry warehouse from slats on a computer modeling stand, *Zalozhnykh Transport Ukraine*, 2, 39–42.

CHAPTER 3

HIERARCHICAL STRUCTURE OF CALCULATION METHODS FOR
ASSESSING THE FIRE RESISTANCE OF ENCLOSURE HORIZONTAL
STRUCTURES UNDER THE LIMIT STATE OF LOSS OF INTEGRITY

ABSTRACT

The paper presents a hierarchical system of calculation methods for assessing the fire resistance of reinforced concrete slabs upon the onset of the limit state of loss of integrity. Three approaches are proposed: tabular, simplified and refined. The tabular method allows to quickly assess the fire resistance of slabs, the simplified method takes into account structural parameters and loads, and the refined method takes into account detailed characteristics of materials and temperature effects for the most accurate results. Such a system provides designers with flexibility during the design phase, allowing them to select the appropriate method depending on the required accuracy and available data. In addition, they help increase the safety of building structures during a fire.

KEYWORDS

Fire resistance, reinforced concrete slabs, limit state, loss of integrity, tabular method, simplified method, refined method, structural parameters, design, temperature effect of fire.

According to EN 1992-1-2, the hierarchical system of methods for the calculation of reinforced concrete slabs is a structure based on simplified methods, and at the top are refined methods, but only according to the loss of bearing capacity. Since floor slabs and coverings, in addition to the load-bearing function, also perform enclosing functions. They prevent the spread of fire and harmful combustion products that pose a threat to people's lives and health. According to EN 1992-1-2, the conformity of boards to the standardized fire resistance class must be confirmed by three limit states, in particular: loss of load-bearing capacity (R), loss of integrity (E) or thermal insulation capacity (I).

However, according to the results of experimental tests on reinforced concrete floor slabs, it was established that the onset of only the limit state of loss of bearing capacity is taken into account [1]. This is explained by the fact that the onset of the loss of heat-insulating ability occurs much later than the loss of bearing capacity, since concrete is a porous material filled with

air, which is the worst heat conductor among all materials except for vacuum, so the heating of the non-heated surface of such structures to critical temperatures occurs very slowly [2]. For example, in work [3], the maximum temperature on the non-heated side of the slab in a hollow slab for 50 minutes was recorded as only 70 °C min, which indicates its high fire resistance indicators upon the onset of the loss of heat-insulating capacity only, without taking into account the loss of load-bearing capacity and integrity. Thus, the question remains unresolved for floor slabs and coatings, which comes first – loss of bearing capacity or loss of integrity.

Since there are no methods for assessing fire resistance based on the limit state of loss of integrity, and during experiments it is difficult to record the formation of cracks due to covering with loads [3], the calculation approach remains the only option.

In [4–7], it was demonstrated that the limit state of fire resistance, the loss of integrity, occurs earlier than the loss of load-bearing capacity, which creates dangerous conditions during the evacuation of people during a fire and the effective elimination of fires by special units.

Therefore, it is proposed to develop a hierarchical system for assessing fire resistance by loss of integrity of reinforced concrete hollow and ribbed slabs, so that designers can guarantee their fire resistance class when using such structures in construction. This will ensure the safety of mankind during evacuation in the event of a fire in buildings with such constructions by preventing the spread of dangerous fire factors and the spread of the fire itself. In addition, the use of such building structures, taking into account the requirements for ensuring integrity during the normalized time specified in the fire resistance class, will allow emergency and rescue units to effectively and quickly localize the fire.

Each of the methods of the hierarchical system of calculating the fire resistance of reinforced concrete hollow and ribbed slabs according to the onset of the limit state of loss of integrity must have three main aspects: a set of initial data, a calculation algorithm and a method of interpreting the calculation results, i.e. a criterion base indicating the onset or non-occurrence of the limit state of loss integrity

3.1 FEATURES OF THE HIERARCHICAL STRUCTURE OF CALCULATION METHODS FOR ASSESSING THE FIRE RESISTANCE OF HOLLOW SLABS BY LOSS OF INTEGRITY

3.1.1 IMPROVEMENT OF THE TABULAR CALCULATION METHOD FOR ASSESSING THE FIRE RESISTANCE OF REINFORCED CONCRETE HOLLOW SLABS

According to EN 1992-1-2, *Table 5.9* shows the minimum geometrical dimensions of the slabs required to ensure the corresponding fire resistance class. However, this table is provided for slabs with a thickness of up to 200 mm, which does not make it possible to use it for assessing the fire resistance of hollow slabs with a thickness of 220 mm to 300 mm. Therefore, in order to carry out a simplified assessment of the fire resistance of hollow slabs upon the onset of the limit

state of loss of integrity, it is necessary to supplement the corresponding *Table 5.9* presented in EN 1992-1-2, using the data obtained using the approaches proposed in [5].

For a comprehensive study, it was proposed to follow the regularity of the dependence of the fire resistance limit of reinforced concrete hollow slabs on their most significant geometric parameters, in this case, it is the axial distance of the reinforcing bars and the thickness of the slab.

According to our assumption, the fire resistance limit is related to the geometric parameters of reinforced concrete hollow slabs by a linear polynomial dependence of the type:

$$y = b_0 + b_1x_1 + b_2x_2 + b_3x_1x_2, \quad (3.1)$$

where x_1, x_2 – factors that correspond to the initial parameters of reinforced concrete hollow slabs, in our case it is the axial distance of reinforcing bars and slab thickness. This type of regression was chosen based on the results of research given in works [8, 9].

In this case, to establish the regression dependence of this type, the matrix of the experimental plan is used, which has the form of a **Table 3.1**.

In the **Table 3.2**, the intervals of factors for the implementation of a full factorial experiment are given.

● **Table 3.1** Planning matrix of a full factorial experiment for building a regression

No.	x_1	x_2	x_1x_2
1	+	+	+
2	+	–	–
3	–	+	–
4	–	–	+

● **Table 3.2** Intervals of variation of factors in a full factorial experiment

Slab thickness, H , mm			Axial distance, w , mm		
Lowest value, H_{-1}	Average value, H_0	Largest value, H_1	Lowest value, w_{-1}	Average value, w_0	Largest value, w_1
220	260	300	10	20	30

To obtain reference data for the implementation of a full factorial experiment, the most common structural characteristics of reinforced concrete hollow slabs were adopted. Mechanical characteristics of concrete and reinforcing steel, as well as geometric characteristics of reinforcement are given in **Table 3.3**.

By varying the relevant parameters according to the matrix of the plan according to the **Table 3.1** and **Table 3.2** according to the results of the calculations according to the proposed

mathematical models of the refined calculation method and using the parameters from the **Table 3.3**, obtained data for conducting a full factorial experiment, which are shown in **Table 3.4**.

● **Table 3.3** Technical data for reinforced concrete hollow slab

Parameter	Units of measurement	Value
Concrete		
Strength class		C 20/25
Density	kg/m ³	2400
Strength limit	MPa	20
Poisson's ratio		0.3
The thickness of the concrete between the cavity and the upper slab	mm	40 mm at H=300 mm 28 mm at H=220 mm
Working armature		
Strength class		A400
Strength limit	MPa	400
Diameter	mm	12
Applied load as a percentage of the maximum	%	70

● **Table 3.4** Parameters of fires in model rooms during a full factorial experiment according to the adopted planning matrix

Experimental situation	1	2	3	4
Limit of fire resistance, U_e , min	75	51	64	41

When using the results of the full factorial experiment given in **Table 3.4**, the corresponding coefficients of the regression dependence (3.1) were calculated according to the formulas [8, 9]:

$$b_0 = \frac{1}{N} \sum_{i=1}^N y_i; b_1 = \frac{1}{N} \sum_{i=1}^N x_1 y_i; b_2 = \frac{1}{N} \sum_{i=1}^N x_2 y_i; b_3 = \frac{1}{N} \sum_{i=1}^N x_1 x_2 y_i, \quad (3.2)$$

where $N=4$ – the number of experimental situations according to the matrix of the full factorial experiment (**Table 3.1**); x_i – values of the corresponding factor according to the matrix of the plan and the ranges of their variation (**Tables 3.1, 3.2**); y_i – the value of the fire resistance limit according to the results of the corresponding numerical experiments according to the **Table 3.4**.

When applying formulas (3.2), regression coefficients were calculated, which are summarized in the **Table 3.5**.

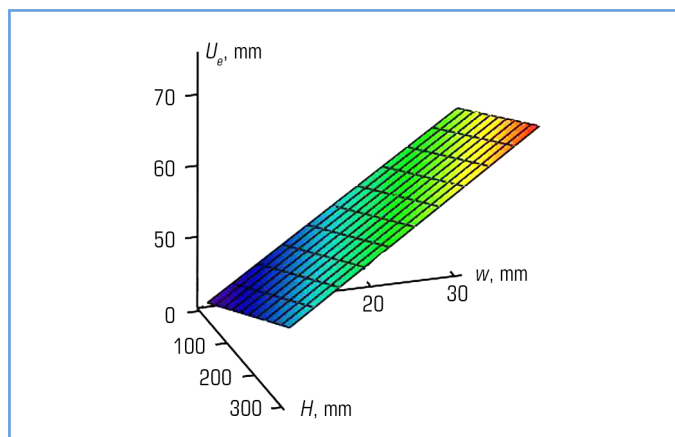
● **Table 3.5** Regression coefficients for determining the limit of fire resistance of reinforced concrete hollow slabs according to the onset of the limit state of loss of integrity

Regression coefficients (7.1)	b_0	b_1	b_2	b_3
Encoded values	57.75	5.25	11.75	0.25
Real values	3.37	0.119	1.01	0.000625

The constructed regression allows to follow the dependence of the fire resistance limit of reinforced concrete hollow slabs on the thickness of the slab and the axial distance of the reinforcing bars. Thus, the revealed regularity of the limit of fire resistance of reinforced concrete hollow slabs upon the onset of the limit state of loss of integrity from the cross-section height (H) and the axial distance from the armature to the heating surface of the slab (w) can be described with the help of a regression dependence:

$$U_e = 3.37 + 0.119H + 1.01w + 0.000625 \times H \times w. \quad (3.3)$$

It is also possible to present it with the help of the corresponding constructed surface, which is presented in **Fig. 3.1**. It can be seen on the constructed surface that it has an almost exact flat shape.



○ **Fig. 3.1** The surface corresponding to the dependence of the fire resistance limit of a reinforced concrete hollow slab upon the onset of the limit state of loss of integrity on its thickness and the axial distance of the reinforcing bars

It is convenient to determine the limit of fire resistance of reinforced concrete hollow slabs upon the onset of the limit state of loss of integrity according to their most significant structural parameters when using the nomogram presented in **Fig. 3.2**.

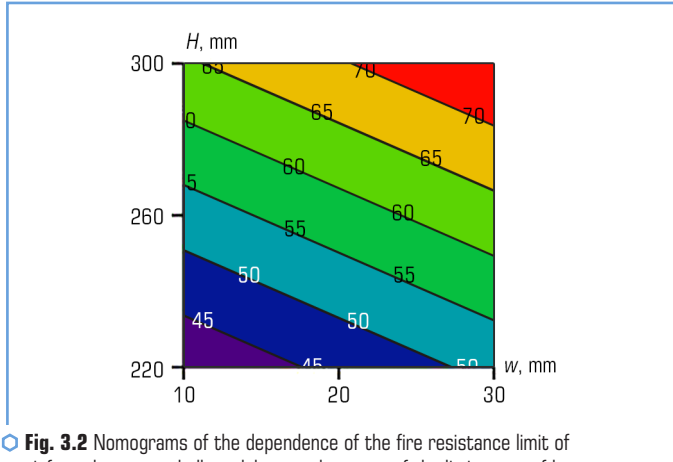


Fig. 3.2 Nomograms of the dependence of the fire resistance limit of a reinforced concrete hollow slab upon the onset of the limit state of loss of integrity on its thickness and the axial distance of the reinforcing bars

When analyzing the results of the calculated fire resistance assessment based on the onset of the limit state of loss of integrity, the value of the fire resistance limit, determined by the regression dependence and by the refined method, was compared. At the same time, absolute deviation and relative deviation were used as criteria for the adequacy of the calculated results. The data obtained during the analysis of the adequacy of the calculation results according to the regression dependence are presented in the **Table 3.6**.

Table 3.6 Adequacy of the results of assessing the fire resistance limit of reinforced concrete hollow slabs, determined by regression dependence

Limit of fire resistance, calculated according to MSE, min	Limit of fire resistance, calculated by regression dependence, min	Absolute deviation, min	Relative deviation, %
Slab thickness $H=220$ mm, Axial distance $w=15$ mm			
51	46.75	4.25	8.33
Slab thickness $H=220$ mm, Axial distance $w=20$ mm			
60.5	52.5	8	13.223
Slab thickness $H=300$ mm, Axial distance $w=15$ mm			
67	57	10	14.925
Slab thickness $H=300$ mm, Axial distance $w=20$ mm			
71	63	8	11.268
Average values			
–	–	7.563	11.937

The results of the adequacy analysis are given in **Table 3.6**, indicate that the error of the assessed fire resistance assessment for reinforced concrete hollow slabs, calculated according to the regression dependence, is insignificant and the obtained regression dependence can be used for the assessed fire resistance assessment of reinforced concrete hollow slabs according to the limit state of loss of integrity.

When using the nomogram shown in **Fig. 3.2**, the *Table 5.9*, given in the guideline EN 1992-1-2, was clarified. The updated table is presented in the form of a **Table 3.7**.

● **Table 3.7** Minimum dimensions and axial distances for reinforced concrete hollow slabs

Standard fire resistance	Minimum dimensions (mm)	
	Slab thickness, h_s	Axial distance, a
REI 30	220	15
REI 45	220	20
REI 60	220/300	30/20
REI 90	300	35

The implementation of the refined tabular method of assessing the fire resistance of reinforced concrete hollow slabs by the onset of the limit state of loss of integrity has the simplest algorithm. Three main parameters are used as initial data: h_s – slab thickness; a – the axial distance of the reinforcing bars to the heating surface; REI – fire resistance class that must be provided.

To implement the algorithm of the tabular method, a **Table 3.6** is used. For the required class of fire resistance, the appropriate line is selected, which contains the minimum values of the slab thickness and the axial distance of the reinforcing bars. If the real parameters are greater, then the required fire resistance class is considered to be provided.

3.1.2 DEVELOPMENT OF A SIMPLIFIED METHOD FOR ASSESSING FIRE RESISTANCE BY LOSS OF INTEGRITY FOR HOLLOW SLABS

To implement the algorithm of the simplified method of calculating the fire resistance of reinforced concrete hollow slabs upon the onset of the limit state of loss of integrity with the use of mathematical models of crack formation, described in [5, 10], a set of initial data is used, which is given in **Table 3.8**.

When calculating according to a mathematical model, a strength criterion was developed, which can be written through the expression:

$$f_{ct,\theta}^2 + \sigma_y f_{ct,\theta} - \tau_{xy}^2 = 0. \quad (3.4)$$

The voltages in equation (3.4) are calculated according to the formulas:

$$\sigma_y = \frac{F_p \operatorname{tg} \varphi_c}{b_s h_p}, \tau_{xy} = \frac{F_p}{b_s h_p}, \quad (3.5)$$

where b_s – the slab width.

By substituting these values into equation (3.4) and solving it with respect to the limit force F_p , the possibility of crack formation was analyzed according to the mechanism reproduced in the diagram of **Fig. 3.3**.

● **Table 3.8** A set of initial data for the implementation of a simplified method of assessing the fire resistance of reinforced concrete hollow slabs according to the limit state of loss of integrity

Materials data

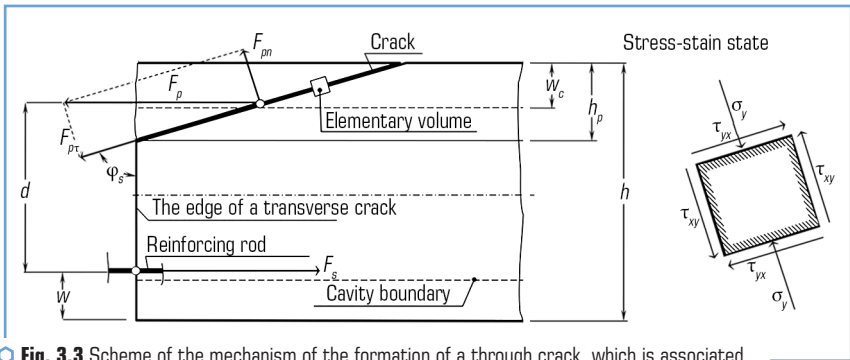
Concrete strength class	Reinforcement strength class	The law of concrete deformation	The law of reinforcement deformation	The law of change of temperature deformation
-------------------------	------------------------------	---------------------------------	--------------------------------------	--

Data on design parameters

Slab dimensions	The geometry of the armature location	Diameters and number of reinforcing bars
-----------------	---------------------------------------	--

Data on the temperature distribution in the cross section

Nomogram of temperature distribution



○ **Fig. 3.3** Scheme of the mechanism of the formation of a through crack, which is associated with the onset of the limit state of loss of integrity

When analyzing all possible solutions of equation (3.4), there are no real roots. Therefore, another mechanism operates during the formation of cracks, which is shown in the diagram of **Fig. 3.4**.

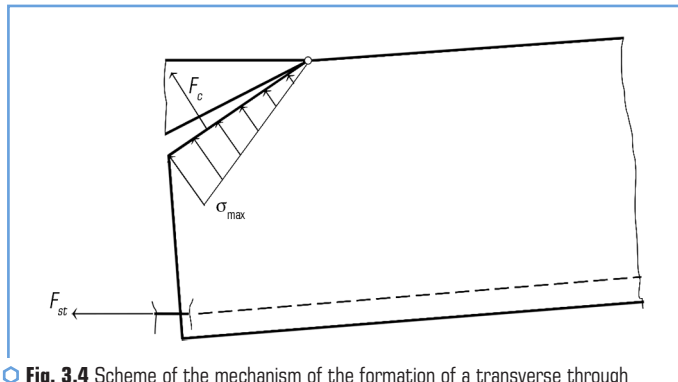


Fig. 3.4 Scheme of the mechanism of the formation of a transverse through crack, which is associated with the onset of the limit state of loss of integrity

According to the calculation scheme shown in Fig. 3.4, the equilibrium equation was compiled:

$$F_{st} (h - w_c) + \frac{2}{3} \frac{F_c h_p}{\sin \varphi_c} = M_E, \quad (3.6)$$

where M_E – the acting moment from the distributed load applied to the slab.

The force in the reinforcing bar and the force of detachment of the lateral surface of the prism of the destruction of a reinforced concrete hollow slab are determined, respectively, by the formulas:

$$F_{st} = f_{s,\theta} \frac{\pi \cdot d_s^2}{4}; F_c = \frac{f_{ct,\theta} h_p b_s}{2 \sin \varphi_c}. \quad (3.7)$$

In view of the given expressions, the distance from the upper surface of the slab to the starting point of the formation of a through crack can be determined by the formula:

$$h_p = \sqrt{\frac{3 \sin^2 \varphi_A}{f_{ct,\theta} b_s} \left(\frac{q_E l^2}{8} - f_{s,\theta} \frac{\pi \cdot d_s^2}{4} \right)} \leq w_c. \quad (3.8)$$

Thus, using this formula, it is possible to determine the danger of the formation of a through crack. The condition for the formation of a through crack is dangerous if the distance h_p exceeds the distance from the upper surface of the slab to the cavity rib w_c .

Another possible prerequisite for the occurrence of the limit state of loss of integrity can be the formation of longitudinal through cracks between the upper rib of the cavity and the upper surface of the slab. The mechanism of formation of this type of cracks can be illustrated by the diagram shown in Fig. 3.5.

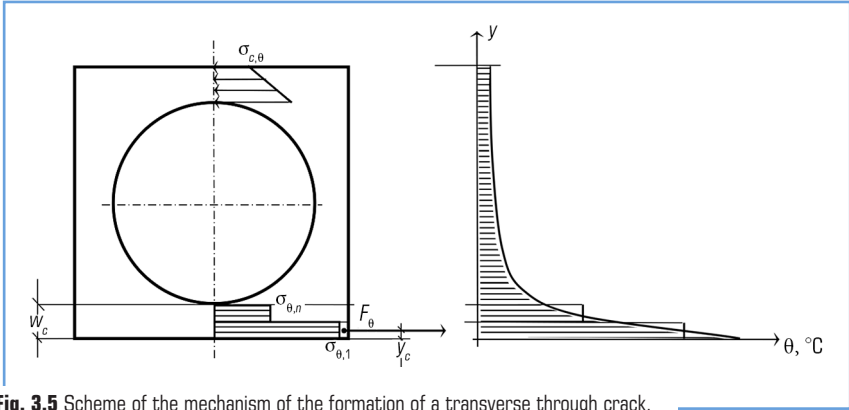


Fig. 3.5 Scheme of the mechanism of the formation of a transverse through crack, which is associated with the onset of the limit state of loss of integrity

Considering the calculation scheme shown in **Fig. 3.5**, it is possible to write the equilibrium equation describing the stress-strain state in the corresponding inner layers of the reinforced concrete slab:

$$\sigma_{c,\theta} = \frac{F_{\theta}}{W_c J} [1 - 6W_c^{-1}(h - 0.5W_c - y_c)]. \quad (3.9)$$

Here, the force acting as a result of thermal expansion in the lower layers of a fragment of a reinforced concrete slab is determined by the formula:

$$F_{\theta} = \frac{1}{n} W_c J \sum_{i=1}^n \sigma_{\theta i}(\varepsilon_c(\theta)). \quad (3.10)$$

Equation (3.9) also includes the distance from the bottom surface of the slab to the point of application of the force F_{θ} , which is determined by the formula:

$$y_c = \frac{\sum_{i=1}^n y_i \sigma_{\theta i}(\varepsilon_c(\theta))}{\sum_{i=1}^n \sigma_{\theta i}(\varepsilon_c(\theta))}. \quad (3.11)$$

Stresses arising as a result of temperature deformations are determined by the formulas given in the first column of the *Table 1*, given in [1]. As deformations, a mathematical model of the dependence of temperature deformations on temperature is used here, which is described by the following expressions:

$$\begin{aligned} \varepsilon_c(\theta) &= -1.8 \cdot 10^{-4} + 9 \cdot 10^{-6} \theta + 2.3 \cdot 10^{-11} \theta^3 \text{ at } 20 \text{ }^{\circ}\text{C} \leq \theta \leq 70 \text{ }^{\circ}\text{C}; \\ \varepsilon_c(\theta) &= 14 \cdot 10^{-3} \text{ at } 700 \text{ }^{\circ}\text{C} \leq \theta \leq 1200 \text{ }^{\circ}\text{C}. \end{aligned} \quad (3.12)$$

The resulting calculation methods allow analyzing the conditions of crack formation, which can be considered as signs of the onset of the limit state of loss of fire resistance in terms of integrity. The proposed methods have a hierarchical structure at the base of which are simplified methods, while at the top the refined methods proposed by us are based on the finite element method.

When performing the calculation according to the mathematical model (3.6)–(3.8), it is necessary to determine the temperature distribution over the thickness of the slab, for this, a diagram (**Fig. 3.6**) is used, which is recommended by the guidelines in the EN 1992-1-2 standard. With its use, it is possible to determine the temperature of the reinforcing bars and the heating temperature of the inner layers of the concrete slab.

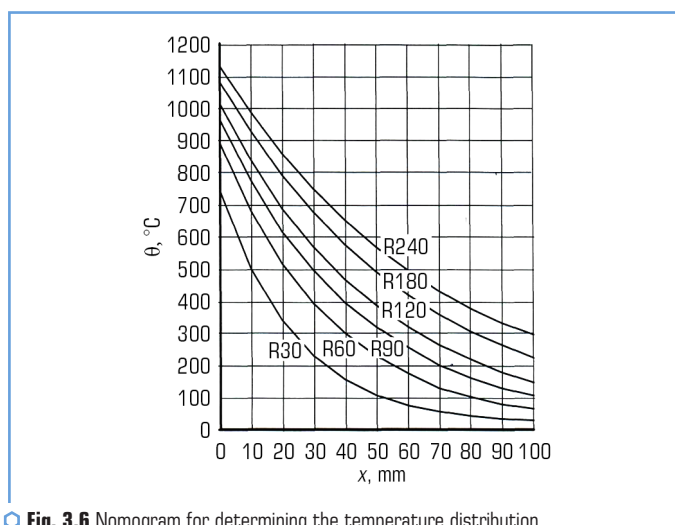


Fig. 3.6 Nomogram for determining the temperature distribution in a reinforced concrete hollow slab

The reduced strength of reinforcing steel is determined by the formula:

$$f_{s,q} = k_t(\theta) f_s, \quad (3.13)$$

where $k_t(\theta)$ – the coefficient of reduction of the tensile strength of reinforcing steel.

The average reduced strength of the reinforcement row depending on the elevated temperatures according to the EN 1992-1-2 guideline is calculated by the formula:

$$k_v(\theta) = \frac{\sum k_t(\theta_i)}{n_v}, \quad (3.14)$$

where $k(\theta_i)$ – the strength reduction factor of the i -th reinforcing bar depending on the temperature θ_i obtained from the nomogram in **Fig. 3.6**; $k_v(\theta)$ – the average strength reduction factor of the v -th reinforcement row; n_v – the number of reinforcing bars in the v -th reinforcing row.

The distance a from the lower surface of the calculated cross-section to the center of gravity of the reinforcement row can be calculated by the formula:

$$a = \frac{\sum a_v k_v(\theta)}{\sum k_v(\theta)}, \quad (3.15)$$

where a_v – the distance from the lower surface of the calculated cross-section to the v -th reinforcement row.

If there are only two rows, the distance w from the lower surface of the calculated cross-section to the center of gravity of the reinforcing row can be calculated using the following formula:

$$w = \sqrt{(a_1 a_2)}. \quad (3.16)$$

If the reinforcing bars have different areas and are placed arbitrarily, the following technique is used.

The average resistance of the reinforcing steel group $k(\varphi) f_{s,fi}$ depending on the elevated temperatures can be calculated by the expression:

$$k(\varphi) f_{s,fi} = \frac{\sum [k_s(\theta_i) f_{s,i} A_i]}{\sum A_i}, \quad (3.17)$$

where $k_s(\theta_i)$ – the strength reduction factor of the i -th reinforcing bar; $f_{s,i}$ – calculated resistance of the i -th reinforcing bar; A_i – cross-sectional area of the i -th reinforcing bar.

The distance w from the calculated cross-section to the center of gravity of the reinforcement group is calculated according to the formula (3.18):

$$w = \frac{\sum [a_i k_s(\theta_i) f_{s,i} A_i]}{\sum [k_s(\theta_i) f_{s,i} A_i]}, \quad (3.18)$$

where a_i – the distance from the calculated cross-section to the axis of the i -th reinforcing bar.

The average coefficient of reduction of concrete strength for the section of the element is determined by the zone method, including the coefficient $(1-0.2/n)$, which takes into account the temperature change of each zone in the calculation according to the formula:

$$k_c = \frac{(1-0.2/n)}{n} \sum_{i=1}^n k_{c,i}(\theta_i), \quad (3.19)$$

where n – the number of zones (minimum $n=3$, recommended $n=5$).

The reduced strength of concrete in the compressed zone of the slab is determined by the formula:

$$f_{ct,q} = k_c(\theta) f_{ct}. \quad (3.20)$$

In this way, the implementation of the proposed method can be carried out according to the algorithm, the scheme of which is presented in **Fig. 3.7**.

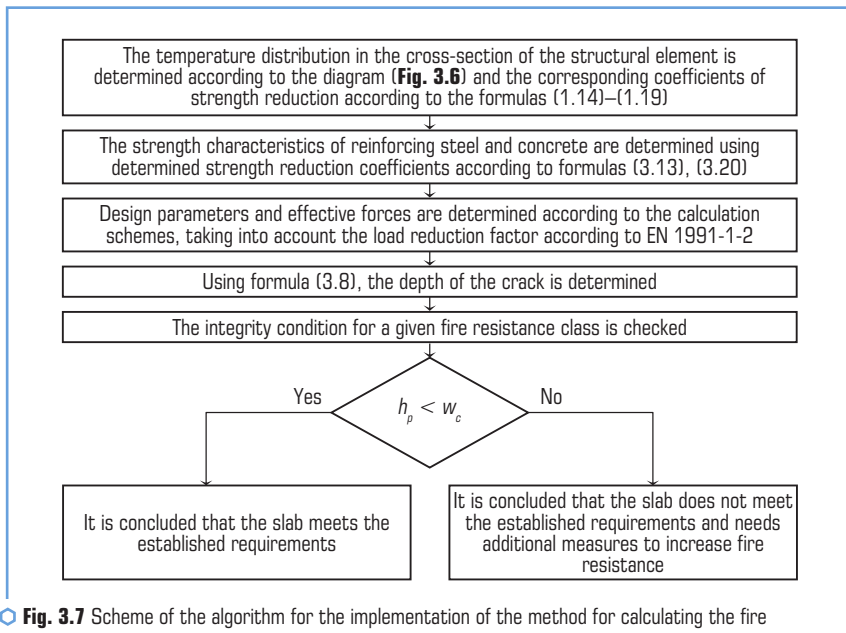


Fig. 3.7 Scheme of the algorithm for the implementation of the method for calculating the fire resistance of a reinforced concrete hollow slab based on the limit state of the loss of integrity when transverse cracks appear

To carry out the calculation according to this method, a set of initial data is also required, which is presented in the form of the **Table 3.8**.

When implementing the algorithm for calculating integrity based on the occurrence of longitudinal cracks, the scheme in **Fig. 3.8** can be used.

Both of the described methods must be applied in a complex and if one of them gives a negative result, it is considered that the slab does not meet the established requirements for fire resistance according to the limit state of loss of integrity.

The next step in the hierarchy of methods for calculating the fire resistance of a reinforced concrete hollow slab based on the limit state of loss of integrity requires the use of refined methods. In [5, 10] it is shown that these methods allow, based on the calculation results, to identify the

moment of onset of the limit state of loss of integrity. To carry out the calculation according to this method, a set of initial data is also required, which is presented in the form of a **Table 3.8**. Basic mathematical models and theoretical references given in the **Table 3.9** are also used for conducting.

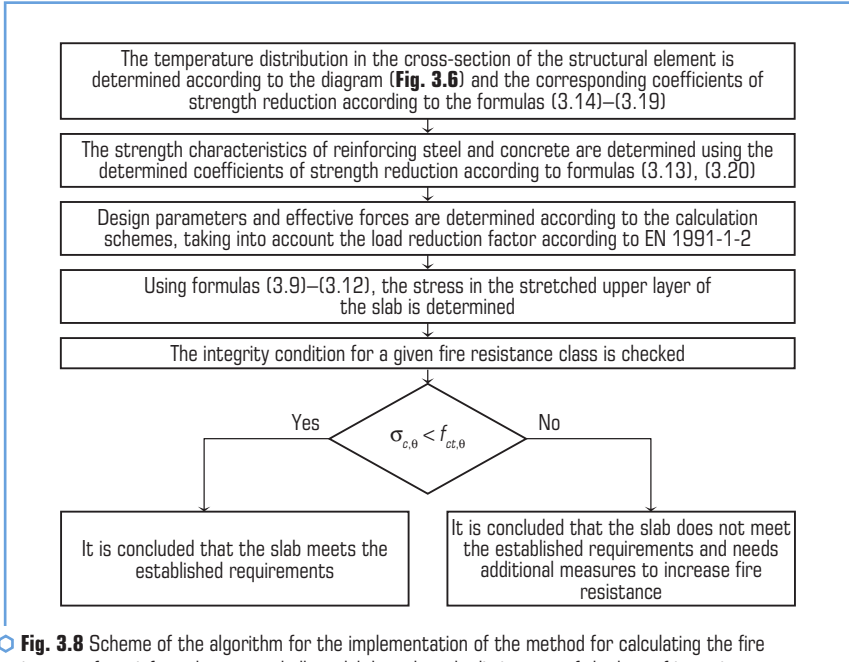


Fig. 3.8 Scheme of the algorithm for the implementation of the method for calculating the fire resistance of a reinforced concrete hollow slab based on the limit state of the loss of integrity when longitudinal cracks appear

Table 3.9 Basic methods of numerical investigation of the integrity of reinforced concrete hollow slabs in case of fire

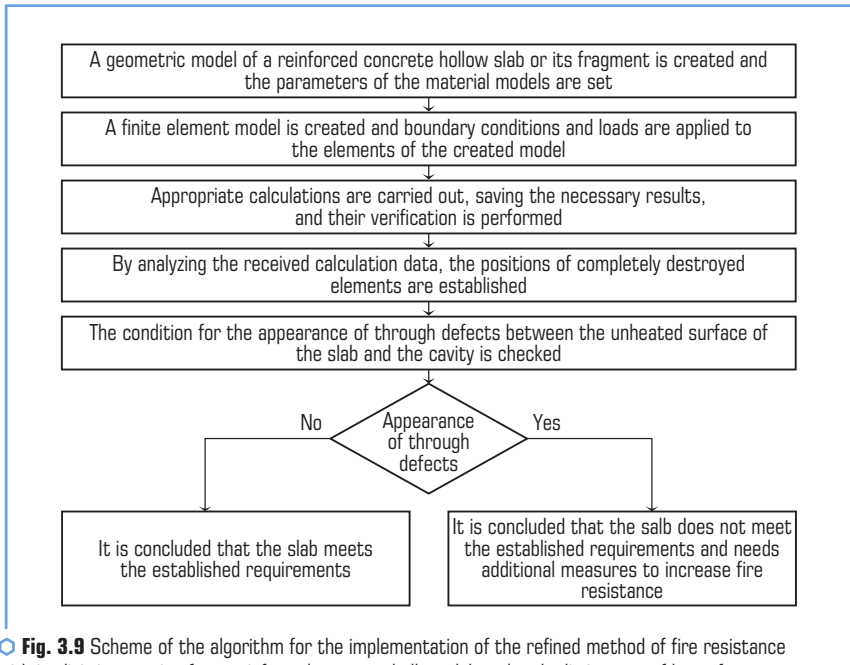
Component of a mathematical model	Used calculation methods
1	2
Heat engineering problem	
Thermal conductivity	Differential non-stationary heat conduction equation, approximated by the finite element method [11]
Boundary conditions	Boundary conditions of the III kind, taking into account convection and radiant heat exchange [11]
Physical nonlinearity	Newton-Raphson method [12]
Thermophysical characteristics	Recommended by EN 1992-1-2
Characteristics of boundary conditions	Recommended by EN 1992-1-2

● Continuation of the Table 3.9

1	2
Structural task	
Stressed and deformed state	Finite element method in nonlinear implementation [12]
Plastic deformation	Associative theory of plasticity [12]
Crack formation criterion	Willem-Warneke concrete strength criterion [12]
Physical and geometric nonlinearity	Newton-Raphson method [12]
Mechanical and thermomechanical characteristics	Deformation diagrams recommended by EN 1992-1-2
Software tools	ANSYS Workbench, ANSYS APDL Mechanical, ABAQUS

When using the method next in the hierarchy, the algorithm for integrating the equations of mechanics by the implicit method is used. This algorithm can be implemented using the scheme presented in **Fig. 3.9**.

At the top of the hierarchical system of methods for calculating the fire resistance of a reinforced concrete hollow slab according to the limit state of the loss of integrity in the scheme of **Fig. 3.10** is a method using explicit integration of the dynamics equations.



○ **Fig. 3.9** Scheme of the algorithm for the implementation of the refined method of fire resistance with implicit integration for a reinforced concrete hollow slab under the limit state of loss of integrity with the appearance of transverse cracks

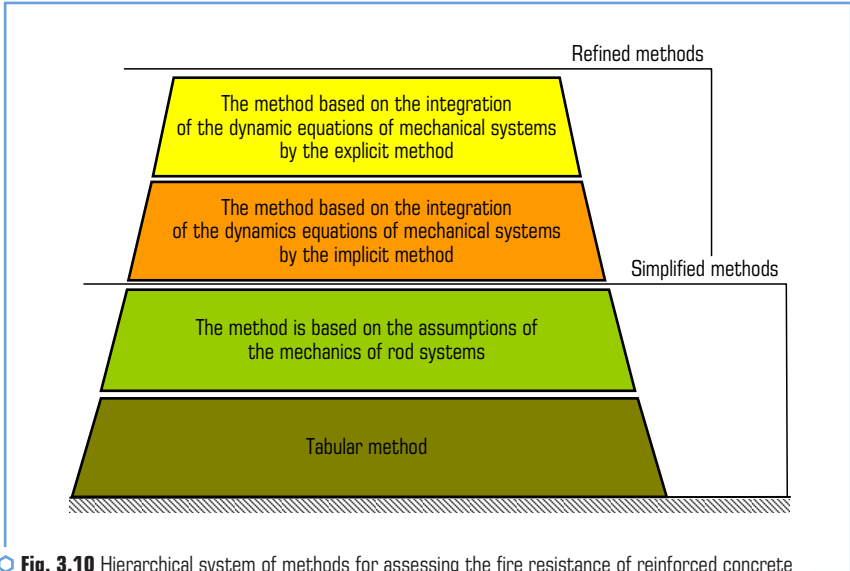


Fig. 3.10 Hierarchical system of methods for assessing the fire resistance of reinforced concrete hollow and ribbed slabs according to the onset of the limit state of loss of integrity

In [10] it is shown that this method also allows to identify the moment of onset of the limit state of loss of integrity based on the calculation results. To carry out the calculation according to this method, a set of initial data is also required, which is presented in the form of a **Table 3.8**, the main mathematical models and theoretical references given in the **Table 3.9** are also used for the implementation.

According to the **Table 3.10** to implement this method, there must be specialized software.

Table 3.10 Basic methods of numerical investigation of the integrity of reinforced concrete hollow slabs in case of fire

Component of a mathematical model	Used calculation methods
1	2
Heat engineering problem	
Thermal conductivity	Differential non-stationary heat conduction equation, approximated by the finite element method [1]
Boundary conditions	Boundary conditions of the III kind, taking into account convection and radiant heat exchange [11]
Physical nonlinearity	Newton-Raphson method [12]
Thermophysical characteristics	Recommended by EN 1992-1-2
Characteristics of boundary conditions	Recommended by EN 1992-1-2

● Continuation of the Table 3.10

1	2
Structural task	
Stressed and deformed state	Finite element method in nonlinear implementation with explicit integration of dynamics equations [13]
Plastic deformation	Associative theory of plasticity [14]
Crack formation criterion	Concrete model CSCM (Continuous Surface Cap Model) [15]
Physical and geometric nonlinearity	Newton-Raphson method [12]
Mechanical and thermomechanical characteristics	Deformation diagrams recommended by EN 1992-1-2
Software tools	ANSYS LS-DYNA

When using this method, the next in the hierarchy, the algorithm for integrating the equations of mechanics according to the explicit method is used. At the same time, the dynamics equations are integrated in the general formulation. This method allows to avoid difficulties with the convergence of processes. Also, this method makes it possible to obtain direct signs of the onset of the limit state of loss of integrity.

The described algorithm can also be implemented using the circuit shown in **Fig. 3.9**.

3.2 FEATURES OF THE HIERARCHICAL STRUCTURE OF CALCULATION METHODS FOR ASSESSING THE FIRE RESISTANCE OF RIBBED SLABS BY LOSS OF INTEGRITY

3.2.1 IMPROVEMENT OF THE TABULAR CALCULATION METHOD FOR ASSESSING THE FIRE RESISTANCE OF REINFORCED CONCRETE RIBBED SLABS

In EN 1992-1-2, as well as for hollow slabs, a similar *Table 5.10* is given for ribbed slabs about certain minimum geometric dimensions of these slabs to ensure the corresponding class of fire resistance. However, this table may be refined in light of new integrity loss data obtained using the approaches proposed in [7]. For a comprehensive study, it was proposed to follow the regularity of the dependence of the fire resistance limit of reinforced concrete ribbed slabs on their most significant geometric parameters, in this case, it is the axial distance of the reinforcing bars and the thickness of the panel in the cell between the ribs of the slab.

According to the accepted assumption, the limit of fire resistance of ribbed slabs is related to the geometric parameters of these structures by a polynomial dependence, just like hollow slabs [8, 9].

In this case, to establish the regression dependence of this type, the matrix of the experimental plan is used, which has the form of a **Table 3.1**.

The **Table 3.11** shows the intervals of factors for the implementation of a full factorial experiment.

● **Table 3.11** Intervals of variation of factors in a full factorial experiment

The thickness of the panel in the cell between the slab ribs, H , mm			The axial distance of the reinforcing bars to the heating surface of the panel between the slab ribs, w , mm		
Lowest value, H_{-1}	Average value, H_0	Largest value, H_1	Lowest value, w_{-1}	Average value, w_0	Largest value, w_1
30	55	80	10	15	20

To obtain reference data for the implementation of a full factorial experiment, the most common structural characteristics of reinforced concrete ribbed slabs were adopted. Mechanical characteristics of concrete and reinforcing steel, as well as geometric characteristics of reinforcement are given in **Table 3.12**.

● **Table 3.12** Technical data on reinforced concrete ribbed slab

Parameter	Units of measurement	Value
Concrete		
Strength class		C 20/25
Density	kg/m ³	2400
Strength limit	MPa	20
Poisson's ratio		0.3
The height of the longitudinal ribs	mm	$H_m = 300$ mm
The height of the transverse ribs	mm	$H_s = 140$ mm
Working reinforcement in longitudinal ribs		
Strength class		A400
Strength limit	MPa	400
Diameter	mm	16
Working fittings in transverse ribs		
Strength class		A400
Strength limit	MPa	400
Diameter	mm	12
Working fittings in the panel between the ribs		
Strength class		A400
Strength limit	MPa	400
Diameter	mm	8
Applied load on the slab		
Applied load as a percentage of the maximum	%	70

By varying the relevant parameters according to the matrix of the plan according to the **Table 3.1** and **Table 3.12** according to the results of the calculations [6, 7] according to the proposed mathematical models of the refined calculation, obtained data for conducting a full factorial experiment, which are shown in **Table 3.13**.

When using the results of the full factorial experiment given in **Table 3.13**, the corresponding coefficients of the regression dependence (3.1) were calculated according to the formulas (3.2) [8, 9].

When applying formulas (3.2), regression coefficients were calculated, which are summarized in the **Table 3.14**.

- **Table 3.13** Parameters of fires in model rooms during a full factorial experiment according to the adopted planning matrix

Experimental situation	1	2	3	4
Limit of fire resistance, U_e , min	46	26	33	18

- **Table 3.14** Regression coefficients for determining the limit of fire resistance of reinforced concrete hollow slabs by the onset of the limit state of loss of integrity

Regression coefficients (7.1)	b_0	b_1	b_2	b_3
Encoded values	30.75	5.25	8.75	1.25
Real values	1.2	0.06	1.2	0.01

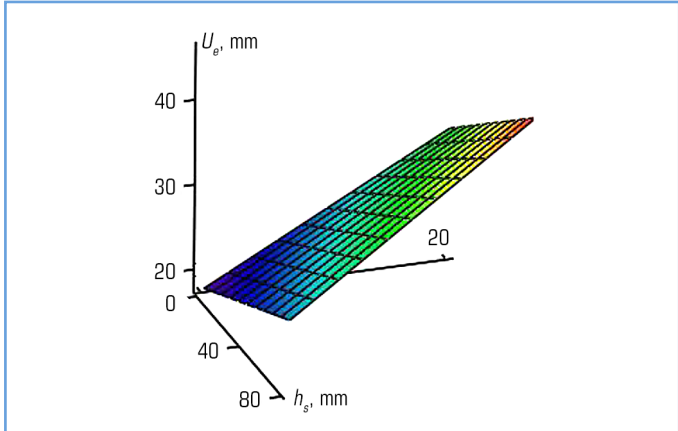
The constructed regression allows to follow the dependence of the fire resistance limit of reinforced concrete ribbed slabs on the panel thickness in the cells between the ribs and the axial distance of the reinforcing rods in this panel.

Thus, the revealed regularity of the limit of fire resistance of reinforced concrete ribbed slabs according to the loss of integrity from the cross-sectional thickness of the panel between the ribs (h_s) and the axial distance from the reinforcement to the heating surface of the panel between the ribs (w_s) can be described using a regression relationship:

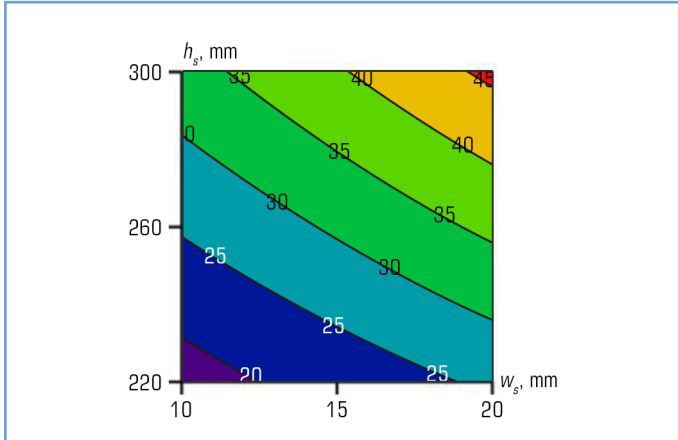
$$U_e = 1.2 + 0.06h_s + 1.2w_s + 0.01 \times h_s \times w_s. \quad (3.21)$$

Also, the detected regularity can be presented using the corresponding constructed surface, which is presented in **Fig. 3.11**. It can be seen on the constructed surface that it has an almost exact flat shape.

It is convenient to determine the limit of fire resistance of reinforced concrete ribbed slabs according to their most significant structural parameters when using the nomogram presented in **Fig. 3.12**.



○ **Fig. 3.11** The surface corresponding to the dependence of the fire resistance limit of a reinforced concrete ribbed slab upon the onset of the limit state of loss of integrity on the slab thickness in the cells between the ribs and the axial distance of the reinforcing rods in the panel



○ **Fig. 3.12** Nomograms of the dependence of the fire resistance limit of a reinforced concrete ribbed slab upon the onset of the limit state of loss of integrity on the slab thickness in the cells between the ribs and the axial distance of the reinforcing rods in the panel

When analyzing the results of the calculated assessment of fire resistance upon the onset of the limit state of loss of integrity, the value of the fire resistance limit, determined by regression dependence and by the refined method, was compared. At the same time, absolute deviation and

relative deviation were used as criteria for the adequacy of the calculated results. The data obtained during the analysis of the adequacy of the calculation results according to the regression dependence are presented in the **Table 3.15**.

● **Table 3.15** Adequacy of the results of assessing the fire resistance limit of reinforced concrete ribbed slabs, determined by regression dependence

Limit of fire resistance, calculated according to MSE, min	Limit of fire resistance, calculated by regression dependence, min	Absolute deviation, min	Relative deviation, %
Slab thickness between the ribs $h_s=30$ mm, Axial distance $w_s=15$ mm			
27.1	25.5	1.6	5.904
Slab thickness $H=50$ mm, Axial distance $w=15$ mm			
32	29.7	2.3	7.188
Slab thickness $H=80$ mm, Axial distance $w=15$ mm			
44	38	6	13.634
Slab thickness $H=80$ mm, Axial distance $w=20$ mm			
48	46	2	4.167
Average values			
–	–	2.975	7.724

The results of the adequacy analysis are given in **Table 3.15**, indicate that the error of the assessed fire resistance for reinforced concrete ribbed slabs, calculated according to the regression dependence, is insignificant and the obtained regression dependence can be used for the assessed fire resistance of reinforced concrete hollow slabs according to the limit state of loss of integrity.

When using the nomogram shown in **Fig. 3.12**, a part of the *Table 5.10* EN 1992-1-2 was clarified. The detailed part of the table is presented below in the form of a **Table 3.16**.

● **Table 3.16** Minimum dimensions and axial distances for reinforced concrete ribbed slabs

Standard fire resistance	Minimum dimensions (mm)				
	Possible combinations of rib width b_{min} and axial distance a		Thickness h_s and axial distance w_s in the slab shelf		
REI 15	$b_{min}=80$ $a=15$			$h_s=30$ $w_s=15$	$h_s=50$ $w_s=10$
REI 30	$b_{min}=80$ $a=15$			$h_s=50$ $w_s=15$	
REI 45	$b_{min}=80$ $a=15$			$h_s=50$ $w_s=25$	
REI 60	$b_{min}=100$ $a=35$	120 25	≥ 200 15	$h_s=80$ $w_s=10$	

The implementation of the tabular method of assessing the fire resistance of reinforced concrete ribbed slabs by the onset of the limit state of loss of integrity has the simplest algorithm. Three main parameters are used as initial data: b_{\min} – slab rib thickness; a – axial distance of reinforcing bars of the rib to the heating surface; h_s – the thickness of the slab panel between the ribs of the slab; w_s – the axial distance of the reinforcing bars of the panel to the heating surface; REI – the fire resistance class that must be provided.

Table 3.16 is used to implement the algorithm of the tabular method. For the required class of fire resistance, the appropriate line is selected, which contains the minimum values of the thickness of the slab shelf and the axial distance of the reinforcing bars. If the real parameters are greater, then the required fire resistance class is considered to be provided.

3.2.2 HIERARCHICAL STRUCTURE OF METHODS FOR ASSESSING THE FIRE RESISTANCE OF REINFORCED CONCRETE RIBBED SLABS ACCORDING TO THE ONSET OF THE LIMIT STATE OF LOSS OF INTEGRITY

The conducted studies, the results of which are described in [7], make it possible to form a hierarchical approach to the methods of calculating the fire resistance of reinforced concrete ribbed slabs upon the onset of the limit state of loss of integrity.

The main tool for achieving such a result is the proposed models of crack formation, which have a through character. In general, the data of the model, obtained as a result of the generalization of a large amount of experimental and computational-theoretical data, are used to justify simplified methods.

According to EN 1992-1-2, the hierarchical system of calculation methods for the loss of load-bearing capacity is a structure based on simplified methods and on top of refined methods. The same system is proposed to be used to assess fire resistance at the limit state of loss of integrity for ribbed and hollow slabs. **Fig. 3.10** presents a hierarchical system of methods for calculating reinforced concrete hollow and ribbed slabs according to the limit state of loss of integrity.

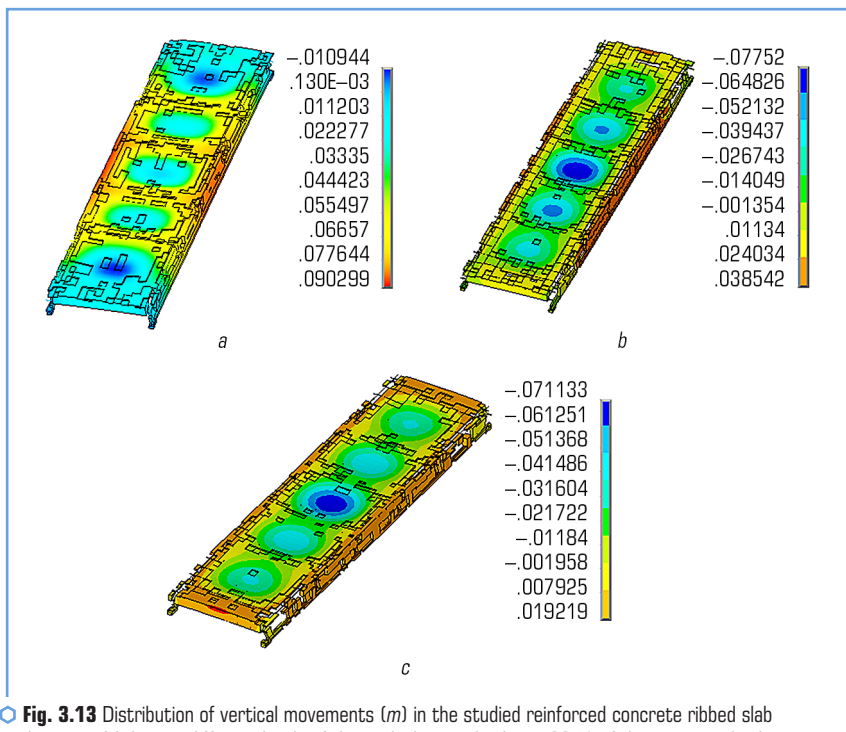
3.2.3 DEVELOPMENT OF A SIMPLIFIED METHOD FOR CALCULATING THE FIRE RESISTANCE OF REINFORCED CONCRETE RIBBED SLABS ACCORDING TO THE LIMIT STATE OF LOSS OF INTEGRITY

To implement the algorithm of the simplified method of calculating the fire resistance of reinforced concrete ribbed slabs upon the onset of the limit state of loss of integrity, the set of initial data presented in **Table 3.8** is used as for hollow slabs. At the same time, other mathematical models of crack formation are used.

According to the results obtained in the studies on modeling the stress-strain state in reinforced concrete ribbed slabs [7], it is possible to describe the main mechanism of the formation of

defects associated with the onset of the limit state of loss of integrity. According to the obtained data, the loss of integrity occurs when the panel is destroyed between the slab ribs. The whole process of deformation and destruction of the slab takes place in several stages. At the first stage, the slab is deformed under the influence of the active load in the form of its downward bending [7]. After the start of the thermal effect of the standard temperature regime of the fire due to the thermal expansion of the concrete of the panel between the ribs, the bend begins to gradually decrease and at a certain point in time the slab bends upwards, however, under the influence of heating, cells are formed between the ribs, in which the panel bends downwards and acquires the shape of holes [7]. The destruction of the formed cells of the panel between the ribs of the slab at the same time occurs by the formation of cracks along the borders of these cells.

In order to study the mechanism of destruction during the research carried out in [7], distributions of the magnitude of vertical displacements were constructed for reinforced concrete ribbed slabs at different levels of the applied effective load. The constructed distributions are shown in **Fig. 3.13**.



○ **Fig. 3.13** Distribution of vertical movements (m) in the studied reinforced concrete ribbed slab at the time of failure at different levels of the applied active load: *a* – 30 % of the maximum load; *b* – 50 % of the maximum load; *c* – 70 % of the maximum load

It is possible to see in **Fig. 3.13** that the nature of the destruction of the panel between the ribs of a reinforced concrete ribbed slab corresponds to the nature of destruction during fire tests of such slabs, described in [16]. **Fig. 3.14** shows a picture of the destruction of reinforced concrete ribbed slabs.



Fig. 3.14 The nature of the destruction of the panel of the ribbed reinforced concrete slab during its fire tests: *a* – during the fire tests; *b* – after the fire tests
Source: [16]

The research conducted in [7] showed a high accuracy of reproduction of the processes occurring in reinforced concrete ribbed slabs, and the possibility of using such an approach [7] as a refined method for assessing the fire resistance of reinforced concrete ribbed slabs according to the limit state of loss of integrity.

Therefore, the partial destruction of the ribbed panel by such a mechanism causes the loss of the integrity of this slab.

In general, the above-described mechanism can be illustrated by a geometric diagram that establishes the main features of the formation of defects (**Fig. 3.15**).

In view of the obtained data on the mechanism of destruction of panels between the ribs of a reinforced concrete ribbed slab, the main prerequisites, hypotheses and assumptions were formulated for the creation of a simplified method for calculating fire resistance at the onset of the limit state of loss of integrity, which are as follows:

1. When breaking, the panel in the cell between the ribs of the reinforced concrete ribbed slab breaks along the lines where the "plastic hinges" are located, of two types: the line delineating the outer contour of the fracture zone and straight lines delineating four facets together with the contour line. These facets make up a geometrically variable system.
2. Calculation of the virtual work of external and internal forces is used for the calculation assessment when applying the principle of possible displacements.

3. The criterion for the destruction of a panel between the ribs of a reinforced concrete ribbed slab is the excess of the total virtual work of external forces over the total virtual work of internal forces.

4. The total work of internal forces is determined using the internal limit moments, which are determined using the recommendations of EN 1992-1-2, taking into account the reduction in the resistance of reinforced concrete according to the zone method.

5. Virtual works are calculated on the possible movements of the kinematic system, which is formed on the lines of "plastic hinges".

6. Taking into account the results of research given in works [17, 18], the contour line of the destruction zone is approximated using Bezier lines.

Using the formulated provisions and the scheme presented in **Fig. 3.15**, the calculation scheme presented in **Fig. 3.16** is built.

The line of the outer contour of the panel failure zone in the cell between the ribs of the reinforced concrete ribbed slab can be approximated using the Bezier curve [17, 18]. The use of this type of approximation is determined by the special properties of Bezier curves. The specified curves are continuous according to the first and second order derivatives, allow to take into account the features of the panel failure zone in the cell between the slab ribs with the calculation of the current values of the geometric characteristics for the calculation of both internal and external moments.

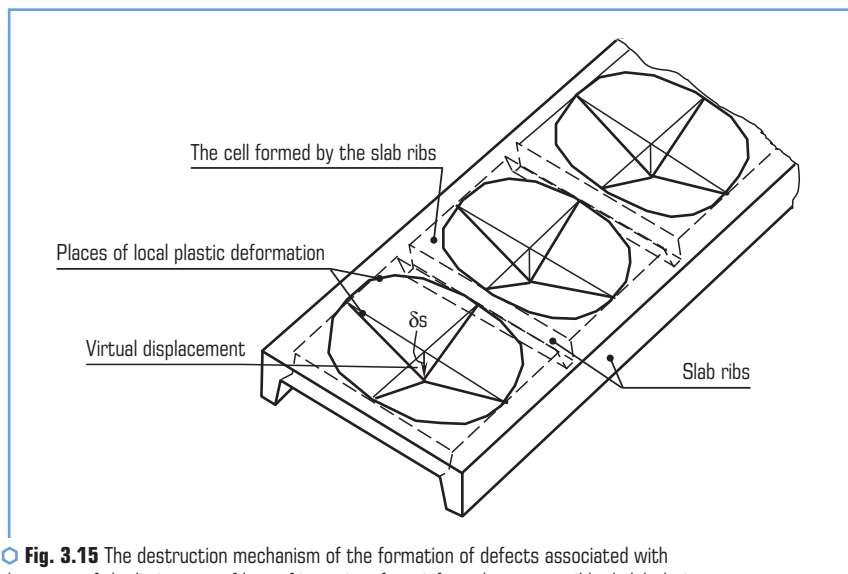


Fig. 3.15 The destruction mechanism of the formation of defects associated with the onset of the limit state of loss of integrity of a reinforced concrete ribbed slab during exposure to the standard fire temperature regime

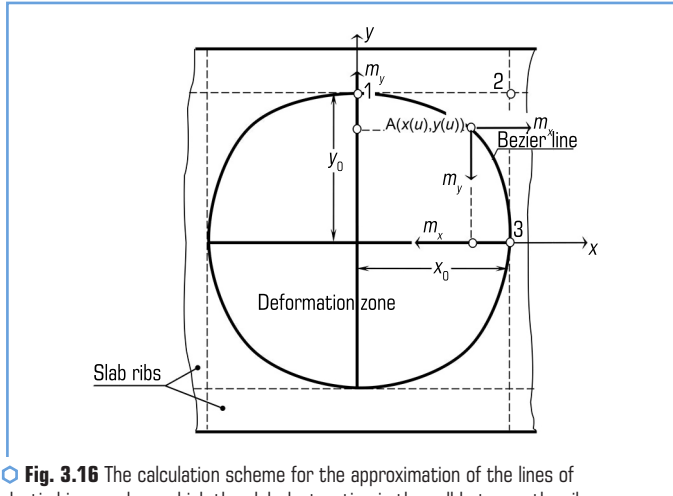


Fig. 3.16 The calculation scheme for the approximation of the lines of plastic hinges, along which the slab destruction in the cell between the ribs of a reinforced concrete ribbed slab occurs

An additional justification for the fact that Bezier lines best reproduce the line of distribution of "plastic joints" in the slab is the geometric representation of the algorithm for their construction, presented in Fig. 3.17 [19].

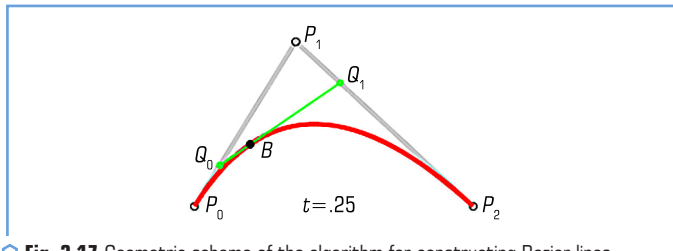


Fig. 3.17 Geometric scheme of the algorithm for constructing Bezier lines

In Fig. 3.17 it can be seen that the effective internal plastic moment is directed along the tangent to the curve, which is built on straight lines that limit the zone of destruction in the cell between the slab ribs.

The vector of coordinates of the reference points, through which the form of the Bezier line function is determined, in the general case is calculated by the expression [20]:

$$F(u) = \sum_{k=1}^n q_k B_{k,n}(u), \quad 0 \leq u \leq 1, \quad (3.32)$$

where $n=3$ – the number of reference points; $B_{k,n}(u)$ – Bernstein polynomials for matching Bezier lines; q_k – vector of coordinates of reference points for constructing a Bezier line.

Bernstein polynomials are described by the formula:

$$B_{k,n}(u) = \frac{n!}{k!(n-k)!} u^k (1-u)^{n-k}. \quad (3.23)$$

In this case, the vector expression (3.22) is decomposed into an algebraic system consisting of two parametric equations:

$$x(u) = \sum_{k=1}^n x_k B_{k,n}(u), \quad y(u) = \sum_{k=1}^n y_k B_{k,n}(u). \quad (3.24)$$

To formulate the expression for calculating the virtual work of internal forces, the calculation scheme presented in **Fig. 3.18**.

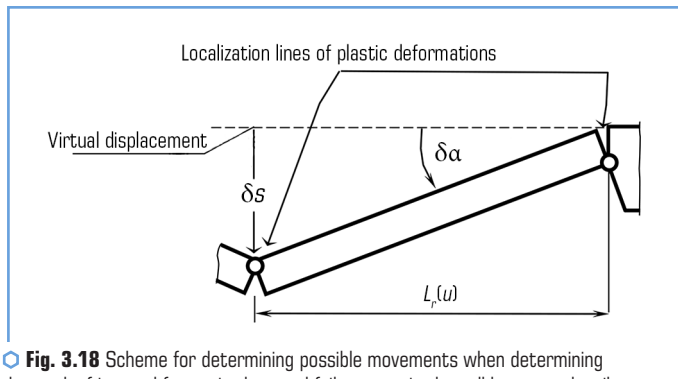


Fig. 3.18 Scheme for determining possible movements when determining the work of internal forces in the panel failure zone in the cell between the ribs of a reinforced concrete ribbed slab

Considering the schemes presented in **Fig. 3.16, 3.18**, the elementary work of internal forces for one symmetric quarter of the facet system at a certain point $A(x(u), y(u))$ in orthogonal directions is determined by the expressions:

$$dW_x = \frac{m_x}{L_{rx}(u)} dl(u) + \frac{m_x}{L_{rx}(u)} x_0, \quad dW_y = \frac{m_y}{L_{ry}(u)} dl(u) + \frac{m_y}{L_{ry}(u)} y_0. \quad (3.25)$$

Here, the elementary section of the curve and the length on the scheme of the elementary kinematic system (**Fig. 3.17**) are determined by the formulas:

$$dl(u) = \sqrt{\left(\frac{dx(u)}{du}\right)^2 + \left(\frac{dy(u)}{du}\right)^2}, L_{rx}(u) = C(u), L_{ry}(u) = x(u). \quad (3.26)$$

Given formulas (3.25) and (3.26), the formula for determining the virtual work of the internal forces of a symmetrical quarter of a mechanical system consisting of facets (**Fig. 3.16**):

$$W = W_x + W_y,$$

$$W_x = m_x \int_0^1 \frac{1}{y(u)} \left(\sqrt{\left(\frac{dx(u)}{du}\right)^2 + \left(\frac{dy(u)}{du}\right)^2} + x_0 \right) du,$$

$$W_y = m_y \int_0^1 \frac{1}{x(u)} \left(\sqrt{\left(\frac{dx(u)}{du}\right)^2 + \left(\frac{dy(u)}{du}\right)^2} + y_0 \right) du. \quad (3.27)$$

The first derivatives of the functions that describe Bezier curves are calculated according to the expressions [20]:

$$\frac{dx(u)}{du} = \sum_{k=1}^n x_k B'_{k,n}(u), \frac{dy(u)}{du} = \sum_{k=1}^n y_k B'_{k,n}(u). \quad (3.28)$$

Derivatives of Bernstein polynomials are calculated by the formula:

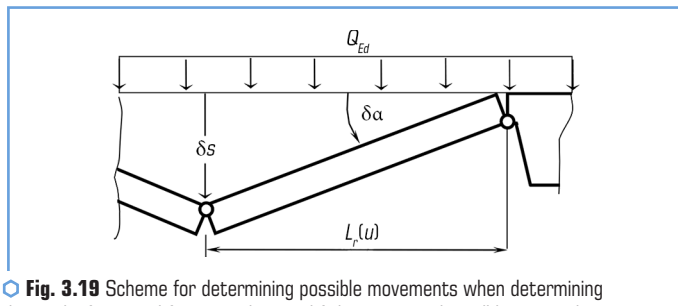
$$B'_{k,n}(u) = B_{k,n}(u) \frac{k - nu}{u(1-u)}. \quad (3.29)$$

In equations (3.27), m_x and m_y are linear limiting moments, which are determined by the formulas:

$$m_x = \frac{M_{Pd,fi,x}}{l_s}, m_y = \frac{M_{Pd,fi,y}}{l_s}, \quad (3.30)$$

where $M_{Pd,fi,x}$ and $M_{Pd,fi,y}$ are the limiting moments of the panel fragments in the cell between the ribs of the reinforced concrete ribbed slab in orthogonal directions along the reinforcing bars. These moments are determined according to the recommendations of EN 1992-1-2, taking into account the reduction in the strength of reinforced concrete by the zone method. Then the obtained value is compared with the moment acting in the slab according to the calculation scheme. If the calculated value of the moment is greater, it means that the limit of fire resistance is not reached.

To determine the virtual work of external forces, the calculation scheme shown in **Fig. 3.19** is used.



○ **Fig. 3.19** Scheme for determining possible movements when determining the work of external forces in the panel failure zone in the cell between the ribs of a reinforced concrete ribbed slab

Considering the schemes presented in **Fig. 3.16, 3.18**, the elementary work of external forces for one symmetric quarter of the facet system at a certain point $A(x(u), y(u))$ in orthogonal directions is determined by the expressions:

$$dU_x = \frac{1}{2} Q_{Ed} \frac{dx(u)}{du} y(u), \quad dU_c = \frac{1}{2} Q_{Ed} \frac{dC(u)}{du} E(u). \quad (3.31)$$

Taking into account formulas (3.31), the final formula for determining the virtual work of external forces of a symmetrical quarter of a mechanical system consisting of facets (**Fig. 3.16**) has the following form:

$$U = U_x + U_y,$$

$$U_x = \frac{1}{2} Q_{Ed} \int_0^1 \frac{dx(u)}{du} y(u) du,$$

$$U_y = \frac{1}{2} Q_{Ed} \int_0^1 \frac{dy(u)}{du} x(u) du. \quad (3.32)$$

To determine compliance with a given class of fire resistance, the corresponding condition should be checked, which has the following form:

$$W \geq U. \quad (3.33)$$

In this way, a simplified method of calculating the fire resistance of a reinforced concrete ribbed slab at the onset of the limit state of loss of integrity is proposed.

When implementing the algorithm for the calculated assessment of integrity according to the energy criterion, the scheme shown in **Fig. 3.20** can be used.

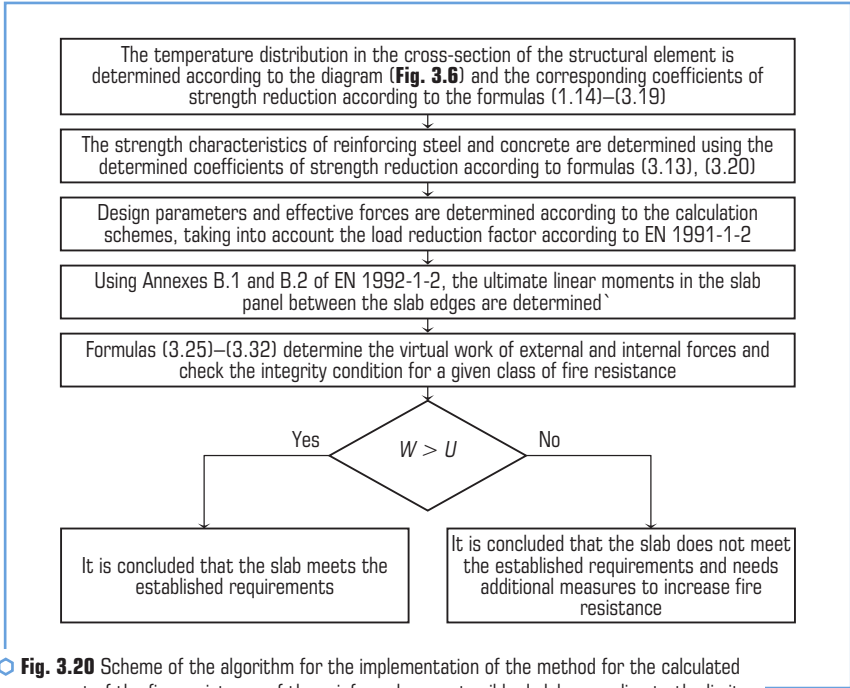


Fig. 3.20 Scheme of the algorithm for the implementation of the method for the calculated assessment of the fire resistance of the reinforced concrete ribbed slab according to the limit state of the loss of integrity according to the energy criterion

The next step in the hierarchy of methods for calculating the fire resistance of reinforced concrete ribbed slabs based on the limit state of loss of integrity requires the use of refined methods. In [7] it was shown that these methods allow, based on the calculation results, to identify the moment of onset of the limit state of loss of integrity. To carry out the calculation according to this approach, a set of initial data is also required, which is presented in the form of a **Table 3.8**, basic mathematical models and theoretical references given in the **Tables 3.9, 3.10** are also used for conducting.

When using the highest methods in the hierarchy, the algorithm of integration of mechanics equations by implicit and explicit methods is used. The algorithm of these methods can be implemented using the scheme presented in **Fig. 3.9**.

Thus, in **Fig. 3.10** the proposed hierarchical system of methods for calculation assessment of reinforced concrete hollow and ribbed slabs according to the limit state of loss of integrity is presented.

The proposed system of approaches to the assessment of fire resistance makes it possible to more accurately determine the fire resistance of structures using tabular, simplified or refined methods. This hierarchical system provides designers with choice at the design stage. If it is possible

to confirm the required class of fire resistance using the tabular method, the use of the simplified method can be avoided. In the case of a negative result, the designer can use a simplified method that takes into account the material, the cross-section of the structure and the load level, allowing to obtain more accurate indicators of fire resistance at the limit state of loss of integrity.

If the simplified method does not give the desired results, it is suggested to apply the refined method. This method more accurately determines the temperature distribution throughout the structure, allowing for a better assessment of concrete and reinforcement degradation, leading to even more accurate results compared to the simplified method.

CONCLUSIONS

Summarizing the obtained results, it can be noted that the actual scientific and technical problem of substantiating the general hierarchical system of methods for calculating the fire resistance of reinforced concrete enclosing structures, in particular reinforced concrete hollow and ribbed slabs upon the onset of the limit state of loss of integrity during the thermal effect of the standard fire temperature regime, was solved. At the same time, the following main results were obtained:

1. The regularities of the onset of the limit state of loss of integrity of reinforced concrete hollow slabs during the thermal effect of the standard temperature regime of fire from their structural parameters were studied.

2. It was found that the studied regularity of the limit of fire resistance of reinforced concrete hollow slabs according to the loss of integrity from the height of the section (H) and the axial distance from the reinforcement to the heating surface of the slab (w) can be described using the regression dependence $U_e = 3.37 + 0.119H + 1.01w + 0.000625 \times H \times w$.

3. It was proved that the obtained regression dependence of the limit of fire resistance of reinforced concrete hollow slabs on their structural parameters allows obtaining adequate results, since the average error does not exceed 12 %.

4. On the basis of the obtained regularities, a nomogram was built to assess the fire resistance limit for reinforced concrete hollow slabs upon the onset of the limit state of loss of integrity.

5. A reference table was created for the assessed fire resistance of reinforced concrete hollow slabs based on the loss of integrity depending on the height of the section and the axial distance from the armature to the heating surface of the slab to justify the corresponding tabular method.

6. On the basis of the results obtained in this work and [5, 10], a hierarchical system of methods for calculating the calculation of reinforced concrete hollow slabs based on the onset of the limit state of loss of integrity was substantiated by creating algorithms for the implementation of simplified and refined methods substantiated in the work.

7. The regularities of the onset of the limit state of loss of integrity of reinforced concrete ribbed slabs during the thermal effect of the standard temperature regime of fire from their structural parameters were studied.

8. The regularity of the limit of fire resistance of reinforced concrete ribbed slabs based on the loss of integrity from the cross-sectional thickness of the panel between the ribs (h_s) and the axial distance from the reinforcement to the heating surface of the panel between the ribs (w_s) has been revealed and can be described using the regression dependence $U_e = 1.2 + 0.06h_s + 1.2w_s + 0.01 \times h_s \times w_s$.

9. It was proved that the obtained regression dependence of the limit of fire resistance of reinforced concrete ribbed slabs on their structural parameters allows obtaining adequate results, since the average error does not exceed 8 %.

10. On the basis of the obtained regularities, a nomogram was built to assess the fire resistance limit for reinforced concrete ribbed slabs upon the onset of the limit state of loss of integrity.

11. A reference table was created for the assessed fire resistance of reinforced concrete ribbed slabs based on the loss of integrity depending on the cross-section thickness of the panel between the ribs and the axial distance from the armature to the heating surface of the panel between the ribs of the slab to justify the appropriate tabular method.

12. Based on the results, in this work and in [6, 7], a hierarchical system of methods for calculating the assessed value of reinforced concrete ribbed slabs based on the onset of the limit state of loss of integrity was substantiated by creating algorithms for the implementation of simplified and refined methods substantiated in the work.

13. On the basis of the proposed approaches, a general hierarchical system of calculation methods for assessing the fire resistance of reinforced concrete hollow and ribbed slabs was created based on the onset of the limit state of loss of integrity.

REFERENCES

1. Pozdieiev, S. V. (20212). Development of scientific basis for determination of fire endurance of bearing reinforced concrete structures [Doctoral dissertation; Instytut derzhavnoho upravlinnia u sferi tsyvilnoho zakhystu].
2. Kovalov, A. I. (2023). Development of the scientific basis of assessing the fire resistance of fireproof reinforced concrete building structures [Doctoral dissertation; Natsionalnyi universytet tsyvilnoho zakhystu Ukrainy Derzhavnoi sluzhby Ukrainy z nadzvychainykh sytuatsii].
3. Kovalov, A., Konoval, V., Khmyrova, A., Dudko, K. (2019). Parameters for simulation of the thermal state and fire-resistant quality of hollow-core floors used in the mining industry. *E3S Web of Conferences*, 123, 01022. <https://doi.org/10.1051/e3sconf/201912301022>
4. Sidnei, S., Nuianzin, V., Kostenko, T., Berezovskyi, A., Waşik, W. (2023). A Method of Evaluating the Destruction of a Reinforced Concrete Hollow Core Slab for Ensuring Fire Resistance. *Journal of Engineering Sciences*, 10 (2), D1–D7. [https://doi.org/10.21272/jes.2023.10\(2\).d1](https://doi.org/10.21272/jes.2023.10(2).d1)
5. Sidnei, S., Myroshnyk, O., Kovalov, A., Veselivskyi, R., Hryhorenko, K., Shnal, T., Matsyk, I. (2024). Identifying the evolution of through cracks in iron-reinforced hollow slabs under the

influence of a standard fire temperature mode. *Applied Mechanics*, 4 (7 (130)), 70–77. <https://doi.org/10.15587/1729-4061.2024.310520>

6. Sidnei, S., Berezovskyi, A., Kasiarum, S., Lytvynenko, O., Chastokolenko, I. (2023). Revealing patterns in the behavior of a reinforced concrete slab in fire based on determining its stressed and deformed state. *Eastern-European Journal of Enterprise Technologies*, 5 (7 (125)), 43–49. <https://doi.org/10.15587/1729-4061.2023.289930>
7. Тут будет ссылка с ВЕЖПТ за октябрь-2024.
8. Vasylykovskiy, O. M., Leshchenko, S. M., Vasylykovska, K. V., Petrenko, D. I. (2016). *Pidruchnyk doslidnyka*. Kirovohrad, 204.
9. Horvat, A. A., Molnar, O. O., Minkovych, V. V. (2019). *Metody obrobky eksperymentalnykh danykh z vykorystanniam MS Excel*. Uzhhorod: Vydavnytstvo UzhNU "Hoverla", 160.
10. Pozdieiev, S., Sidnei, S., Nekora, O., Subota, A., Kulitsa, O. (2023). Study of the Destruction Mechanism of Reinforced Concrete Hollow Slabs Under Fire Conditions. *Smart Technologies in Urban Engineering*, 447–457. https://doi.org/10.1007/978-3-031-46877-3_40
11. Wickström, U. (2016). *Temperature Calculation in Fire Safety Engineering*. Springer International Publishing. <https://doi.org/10.1007/978-3-319-30172-3>
12. S. Ma, S. Y. A., May, I. M. (1986). The Newton-Raphson method used in the non-linear analysis of concrete structures. *Computers & Structures*, 24 (2), 177–185. [https://doi.org/10.1016/0045-7949\(86\)90277-4](https://doi.org/10.1016/0045-7949(86)90277-4)
13. Cremonesi, M., Franci, A., Idelsohn, S., Oñate, E. (2020). A State of the Art Review of the Particle Finite Element Method (PFEM). *Archives of Computational Methods in Engineering*, 27 (5), 1709–1735. <https://doi.org/10.1007/s11831-020-09468-4>
14. Rainone, L. S., Tateo, V., Casolo, S., Uva, G. (2023). About the Use of Concrete Damage Plasticity for Modeling Masonry Post-Elastic Behavior. *Buildings*, 13 (8), 1915. <https://doi.org/10.3390/buildings13081915>
15. Murray, Y. D., Abu-Odeh, A., Bligh, R. (2006). Evaluation of Concrete Material Model 159. FHWA-HRT-05-063.
16. Janssen, R. (2013). *Fire Spalling of Concrete*. Doctoral thesis in Concrete structures. Stockholm.
17. Pozdieiev, S., Nekora, O., Kryshstal, T., Sidnei, S., Shvydenko, A. (2019). Improvement of the estimation method of the possibility of progressive destruction of buildings caused by fire. *IOP Conference Series: Materials Science and Engineering*, 708 (1), 012067. <https://doi.org/10.1088/1757-899x/708/1/012067>
18. Pozdieiev, S., Nekora, O., Kryshstal, T., Zazhoma, V., Sidnei, S. (2018). Method of the calculated estimation of the possibility of progressive destruction of buildings in result of fire. *MATEC Web of Conferences*, 230, 02026. <https://doi.org/10.1051/mateconf/201823002026>
19. Vambersky, J. N. J. A. (1994). Precast concrete in buildings today and hi the future. *The Structural Engineer*, 72 (15).
20. Khern, D., Beiker, M. P. (2005). *Kompiuternaia hrafyka y standart OpenGL*. Moscow: Vyliams, 1168.

CHAPTER 4

ESTABLISHING A HIGH-QUALITY TECHNICAL CONDITION AT
THE DESIGN STAGE: PROMISING CONCEPTS OF LOAD-BEARING
COMPONENTS OF CAR STRUCTURES

ABSTRACT

Most often in the practice of creating multifunctional technical means, a combination of elements that are separate in terms of their functions is used. Its main directions include: connecting different levels of the constructive hierarchy (modules, nodes, basic elements) of components without changing their forms and properties, and with mutual coordination of forms and properties; introducing new principles of functioning to car constructs on the existing element base and on a new element base; taking into account at the design stage the prerequisites for the constructive implementation of future innovative design solutions.

Today, the most promising from the point of view of the practical creation of multifunctional freight car components are the following directions identified and presented in detail in the article: elastic-dissipative, non-rigid articulated and multi-material. It was the solution of such a scientific and applied task that became the aim of the research, the results of which are presented in this section of the monograph.

To achieve the aim, the following scientific and applied objectives were identified and solved: analysis of information sources that highlight the issues of the prospects for the development of non-load-bearing components of freight car structures; development of a mathematical description of the procedure for creating car components with a useful pre-stressed and/or deformed state; development of theoretical aspects of creating useful pre-stressed and/or deformed non-load-bearing components of car structures; development of a promising useful pre-stressed and/or deformed concept of a covered hopper car for transporting cement and a pellet car, a platform car from leaf springs, a hopper car for transporting grain from leaf springs, a hopper car for transporting mineral fertilizers from leaf springs, a hollow-bottomed gondola car made of leaf springs, a universal covered car with racks with damping properties, a universal hopper car for transporting grain with racks with damping properties; development of a promising concept of a railway tank car with supports in the form of leaf and disc springs; development of a promising articulated concept of a 4-axle dump car, a hopper car for transporting grain and mineral fertilizers, a universal platform car, a universal covered car, a hollow-bottomed gondola, a railway tank; development of a promising multi-material concept of a covered car and a railway tank; development of a promising railway

tank with a multi-material concept of supports; systematization of the obtained developments and formulation of general conclusions.

The presented directions for creating multifunctional components of freight cars will allow to obtain positive results in their manufacture and operation. Such positive results include: increasing the life cycle of the studied means, reducing their material consumption and increasing the load-bearing capacity, improving maintainability, increasing crack resistance, reducing/completely eliminating stresses of different signs.

KEYWORDS

Transport mechanics, railway transport, cars, load-bearing systems, promising structures.

The results of the analysis of world and national trends in the development of means of transport have shown that a promising direction for improving their structures is the implementation of innovative principles of functioning into the components. The corresponding trends are defined in various levels of transport development strategies and programs. Of particular importance in this regard is the resolution of relevant issues for the load-bearing systems of means of transport. Among means of railway transport, in the development of this direction, special attention should be paid to freight cars, the structures of which mainly represent general load-bearing mechanical systems.

The aim of the publication is to highlight the obtained scientific and practical developments in the creation of promising concepts of load-bearing component structures of freight cars.

To achieve the aim, a number of the following scientific and technical objectives were identified and solved:

- 1) analysis of information sources that highlight the issues of the prospects for the development of non-load-bearing components of freight car structures;
- 2) development of a mathematical description of the procedure for creating car components with a useful pre-stressed and/or deformed state;
- 3) creation of theoretical aspects of creating useful pre-stressed and/or deformed non-load-bearing components of car structures;
- 4) development of a promising useful pre-stressed and/or deformed concept of a covered hopper car for transporting cement;
- 5) development of a promising useful pre-stressed and/or deformed concept of a pellet car;
- 6) development of a promising elastic-dissipative concept of a platform car made of leaf springs;
- 7) development of a promising elastic-dissipative concept of a hopper car for transporting grain with leaf springs;
- 8) development of a promising elastic-dissipative concept of a hopper car for transporting mineral fertilizers with leaf springs;

9) development of a promising elastic-dissipative concept of a hollow-bottomed gondola car with leaf springs;

10) development of a promising elastic-dissipative concept of a universal covered car with racks with damping properties;

11) development of a promising elastic-dissipative concept of a universal hopper car for transporting grain with racks with damping properties;

12) development of a promising concept of a railway tank with supports in the form of leaf springs;

13) development of a promising concept of a railway tank with supports in the form of disc springs;

14) development of a promising articulated concept of a 4-axle dump car;

15) development of a promising articulated concept of a hopper car for transporting grain;

16) development of a promising articulated concept of a hopper car for transporting mineral fertilizers;

17) development of a promising articulated concept of a universal platform car;

18) development of a promising articulated concept of a universal covered car;

19) development of a promising articulated concept of a hollow-bottomed gondola car;

20) development of a promising articulated concept of a railway tank;

21) development of a promising multi-material concept of a covered car;

22) development of a promising multi-material concept of a railway tank;

23) development of a promising railway tank with a multi-material concept of supports;

24) systematization of the obtained developments and formulation of general conclusions.

4.1 ANALYSIS OF INFORMATION SOURCES THAT HIGHLIGHT THE ISSUES OF THE PROSPECTS FOR THE DEVELOPMENT OF NON-LOAD-BEARING COMPONENT STRUCTURES OF FREIGHT CARS

The search for information sources was aimed at finding works that are devoted to highlighting the developments and results of research on the creation of promising concepts of non-load-bearing component structures of transport engineering.

Works [1–4] present the prospects for the development of freight car structures determined by the authors. At the same time, the need to apply the latest achievements in materials science is identified as the main areas of development.

Research [5–9] is aimed at finding scientific and practical solutions to improve transport processes. And as one of the key aspects, the need to update transport fleets with new generation models is highlighted, which requires the creation of appropriate scientific and practical tools.

Works [10–13] present the scientific results of theoretical and practical developments on the prospects for the development of machine-building structures. The importance of scientists and engineers paying attention to the problems of structural and material innovative solutions is

separately highlighted, which is certainly connected with the deployment of design works of materials science and architectural and structural search.

In articles [14–16], the authors presented scientific results on the optimization of processes occurring in the power module of a vehicle. At the same time, the main attention was paid to increasing energy efficiency.

In scientific works [17–20], damage to cars at the final stages of the life cycle (corrosion, accident, impacts) was considered. The feasibility of deploying scientific research and development work to reduce and correct operational deformations was determined.

Scientific research highlights a new approach to improving energy transfer processes between various components of vehicles. However, not enough attention has been paid to the redistribution of stresses.

In works [24–26], the results of experimental studies of subway rolling stock are presented. The main attention is paid to energy efficiency. However, the force interaction of the corresponding modules and blocks has not been studied.

Summarizing the above, it can be noted that in all the above scientific works, the features of determining promising concepts of load-bearing component structures have not been studied.

4.2 MATHEMATICAL DESCRIPTION OF THE PROCEDURE FOR CREATING CAR COMPONENTS WITH A USEFUL PRE-STRESSED AND/OR DEFORMED STATE

This section focuses on the author's hypothesis about the feasibility of introducing pre-stressed and/or deformed load-bearing elements into the design of freight cars. Pre-stressing and/or deformation of structures should be understood as various methods of artificially regulating stresses (manipulating the stressed-deformed state) in structures to increase their efficiency.

Intervention in the natural operation of an object to directional change its potential deformation energy can occur at different stages of the life cycle: during manufacturing, during repairs, during operation or modernization and at different levels: structural elements or assemblies, modules and the system as a whole.

The criteria for the effectiveness of applying prestressing in metal structures can be both economic requirements for reducing the mass and cost of objects, and technological (increasing rigidity, preserving the shape of load-bearing structural elements, changing dynamic characteristics, increasing crack resistance and reducing fatigue strength, etc.). In this regard, metal structures have wider possibilities for applying prestressing and/or deformation than reinforced concrete and reinforced concrete structures, where this technique has developed primarily as a means of combating low strength of concrete during tension.

Generalizing the universal mathematical record of the procedure for implementing a useful prestressed and/or deformed state in the components of railcar structures, it is necessary to take into account the following requirements:

- 1) systematically consider economic efficiency at the stages of the freight car life cycle;
- 2) as the main criterion for the implementation of the useful prestressed and/or deformed state, the total vector of the useful prestressed and/or deformed state is used, which in magnitude and direction is directed towards counteracting the total vector of operational loads;
- 3) the mathematical model must include an objective function (OF), which is a vector for finding (searching for) the optimal design option from the region of admissible solution area (ASA) selected from the possible solution area (PSA).

Due to the fact that the application of a mathematical notation (model) must effectively operate as an implementation of the prestressed and/or deformed state, or their combinations, it is necessary to create sufficient prerequisites for describing the corresponding states, namely, for example, the dependences of various deflections and bends, internal and external mechanical stresses on thermal or mechanical effects.

As noted above, the main criterion for creating a useful prestressed and/or deformed state is the total vector of the useful prestressed and/or deformed state, which in magnitude and direction is directed towards counteracting the total vector of operational loads:

$$\sum \overline{F^{UPSDS}}(\bar{Y}) \rightarrow -\sum \overline{F^{OPER}}, \quad (4.1)$$

where $\sum \overline{F^{UPSDS}}(\bar{Y})$ – where the total vector of the useful pre-stressed and/or deformed state;
 $\sum \overline{F^{OPER}}$ – the total vector of operational loads.

In this case, the total vector of the useful pre-stressed and/or deformed state is a function of the scalar sum of the vectors of stresses and deformation of the component. That is, the possible solution area (PSA) is formed by the fields of possible changes in the factors of the implementation of the corresponding methods for creating a pre-stressed and/or deformed state:

$$PSA = \left\{ \bar{Y} \left| \begin{array}{l} \sum \bar{a}_x^{\min} \leq \sum \bar{a}_x \leq \sum \bar{a}_x^{\max}; \quad \sum \bar{a}_y^{\min} \leq \sum \bar{a}_y \leq \sum \bar{a}_y^{\max}; \quad \sum \bar{a}_z^{\min} \leq \sum \bar{a}_z \leq \sum \bar{a}_z^{\max}; \\ \sum \bar{b}_x^{\min} \leq \sum \bar{b}_x \leq \sum \bar{b}_x^{\max}; \quad \sum \bar{b}_y^{\min} \leq \sum \bar{b}_y \leq \sum \bar{b}_y^{\max}; \quad \sum \bar{b}_z^{\min} \leq \sum \bar{b}_z \leq \sum \bar{b}_z^{\max}; \\ a \in [1; s]; b \in [1; k] \end{array} \right. \right\}, \quad (4.2)$$

where $\sum \bar{a}_x^{\min} \leq \sum \bar{a}_x \leq \sum \bar{a}_x^{\max}; \sum \bar{a}_y^{\min} \leq \sum \bar{a}_y \leq \sum \bar{a}_y^{\max}; \sum \bar{a}_z^{\min} \leq \sum \bar{a}_z \leq \sum \bar{a}_z^{\max}; a \in [1; s]$ – the specified variable parameters: the magnitude and direction of the useful prestresses;
 $\sum \bar{b}_x^{\min} \leq \sum \bar{b}_x \leq \sum \bar{b}_x^{\max}; \sum \bar{b}_y^{\min} \leq \sum \bar{b}_y \leq \sum \bar{b}_y^{\max}; \sum \bar{b}_z^{\min} \leq \sum \bar{b}_z \leq \sum \bar{b}_z^{\max}; b \in [1; k]$ – the specified variable parameters: the magnitude and direction of the useful prestresses.

The admissible solution area (ASA) in which the desired solution is located, is separated from the possible solution area (PSA) by the functional requirements and constraints of the secondary criteria:

$$\bar{Y} \in ASA \in PSA. \quad (4.3)$$

Previous studies have shown that the above criteria and their corresponding limitations for freight cars should be considered taking into account technical, economic and operational limitations. The above criteria and limitations for freight cars should be considered the following technical, economic and operational characteristics:

M_C – tare weight of the car, which must be within the specified design limitations;

P_C – load capacity, which must be within the specified design limitations;

V_C – full (loading) volume of the body, which must be within the specified design limitations (in particular, taking into account the dimensions and features of the cargo to be transported);

P_C^{run} – running load, which must be within the specified design limitations and is determined by the formula:

$$P_C^{run} = \frac{M_C + P_C}{L_{coup.}}, \quad (4.4)$$

where $L_{coup.}$ – coupling length of the car, m;

C_B – characteristics of the chassis module (for example: flexibility and static deflection of the spring suspension, design speed, etc.), within the specified design limitations established by the NTD;

f_C – structural rigidity, which must be no less than the specified allowable value;

n_y^C – structural stability, which must be no less than the specified allowable value;

n_C – fatigue strength of the structure, which must be no less than the specified allowable value;

B_C – maximum costs for the production of the component, which must be within the specified limitations;

E_C – energy consumption of the absorbing device, which must be within the specified design limitations;

T_C – characteristics of the brake equipment module (for example: calculated brake pressure coefficient, pressure loss in the brake line per unit of time, etc.), which must be within the specified design limitations;

σ_C^I – strength according to the first design mode according to the car design standards, the value of which should not exceed the permissible;

σ_C^{II} – strength according to the second design mode according to the car design standards, the value of which should not exceed the permissible;

σ_C^{III} – strength according to the third design mode according to the car design standards, the value of which should not exceed the permissible;

σ_C^{imp} – impact strength according to the car design standards, the value of which should not exceed the permissible;

P_C – calculated static load from the wheelset on the rails, which should not exceed the permissible value established by the regulatory and technical documentation.

It is possible to take into account other functional requirements and restrictions of the corresponding secondary criteria, which are added depending on the design features of the studied car model.

Then the admissible solution area (ASA) will take the following form:

$$ASA = \left\{ \bar{Y} \left[\begin{array}{l} \min \leq M_C \leq \max; P_{\min} \leq P_C \leq P_{\max}; V_{\min} \leq V_C \leq V_{\max}; \\ P_{\min}^{run} \leq P_C^{run} \leq P_{\min}^{run}; I_{\min} \leq C_C \leq C_{\max}; [f] \leq f_C; [n_y] \leq n_y^C; [n] \leq n^C; \\ B_{\min} \leq B_C \leq B_{\max}; \min \leq E_C \leq E_{\max}; T_{\min} \leq T_C \leq T_{\max}; \\ [\sigma] \leq \sigma_C; [\sigma] \leq \sigma_C; [\sigma] \leq \sigma_C; [\sigma^{imp}] \leq \sigma_C^{imp}; [P_C] \leq P_C^C; \\ \sum_{\theta \in [1,s]} \bar{a}_x^{\min} \leq \sum \bar{a}_x \leq \sum \bar{a}_x^{\max}; \sum \bar{a}_y^{\min} \leq \sum \bar{a}_y \leq \sum \bar{a}_y^{\max}; \sum \bar{a}_z^{\min} \leq \sum \bar{a}_z \leq \sum \bar{a}_z^{\max}; \\ \sum \bar{b}_x^{\min} \leq \sum \bar{b}_x \leq \sum \bar{b}_x^{\max}; \sum \bar{b}_y^{\min} \leq \sum \bar{b}_y \leq \sum \bar{b}_y^{\max}; \sum \bar{b}_z^{\min} \leq \sum \bar{b}_z \leq \sum \bar{b}_z^{\max} \end{array} \right] \right\}. \quad (4.5)$$

The highlighted approach to creating a generalizing universal mathematical notation of the procedure for implementing a useful prestressed and/or deformed state in the components of car structures and the results of its implementation can be used in solving other similar problems.

4.3 THEORETICAL ASPECTS OF CREATING USEFUL PRESTRESSED AND/OR DEFORMED LOAD-BEARING COMPONENTS OF CAR STRUCTURES

One of the main scientific and technical tasks, the results of which directly affect the efficiency of the freight car fleet, is the development of new or modernization of existing models of freight cars in order to reduce their material consumption. At the same time, a promising method for reducing the material consumption (with a corresponding increase in load capacity) of freight cars is the search and implementation of structural excess safety margins, by providing their component elements with optimal structural forms and their execution from materials with directional properties while meeting the conditions of strength and operational reliability. In addition, the results of the analysis of the impact of operational factors on the structures of the load-bearing systems of freight cars showed that one of the main types of damage to their elements is cracks.

As the positive experience of other industries related to the manufacture of metal structures shows, one of the promising directions for solving both of the above scientific and technical problems is the use of useful pre-stressed and/or deformed multifunctional structures in the load-bearing systems of mechanical engineering. However, consideration of the current scientific and technical background on the profile of the issues studied showed the lack of meaningful information on the creation of relevant theoretical aspects of solving such a problem for freight cars.

The main purpose of considering and applying the specified approach is to increase the life cycle of railway rolling stock, reduce their material consumption and increase load capacity, improve maintainability, increase crack resistance, reduce/completely eliminate stresses of different signs.

According to the current and prospective regulatory documentation, when calculating all types of cars, two main calculation modes are established: I and III [1–4].

According to the I calculation mode (rare combination of extreme loads), the permissible stresses are selected close to the yield point of the material used, taking into account the nature of the load action and the properties of the material (from 0.85 to 1.1 of the minimum yield point σ_t) in order to prevent the appearance of residual deformations and destruction of the elements and parts of the car.

According to the III calculation mode (frequent combination of moderate operational loads), the permissible stresses are selected based on the endurance limit of the material at a level of from 0.5 σ_t to 0.65 σ_t in order to prevent fatigue destruction of the assembly or part.

General rules for calculating the bearing capacity of railcar structures provide:

- calculation of body elements shall be performed according to permissible stresses and a margin of stability;
- calculation of individual frame elements shall be performed according to permissible stresses and a margin of fatigue resistance.

The basic parameters in the calculation and design of freight cars of all types are:

1) permissible stresses, the value of which, taking into account the margin factors, is determined by the yield strength of the material (σ_t). The margin factor for rolled metal is 0.9–0.95, depending on the operating conditions. The value of the yield strength, as well as other indicators of the mechanical properties of the material;

2) a margin of stability, the value of which, among other things, is determined by the yield strength of the material (σ_t).

The useful prestressing of structures is understood as various methods of directed artificial regulation of stresses (control of the stressed-deformed state) in structures to increase their efficiency in perceiving loads at the stages of the life cycle. In this case, intervention in the natural operation of the object for a directed change in its potential deformation energy can occur at different stages of the life cycle: during manufacturing, during installation, during operation or reconstruction and at different levels. For example, for freight cars: in modules, components, assemblies or basic elements.

The main task of introducing a pre-stressed and/or deformed state is to reduce the magnitude of stresses and/or deformations in the structural components of freight cars by using one or a combination of methods for their creation:

1. Compression of individual stretched, compressed and bent hollow/solid closed/unclosed profiles and entire elements (beams, frames) with various types of tightening from high-strength materials.
2. Preliminary elastic bending of individual elements with subsequent fixation (or welding) of them in a bent state into a whole structural element (beam).
3. Pre-stretching of entire structures or their individual parts in order to increase the elastic work area of the material.

4. Pre-tensioning of individual included flexible rods (cables, wire bundles, reinforcement) in order to perceive compressive forces by them.

5. Temporary loading during the manufacturing and installation of individual elements of structures or the entire structure with or without subsequent fixation, of the structure under load for rational distribution of forces and increasing its rigidity and stability.

6. Creation of pre-stress in rolled profiles by rolling pre-tensioned high-strength wire into them (for example, when creating flexible car joints).

7. Pre-heating/cooling of individual parts in order to increase/decrease their geometric dimensions). An example of an application for freight cars is preheating, which can be used to prevent the formation of cracks and/or to provide the required mechanical properties, for example, impact strength. Preheating can be performed in a furnace or using heating burners, electric plate radiators or induction or radiant heaters.

Next, it is necessary to analyze the load application schemes (**Fig. 4.1**) in accordance with the regulatory framework, which must be taken into account when assessing the strength of the elements of the car bodies according to the modes.

The criteria for the effectiveness of the use of useful prestressing and/or deformation in metal structures can be both economic requirements for reducing material consumption and the cost of objects, and structural and technological (increasing rigidity, preserving the shape of load-bearing structural elements after the influence of technologically determined factors (for example, welding), improving dynamic characteristics, etc.). In this regard, metal structures have broader opportunities and greater prospects for the use of prestressing than reinforced concrete and steel-reinforced concrete, where this technique has developed primarily as a means of combating the low strength of concrete during tension.

In all cases, additional labor is required to regulate internal forces in structures and there remains the possibility of loss or restructuring of the induced background of internal stresses over time due to the development of long-term processes in materials and joints. Therefore, the introduction of rational methods of stress-strain state management into the practice of creating modern railway engineering structures requires the development of appropriate theoretical provisions, methodological foundations and practical tools for each structural form.

The goals of creating useful prestressed and/or deformed multifunctional structures:

1) saving metal and resources in the structures being constructed due to a more favorable distribution of external forces, increasing the area of elastic work;

2) increasing the bearing capacity of structures that are at the stage of operation or reconstruction due to increased loads;

3) reducing the deformability of the entire structure or its individual elements, reducing the frequency or amplitude of oscillations;

4) increasing the stability of individual elements or the entire structure as a whole;

5) increasing the endurance of individual elements under cyclic loads by improving the cycle characteristics;

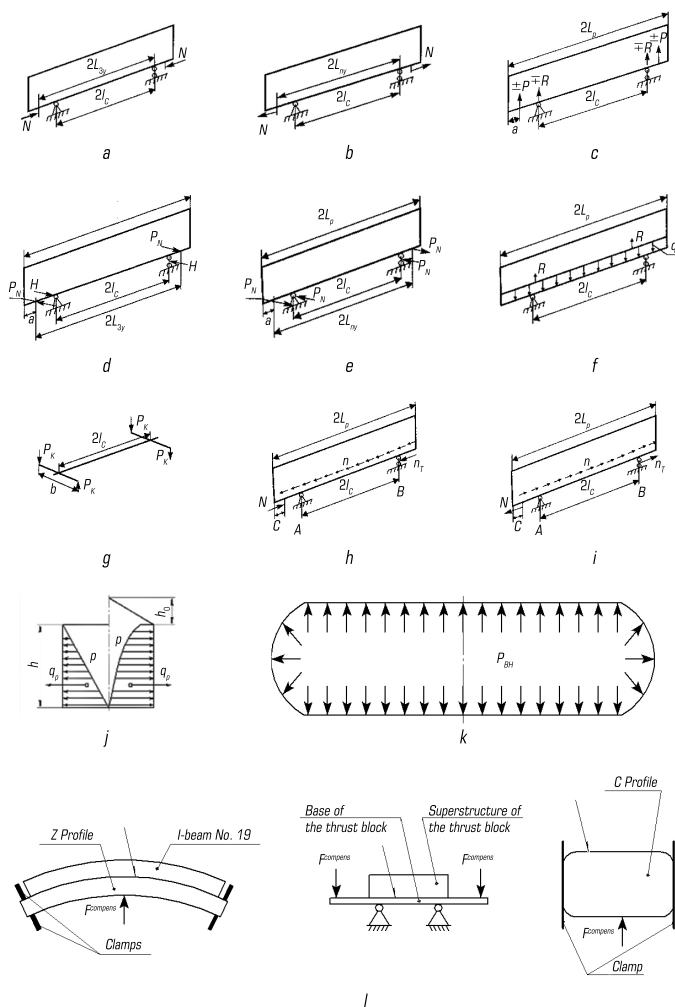


Fig. 4.1 Expanded scheme of applying loads to car structures in various design cases of the life cycle: *a* – longitudinal quasi-static compression force; *b* – longitudinal quasi-static tensile force; *c* – vertical force due to eccentricity between the axes of the auto couplers; *d* – transverse forces in curves under quasi-static compression; *e* – transverse forces in curves under quasi-static tensile force; *f* – vertical load from the mass of the cargo and its own mass; *g* – oblique symmetrical loading (for cars with a base of more than 16 m); *h* – hitting the auto-coupler; *i* – spurt; *j* – expansion (pressure) forces of loose and bulk cargo; *k* – pressure forces of liquids and gases and water hammer forces in tank boilers, reservoirs, tanks; *l* – forces for creating a deformed state (vertical bending) during assembly and welding work

6) favorable change in some properties of the structure (dynamic characteristics under dynamic and seismic influences, aerodynamic characteristics under wind influences, increased resistance to temperature loads (for example, frost resistance);

7) ensuring in some cases ease of installation, and in this regard, a reduction in labor costs;

8) counteracting the occurrence of negative residual deformations from technological factors.

For example, in freight car construction, preliminary deflection of the fixed overall structure when applying large welds: welding an I-beam to welded Z-shaped profiles of the backbone beam of gondolas, assembly structures of the upper gondolas' straps, etc.

The same goals can be achieved by other methods (increasing the area or changing the type of cross-section, the method of connecting elements, etc.) that are more materially expensive. Preliminary useful stress and/or deformation is advisable if the effect obtained from it fully pays off the additional costs. The choice of the final design option should be made on the basis of a feasibility study.

4.4 A PROMISING USEFUL PRESTRESSED AND/OR DEFORMED CONCEPT OF A COVERED HOPPER CAR FOR CEMENT TRANSPORTATION

A promising useful prestressed and/or deformed concept of a covered hopper car for cement transportation relates to car construction and can be used for railway transportation of bulk and bulk cargoes that require protection from precipitation, in particular cement.

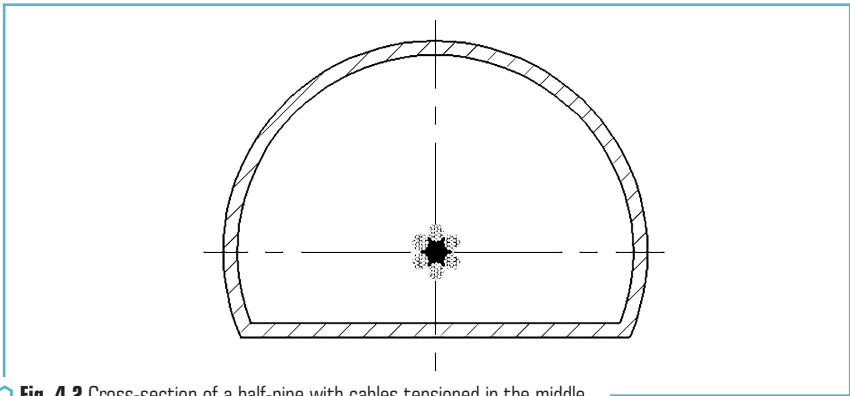
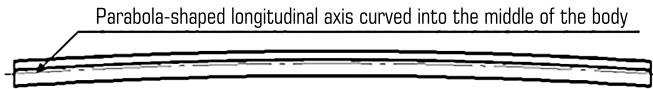


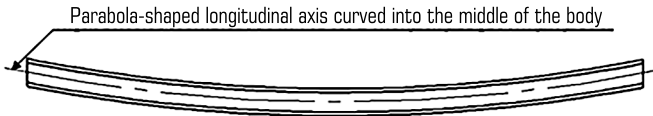
Fig. 4.2 Cross-section of a half-pipe with cables tensioned in the middle

The concept is based on the task of improving the design of the main elements of the frame and body modules, based on the execution of the backbone, end, pivot, middle intermediate beams of the frame module, the strapping of the upper and vertical side wall racks, the strapping of the upper, side racks and intermediate end walls from half-pipes (Fig. 4.2) with cables stretched (usefully

pre-tensioned) in their middles, the backbone beam (**Fig. 4.3**), the frames (**Fig. 4.4**) of the side and end (**Fig. 4.5**) walls are curved parabolically (usefully pre-tensioned) curved into the middle of the body, while meeting the conditions of strength and operational reliability, which will allow reducing its material consumption and wear of non-bearing elements, and as a result, reducing the cost of manufacturing and operating the covered hopper car for cement transportation.



○ **Fig. 4.3** Side view of a useful pre-deformed backbone beam of a covered hopper car concept for transporting cement



○ **Fig. 4.4** Top view of a useful pre-deformed side wall of a covered hopper car concept for transporting cement and pellet car



○ **Fig. 4.5** Top view of a useful pre-deformed end wall of a covered hopper car concept for transporting cement and pellet car

4.5 PROMISING USEFUL PRESTRESSED AND/OR DEFORMED PELLET CAR CONCEPT

Promising useful prestressed and/or deformed pellet car concept relates to railcar construction and can be used for rail transportation of hot pellets and sinter with temperatures up to 700 °C from the production site to the receiving hoppers of the blast furnace.

The concept is based on the task of improving the railway gondola-hopper car for hot pellets and sinter by improving the design of the main elements of the frame and body modules, based on the execution of the backbone, end, pivot, middle intermediate beams of the frame module, the strapping of the upper and uprights of the vertical side walls, the strapping of the upper, uprights of the side and intermediate end walls from half-pipes (**Fig. 4.2**) with cables stretched (usefully pre-tensioned)

in their middles, the backbone beam (Fig. 4.3), the frames (Fig. 4.4) of the side and end (Fig. 4.5) walls are curved parabolically (usefully pre-tensioned) into the middle of the body, while meeting the conditions of strength and operational reliability, which will allow reducing its material consumption and wear of load-bearing elements, and as a result, reducing the cost of manufacturing and operation.

4.6 PROMISING ELASTIC-DISSIPATIVE CONCEPT OF A PLATFORM CAR MADE OF LEAF SPRINGS

The promising elastic-dissipative concept of a platform car made of leaf springs relates to car construction and can be used for railway transportation of wheeled and tracked vehicles, piece goods, forest and long-length goods, box-packed goods, containers and other goods that do not require protection from atmospheric precipitation.

The concept is based on the task of improving the platform car by making the middle part of the backbone beam (Fig. 4.6), transverse and end beams in the form of leaf springs (Fig. 4.7).

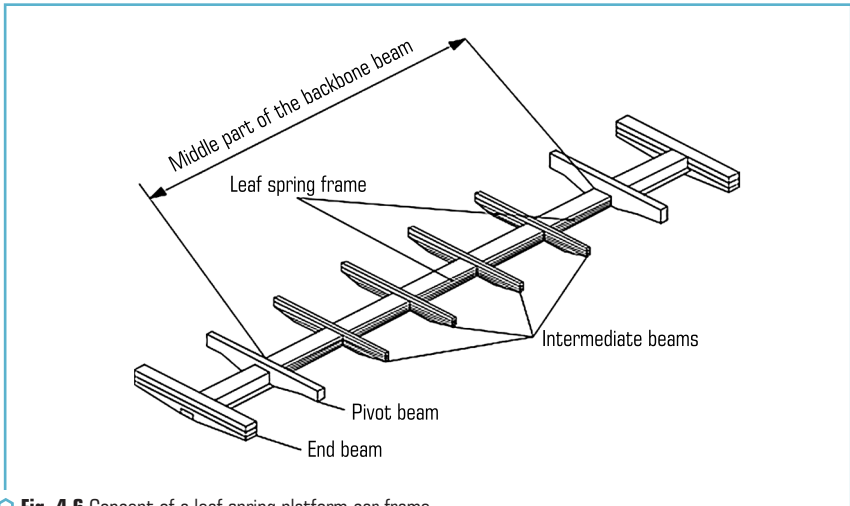


Fig. 4.6 Concept of a leaf spring platform car frame

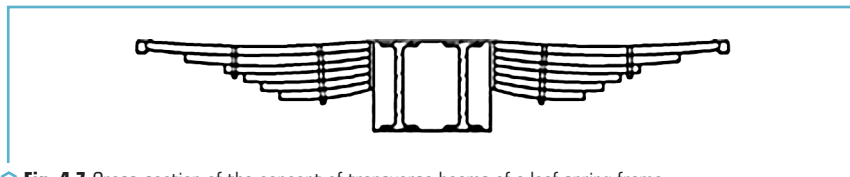


Fig. 4.7 Cross-section of the concept of transverse beams of a leaf spring frame

The introduction of new features in interaction with known ones ensures the absorption of vibration and impact energy, which, as a result, improves the dynamics and strength of the platform car, reduces material consumption, accordingly increases load capacity and increases the service life of the car.

4.7 PROMISING ELASTIC-DISSIPATIVE CONCEPT OF A HOPPER CAR FOR TRANSPORTING GRAIN FROM LEAF SPRINGS

The promising elastic-dissipative concept of a hopper car for transporting grain from leaf springs relates to railcar construction and can be used for freight rail transportation of bulk cargo that requires protection from precipitation, in particular grain.

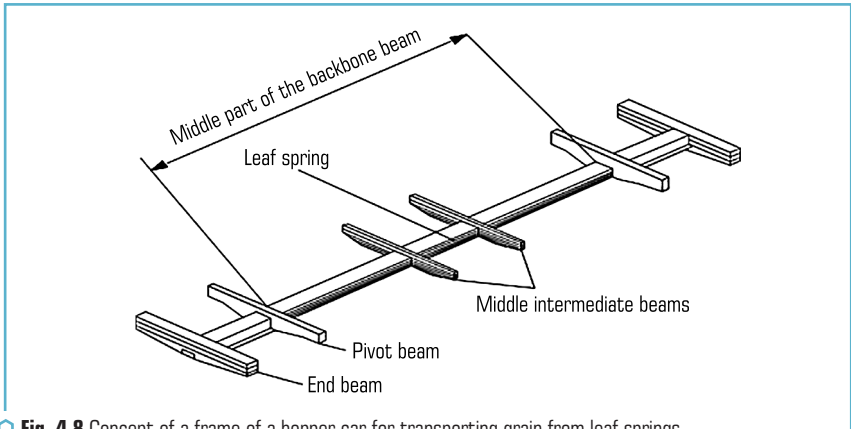


Fig. 4.8 Concept of a frame of a hopper car for transporting grain from leaf springs

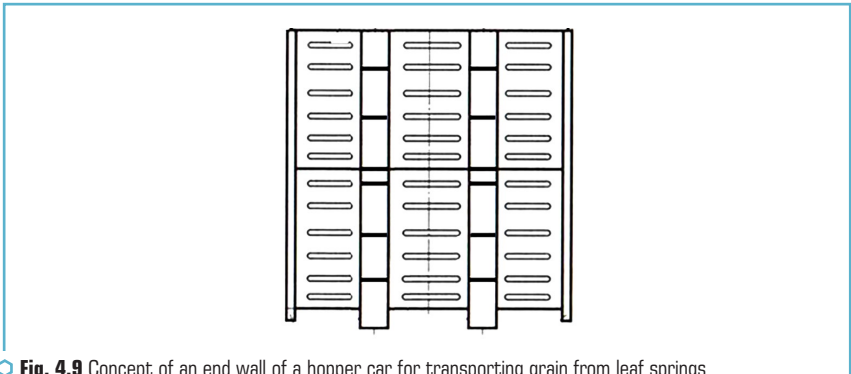


Fig. 4.9 Concept of an end wall of a hopper car for transporting grain from leaf springs

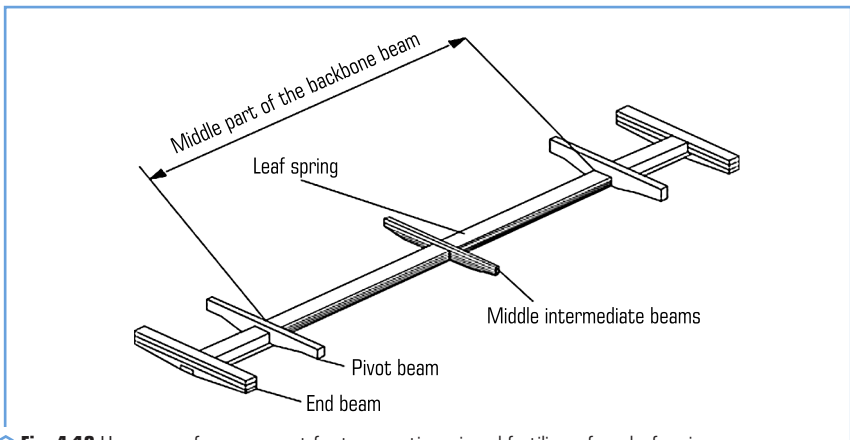
The concept is based on the task of improving a hopper car for transporting grain by making the middle part of the backbone beam (**Fig. 4.8**), end beams, middle intermediate beams and vertical racks of the side walls and intermediate racks of the end walls (**Fig. 4.9**) in the form of leaf springs.

The introduction of new features in interaction with known ones ensures the absorption of vibration energy, which, as a result, improves the dynamics and strength of the hopper car for transporting grain, provides a reduction in material consumption and, accordingly, increases the load capacity and extends the service life of the car.

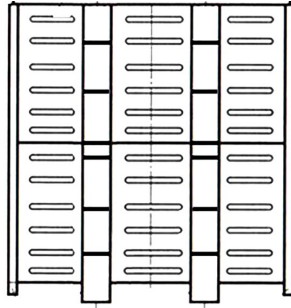
4.8 PROMISING ELASTIC-DISSIPATIVE CONCEPT OF A HOPPER CAR FOR TRANSPORTING MINERAL FERTILIZERS FROM LEAF SPRINGS

The promising elastic-dissipative concept of a hopper car for transporting mineral fertilizers from leaf springs relates to railcar construction and can be used for freight rail transportation of bulk cargo that requires protection from precipitation, in particular mineral fertilizers.

The concept is based on the task of improving a hopper car for transporting mineral fertilizers by making the middle part of the backbone beam (**Fig. 4.10**), end beams, middle intermediate beam and vertical racks of the side walls and intermediate racks of the end walls (**Fig. 4.11**) in the form of leaf springs. The introduction of new features in interaction with known ones ensures the absorption of vibration energy, which, as a result, improves the dynamics and strength of the hopper car for transporting mineral fertilizers, reduces material consumption and, accordingly, increases the load capacity and extends the service life of the car.



○ **Fig. 4.10** Hopper car frame concept for transporting mineral fertilizers from leaf springs

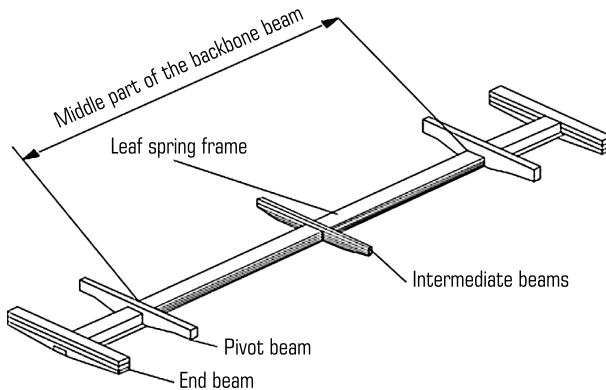


○ Fig. 4.11 Hopper car end wall concept for transporting mineral fertilizers from leaf springs

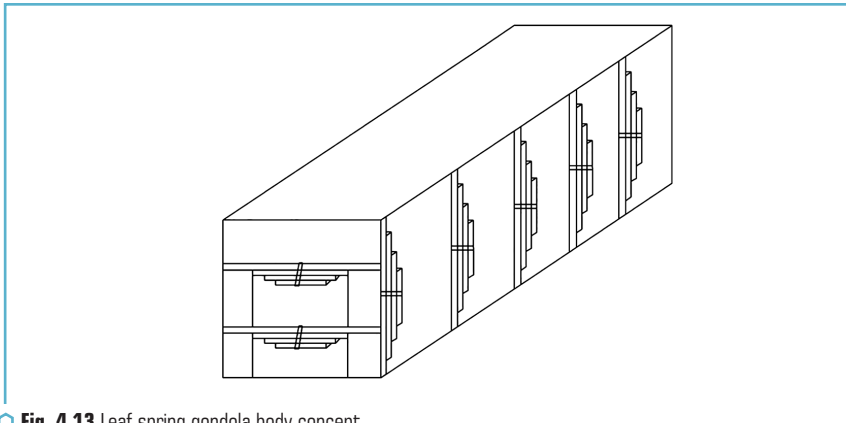
4.9 PROMISING ELASTIC-DISSIPATIVE CONCEPT OF A HOLLOW-BOTTOMED GONDOLA WITH LEAF SPRINGS

The promising elastic-dissipative concept of a hollow-bottomed gondola with leaf springs relates to car construction and can be used for railway transportation of bulk and bulk cargo that does not require protection from precipitation.

The concept is based on the task of improving the hollow-bottomed gondola by making the middle part of the backbone beam (Fig. 4.12), intermediate beams, vertical side wall uprights and horizontal end wall belts (Fig. 4.13) in the form of leaf springs.



○ Fig. 4.12 Leaf spring gondola frame concept



○ **Fig. 4.13** Leaf spring gondola body concept

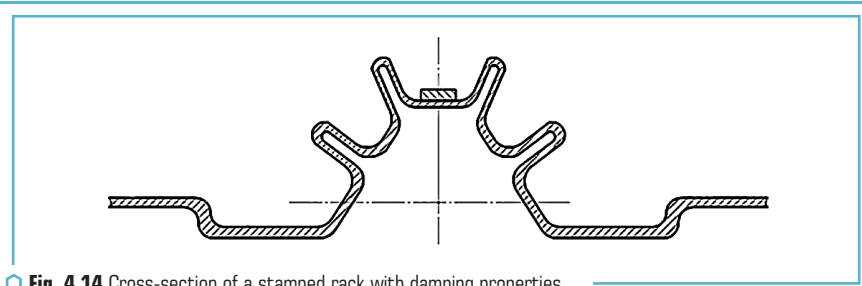
The introduction of new features in interaction with known ones ensures the absorption of vibration energy, which, as a result, improves the dynamics and strength of the hollow-bottom gondola, reduces material consumption, accordingly increases load capacity and increases the service life of the car.

4.10 PROMISING ELASTIC-DISSIPATIVE CONCEPT OF A UNIVERSAL COVERED CAR WITH RACKS WITH DAMPING PROPERTIES

The promising elastic-dissipative concept of a universal covered car with racks with damping properties relates to car construction and can be used for freight rail transportation of goods that require protection from precipitation.

The concept is based on the task of improving the technical and economic indicators of a universal covered car by making parts of the body module in a stamped manner, namely, making the side walls and intermediate racks of the side walls solid, in a stamped manner, with additional stiffening edges (**Fig. 4.14**); making the end walls and end racks solid, in a stamped manner, with additional stiffening edges; making the roof of the car solid in a stamped manner with additional stiffening edges.

The introduction of new features in interaction with known ones ensures the appearance of damping of the body module design, which implements in it the principle of adaptive perception of operational loads in the loaded or unloaded states, which, as a result, improves the dynamics and strength indicators of the universal covered car, reduces the mass of material for the manufacture of the universal covered car, simplifies the technological process of manufacturing the universal covered car, increases the load capacity, and its service life.



○ **Fig. 4.14** Cross-section of a stamped rack with damping properties

4.11 PROMISING ELASTIC-DISSIPATIVE CONCEPT OF A UNIVERSAL HOPPER CAR FOR TRANSPORTING GRAIN WITH RACKS WITH DAMPING PROPERTIES

The promising elastic-dissipative concept of a universal hopper car for transporting grain with racks with damping properties relates to railcar construction and can be used for freight rail transportation of bulk cargo that requires protection from precipitation, in particular grain.

The concept is based on the task of improving the technical and economic indicators of the grain hopper car by making parts of the body module stamped, namely, making the side walls and intermediate racks of the side walls solid, stamped, with additional stiffening edges (**Fig. 4.14**); making the end walls and end racks solid, stamped, with additional stiffening edges; making the roof of the car solid, stamped, with additional stiffening edges. The introduction of new features in interaction with the known ones ensures the appearance of damping of the body module design, which implements the principle of adaptive perception of operational loads in the loaded or unloaded states, which, as a result, improves the dynamics and strength of the grain hopper car, reduces the mass of material for manufacturing the grain hopper car, simplifies the technological process of manufacturing the grain hopper car, increases the carrying capacity, and its service life.

4.12 PROMISING CONCEPT OF A RAILWAY TANK WITH SUPPORTS IN THE FORM OF LEAF SPRINGS

The concept is based on the task of improving a railway tank by replacing the supports located between the boiler and the frame with leaf springs that absorb vibration energy, which, as a result, improves the dynamics of the railway tank.

The task is achieved by the fact that in a railway tank, which contains bogies, a frame, braking equipment, automatic coupling devices, a boiler, fastening the boiler to the frame and boiler supports on the frame, according to the concept, the boiler supports on the frame are made in the form of leaf springs (**Fig. 4.15**).

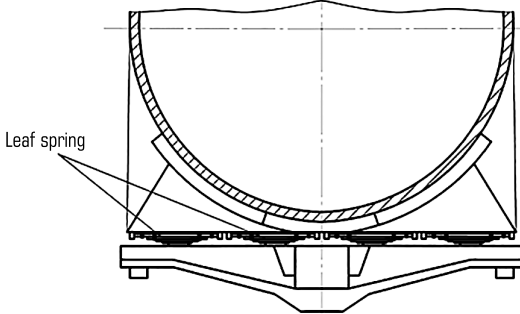


Fig. 4.15 Concept of a railway tank with supports of the boiler on the frame in the form of leaf springs

4.13 PROMISING CONCEPT OF A RAILWAY TANK WITH SUPPORTS IN THE FORM OF DISC SPRINGS

The concept of a railway tank with supports in the form of disc springs belongs to railway transport, namely railway tanks and can be used for the transportation of liquid cargo.

The concept is based on the task of improving the railway tank by replacing the supports located between the boiler and the frame with disc springs that absorb vibration energy, which, as a result, improves the dynamics of the railway tank.

The task is achieved by the fact that in a railway tank containing bogies, a frame, braking equipment, automatic coupling devices, a boiler, fastening of the boiler to the frame and boiler supports on the frame, according to the concept, the boiler supports on the frame are made in the form of disc springs (Fig. 4.16).

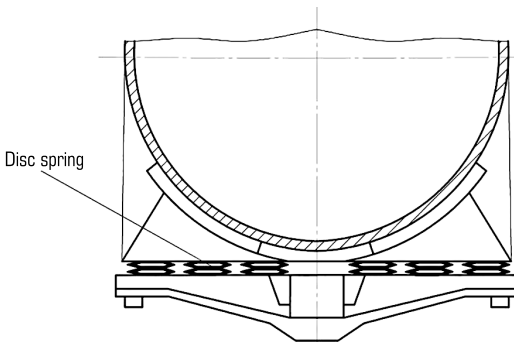
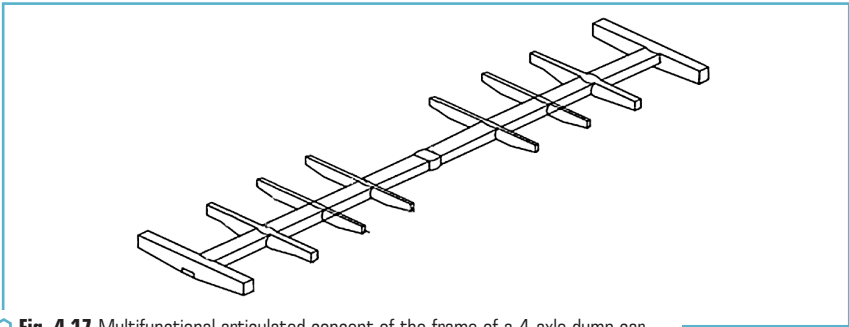


Fig. 4.16 Concept of a railway tank with supports in the form of disc springs

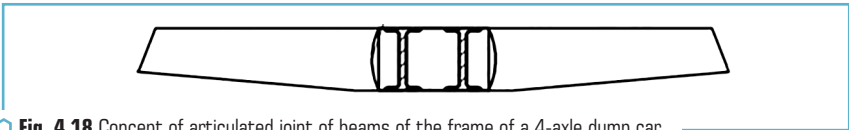
4.14 PROMISING ARTICULATED CONCEPT OF A 4-AXLE DUMP CAR

The promising articulated concept of a 4-axle dump car refers to railcar construction and can be used for rail freight transportation of bulk cargo that does not require protection from precipitation and mechanical unloading.

The concept is based on the task of improving the dump car by having articulated elements in its design instead of existing fixed elements (solid beams, welded joints), namely the presence of an articulated element in the middle part of the backbone beam (**Fig. 4.17**), the presence of articulated elements (**Fig. 4.18**) at the points of joint of the backbone beam with: buffer walls, pivot and cylinder beams. The introduction of new features in interaction with known ones provides the appearance of additional degrees of freedom of the design and implements in it the principle of adaptive perception of operational loads in the loaded or unloaded states, which, as a result, improves the dynamics and strength of the dump car, ensures a reduction in material consumption and, accordingly, increases the load-bearing capacity and extends the service life of the dump car.



◉ **Fig. 4.17** Multifunctional articulated concept of the frame of a 4-axle dump car



◉ **Fig. 4.18** Concept of articulated joint of beams of the frame of a 4-axle dump car

4.15 PROMISING ARTICULATED CONCEPT OF A HOPPER CAR FOR GRAIN TRANSPORTATION

The promising articulated concept of a hopper car for grain transportation relates to car construction and can be used for rail freight transportation of bulk cargoes that require protection from precipitation, in particular grain.

The concept is based on the task of improving the hopper car for transporting grain by using articulated elements in its design instead of existing fixed elements (solid beams, welded joints), namely, installing an articulated element in the middle part of the backbone beam (**Fig. 4.19**), installing articulated elements (**Fig. 4.20**) at the joints of the end beams, pivot beams and middle intermediate beams.

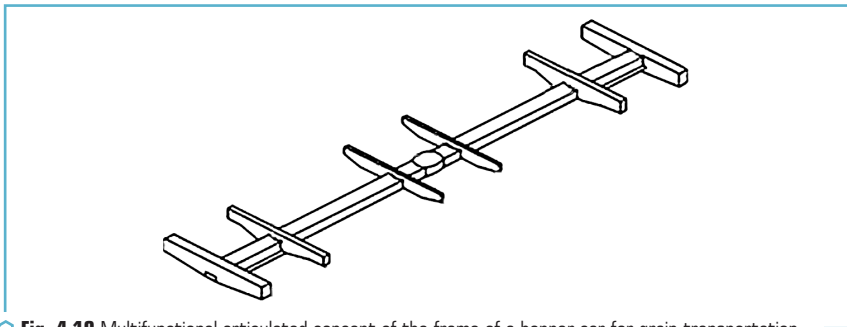


Fig. 4.19 Multifunctional articulated concept of the frame of a hopper car for grain transportation

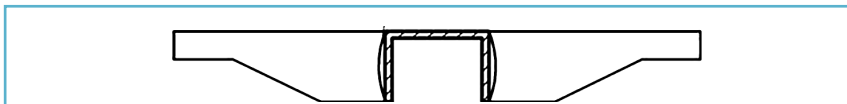
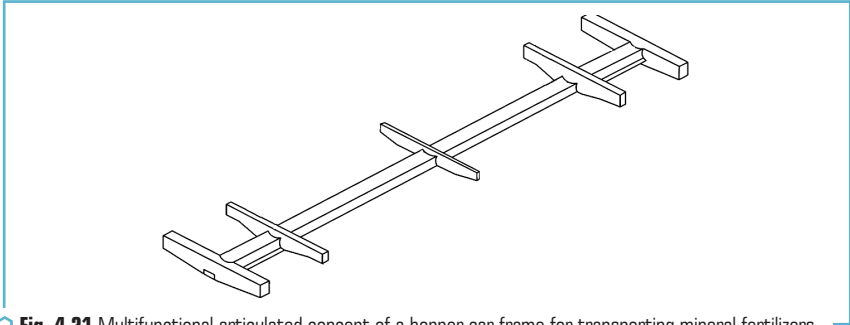


Fig. 4.20 Concept of articulated joint of beams of the frame of a hopper car for grain transportation

The introduction of new features in interaction with known ones provides the appearance of additional degrees of freedom of the structure and implements in it the principle of adaptive perception of operational loads in the loaded or unloaded states, which, as a result, improves the dynamics and strength of the hopper car for grain transportation, provides a reduction in material consumption and, accordingly, increases the load-bearing capacity and increases the service life of the car.

4.16 PROMISING ARTICULATED CONCEPT OF A HOPPER CAR FOR TRANSPORTING MINERAL FERTILIZERS

The concept is based on the task of improving a hopper car for transporting mineral fertilizers by using articulated elements in its design instead of existing fixed elements (solid beams, welded joints), namely, installing an articulated element in the middle part of the backbone beam (**Fig. 4.21**), installing articulated elements at the joints of the end beams, pivot beams and the central intermediate beam.



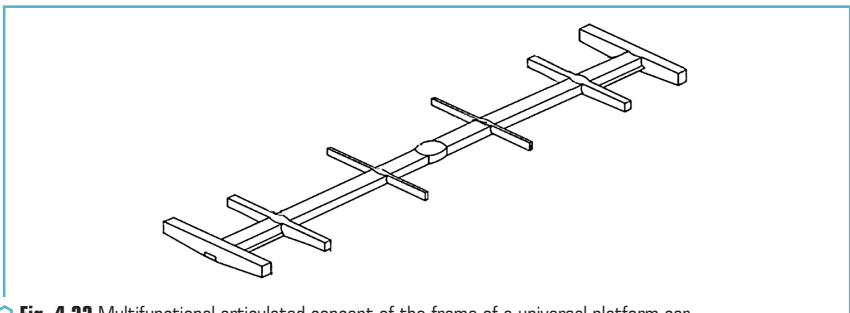
◉ **Fig. 4.21** Multifunctional articulated concept of a hopper car frame for transporting mineral fertilizers

The introduction of new features in interaction with known ones provides the appearance of additional degrees of freedom of the design and implements in it the principle of adaptive perception of operational loads in the loaded or unloaded states, which, as a result, improves the dynamics and strength of the hopper car for transporting mineral fertilizers, provides a reduction in material consumption and, accordingly, increases the load capacity and increases the service life of the car.

4.17 PROMISING ARTICULATED CONCEPT OF A UNIVERSAL PLATFORM CAR

The promising articulated concept of a universal platform car refers to car construction and can be used for railway transportation of wheeled and tracked vehicles, long-sized, piece, forest and other cargo, containers and equipment that does not require protection from atmospheric influences.

The concept is based on the task of improving the universal platform car by using articulated elements in its design instead of existing fixed elements (solid beams, welded joints), namely, installing a articulated element in the middle part of the backbone beam (**Fig. 4.22**), installing articulated elements at the joints of the end beams, pivot beams and main cross beams.



◉ **Fig. 4.22** Multifunctional articulated concept of the frame of a universal platform car

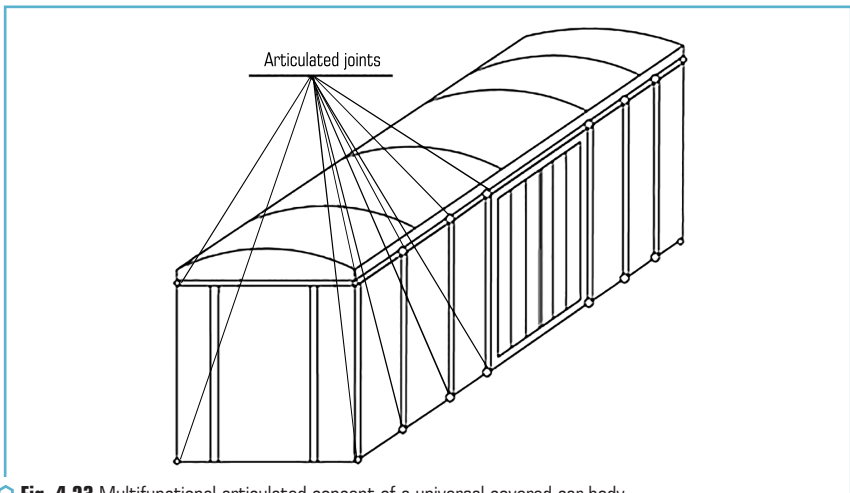
The introduction of new features in interaction with known ones provides the appearance of additional degrees of freedom of the structure and implements in it the principle of adaptive perception of operational loads in the loaded or unloaded states, which, as a result, improves the dynamics and strength of the universal platform car, provides a reduction in material consumption and, accordingly, increases the load capacity and increases the service life of the car.

4.18 PROMISING ARTICULATED CONCEPT OF A UNIVERSAL COVERED CAR

The utility model relates to car construction and can be used for freight railway transportation of goods that require protection from atmospheric precipitation.

The concept is based on the task of improving a universal covered car by using articulated elements in its design (**Fig. 4.23, 4.24**) instead of existing fixed elements (solid beams, welded joints), namely the presence of an articulated element in the middle part of the backbone beam, the presence of articulated elements at the joints of the end beams, pivot beams and main beams, the presence of articulated elements at the joints of the side wall uprights with the lower skin and at the joints of the roof with the side wall uprights.

The introduction of new features in interaction with the known ones ensures the emergence of additional degrees of freedom of the structure and implements in it the principle of adaptive perception of operational loads in the loaded or unloaded states, which, as a result, improves the dynamics and strength indicators of the universal covered car, provides a reduction in material consumption and, accordingly, increases the load capacity and increases the service life of the car.



○ **Fig. 4.23** Multifunctional articulated concept of a universal covered car body

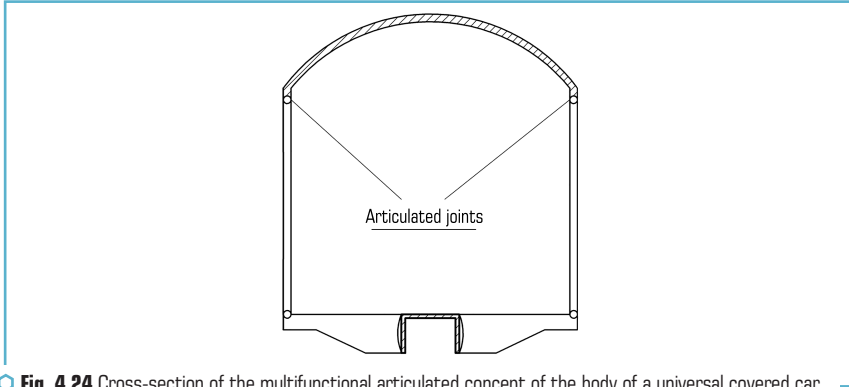


Fig. 4.24 Cross-section of the multifunctional articulated concept of the body of a universal covered car

4.19 PROMISING ARTICULATED CONCEPT OF A HOLLOW-BOTTOMED GONDOLA

The concept is based on the task of improving the hollow-bottomed gondola by using articulated elements in its design (Fig. 4.25–4.27) instead of existing fixed elements (solid beams, welded joints), namely, installing an articulated element in the middle part of the backbone beam; installation of articulated elements at the points of joint of the backbone beam with: end, pivot and intermediate beams; installation of articulated elements at the points of joint of end, pivot and intermediate beams with side walls; installation of articulated elements at the points of joint of vertical side wall uprights with upper strapping.

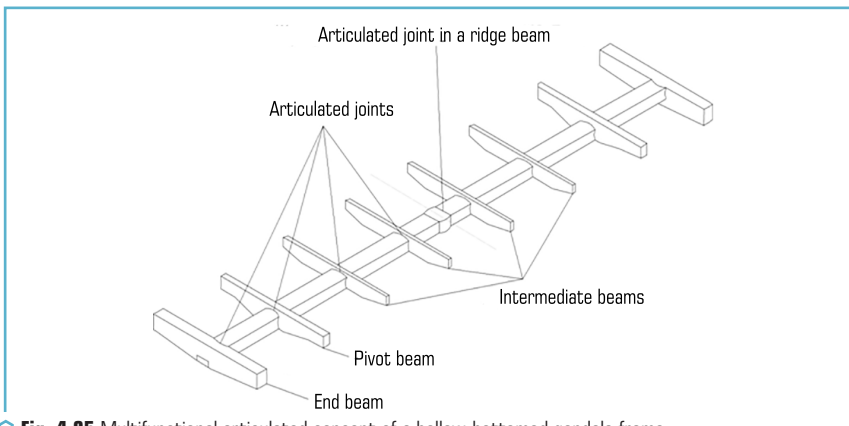


Fig. 4.25 Multifunctional articulated concept of a hollow-bottomed gondola frame

The introduction of new features in interaction with known ones provides the appearance of additional degrees of freedom of the structure and implements in it the principle of adaptive perception of operational loads in loaded or unloaded states, which, as a result, improves the dynamics and strength of the hollow-bottomed gondola, provides a reduction in material consumption and, accordingly, increases the load-bearing capacity and increases the service life of the car.

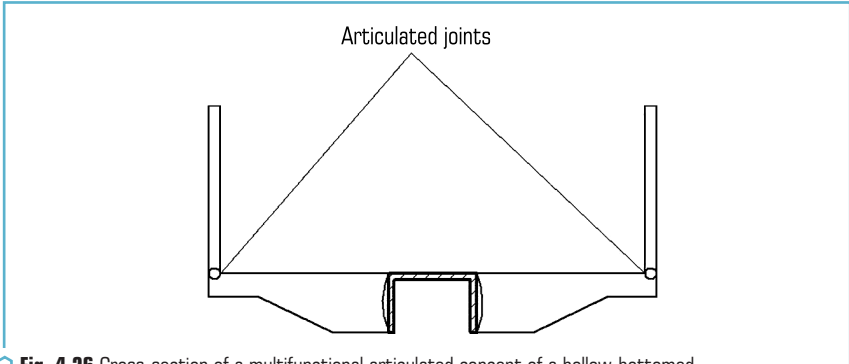


Fig. 4.26 Cross-section of a multifunctional articulated concept of a hollow-bottomed gondola body

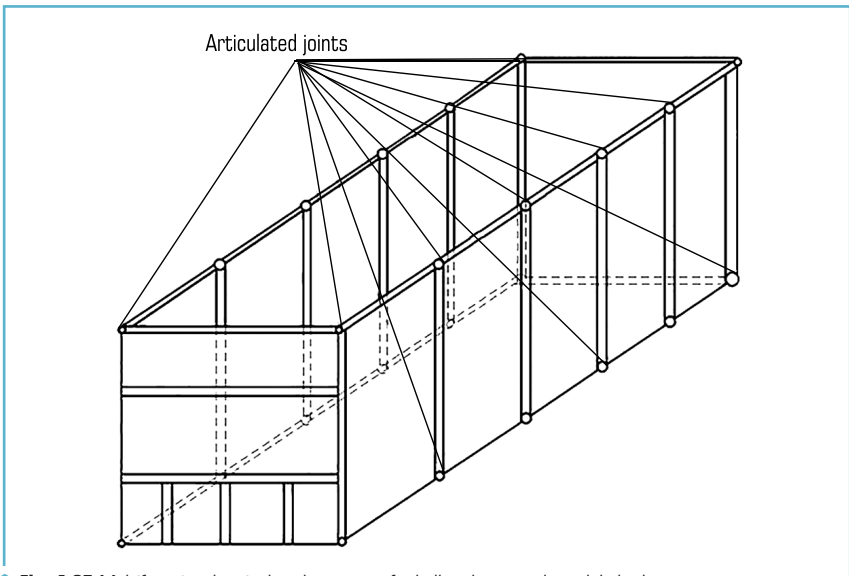


Fig. 4.27 Multifunctional articulated concept of a hollow-bottomed gondola body

4.20 PROMISING ARTICULATED RAILWAY TANK CONCEPT

The promising articulated railway tank concept belongs to railway transport, namely railway tanks and can be used for the transportation of liquid cargo.

The concept is based on the task of improving the railway tank for the transportation of liquid cargo by using articulated elements in its design (**Fig. 4.28**) instead of existing fixed elements (solid beams, welded joints), namely, installing the articulated element in the middle part of the backbone beam, installing articulated elements at the joints of the end and pivot beams.

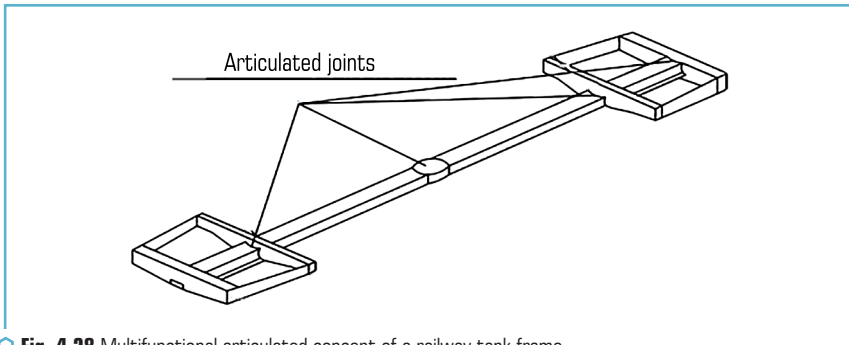


Fig. 4.28 Multifunctional articulated concept of a railway tank frame

The introduction of new features in interaction with known ones provides the appearance of additional degrees of freedom of the structure and implements in it the principle of adaptive perception of operational loads in the loaded or unloaded states, which, as a result, improves the dynamics and strength of the railway tank for the transportation of liquid cargo, provides a reduction in material consumption and, accordingly, increases the load capacity and increases the service life of the railway tank for liquid cargo.

4.21 PROMISING MULTI-MATERIAL CONCEPT OF A COVERED CAR

The promising multi-material concept of a covered car (**Fig. 4.29**) refers to car construction and can be used for railway transportation and is intended for the transportation of a wide range of piece, grain and other cargo that requires protection from atmospheric influences.

The concept is based on the task of improving the covered car to increase the efficiency of its use, namely: reducing material consumption, increasing the load capacity and loading volume of the body, and reducing the corrosion wear of the body module (**Fig. 4.30**), by improving its design, based on the execution of the body module as a solid composite material and cross-sectional

configurations of equal resistance to the actions of the total corresponding operational loads, while meeting the conditions of strength and operational reliability.

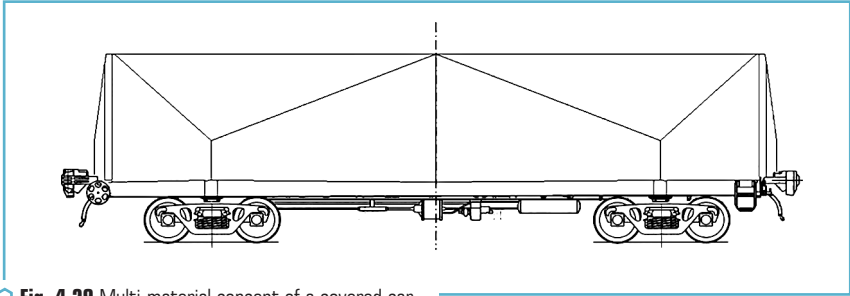


Fig. 4.29 Multi-material concept of a covered car

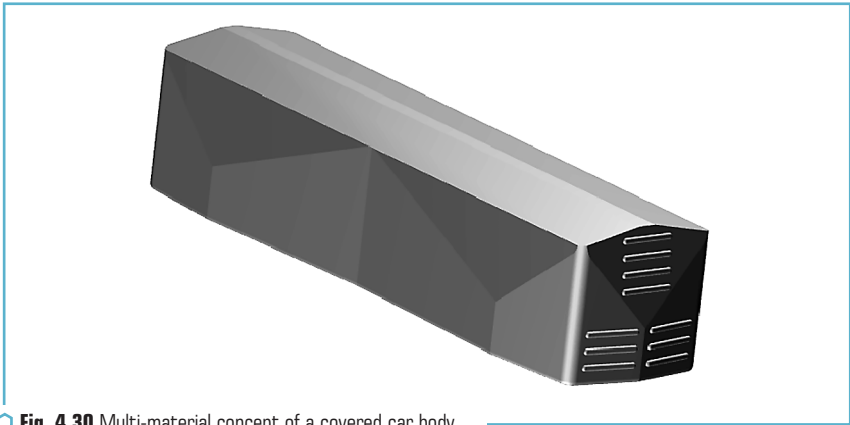


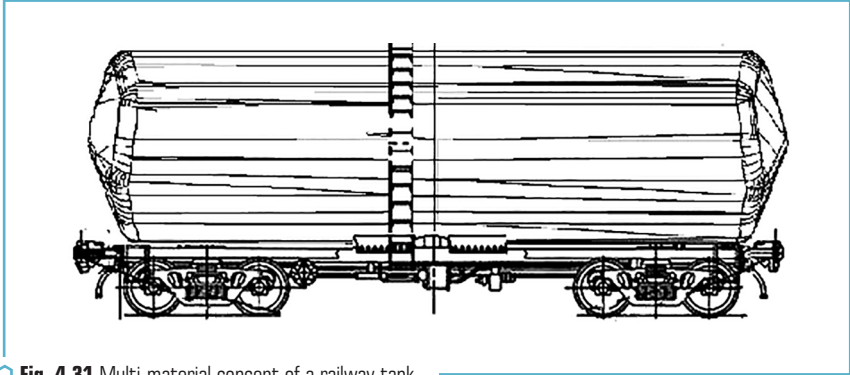
Fig. 4.30 Multi-material concept of a covered car body

The introduction of new features in interaction with known ones ensures a reduction in material consumption, an increase in the load capacity and loading volume of the body, an increase in the corrosion resistance of the body module and, as a result of all the above, a reduction in the cost of manufacturing and operating a covered car.

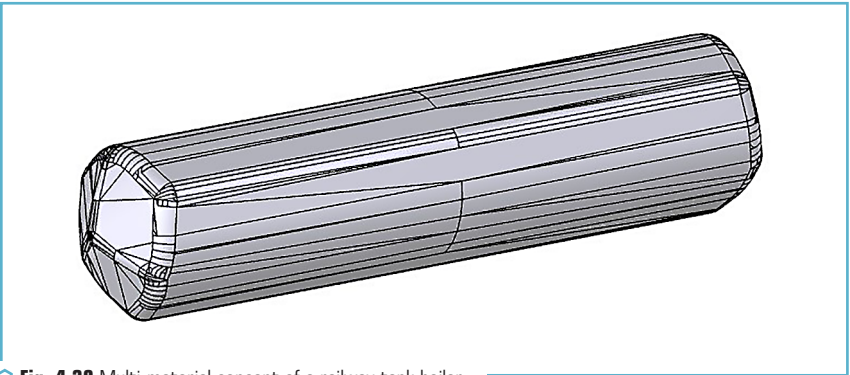
4.22 A PROMISING MULTI-MATERIAL CONCEPT OF A RAILWAY TANK CAR

A promising multi-material concept of a railway tank car (**Fig. 4.31**) belongs to railway transport, namely railway tanks and can be used for the transportation of liquid cargo.

The concept is based on the task of improving a railway tank car for transporting liquid cargo, namely: reducing material capacity, increasing the load capacity and loading volume of the body, and reducing the corrosion wear of the body module (**Fig. 4.32**), by improving its design, based on the continuous execution of the boiler from composite material and cross-sectional configurations of equal resistance to the effects of the total corresponding operational loads, while meeting the conditions of strength and operational reliability.



○ **Fig. 4.31** Multi-material concept of a railway tank



○ **Fig. 4.32** Multi-material concept of a railway tank boiler

The introduction of new features in interaction with known ones ensures a reduction in material consumption, an increase in the load capacity and loading volume of the body, an increase in the corrosion resistance of the body module and, as a result of all the above, a decrease in the cost of manufacturing and operating a railway tank for transporting liquid cargo.

4.23 A PROMISING RAILWAY TANK WITH A MULTI-MATERIAL CONCEPT OF SUPPORTS

A promising railway tank with a multi-material concept of supports belongs to railway transport, namely railway tanks and can be used for transporting liquid cargo.

The concept is based on the task of improving the railway tank by replacing the supports located between the boiler and the frame with rubber-metal elements that absorb vibration energy, which, as a result, improves the dynamics of the railway tank.

The task is achieved by the fact that in a railway tank car, which contains bogies, a frame, braking equipment, automatic coupling devices, a boiler, fastening of the boiler to the frame and supports of the boiler on the frame, according to the concept, the supports of the boiler on the frame are made in the form of rubber-metal elements (**Fig. 4.33**).

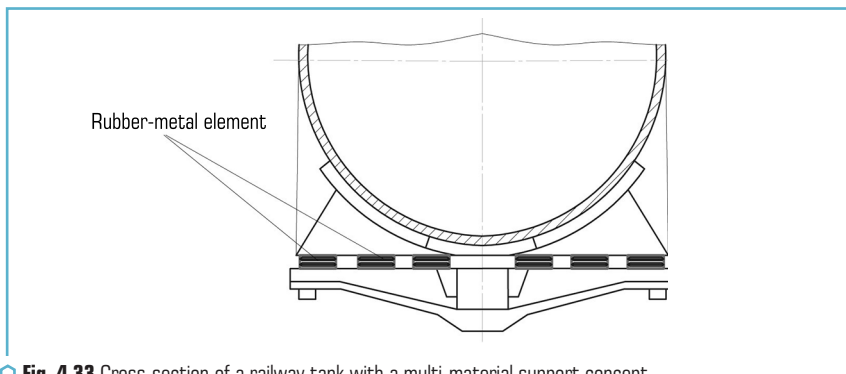


Fig. 4.33 Cross-section of a railway tank with a multi-material support concept

CONCLUSIONS

1. The creation and development of multifunctional components of freight cars is a promising direction for improving their designs. Today, there are a significant number of ways to create multifunctional components of freight cars. In general, among them it is possible to distinguish: a combination of elements that are separate in terms of their functions; transformation of a functional element or functional grouping of elements; identification and implementation of additional functions on the same resource base; identification and implementation of additional functions on a new resource base.

2. Most often in the practice of creating multifunctional technical means, a combination of elements that are separate in terms of their functions is used. Its main directions include: connection of different levels of the constructive hierarchy (modules, nodes, basic elements) of components without changing their forms and properties, and with mutual coordination of forms and properties;

introduction of new principles of functioning to car constructs on the existing element base and on a new element base; consideration at the design stage of the prerequisites for the constructive implementation of future innovative design solutions.

3. Today, the most promising from the point of view of practical creation of multifunctional components of freight cars are the following directions identified and presented in detail in the article: elastic-dissipative, non-rigid articulated and multi-material.

4. The expected results of the development and implementation of multifunctional components of freight cars include: reducing their own mass; improving operational properties; reducing the number of elements and redundant connections; increasing reliability and safety of movement; increasing the permissible values of the speeds of cars in empty and loaded states; reducing the costs of their: manufacturing, operation, maintenance, repairs, etc.

5. The presented directions for creating multifunctional components of freight cars will allow obtaining positive results in their manufacture and operation. Such positive results include: increasing the life cycle of the studied means, reducing their material consumption and increasing load capacity, improving maintainability, increasing crack resistance, reducing/completely eliminating stresses of different signs.

6. The possibilities of constructive and technological implementation of prestressed and/or deformed components of freight cars, structured in a graphical form and presented in the work, should be used in further research and development work on the creation of new generation freight cars, as well as increasing the systemic efficiency of their existing models.

7. The proposed theoretical provisions for the implementation of prestressed and/or deformed components in the design of freight cars in accordance with possible cases of loading at the stages of the life cycle should be used in solving similar scientific and applied problems for other types of rolling stock, as well as objects of transport engineering.

8. When introducing a directed stress-strain state into the components of freight cars, it is advisable to use the given mathematical notation.

REFERENCES

1. Koshel, O., Saponova, S., Kara, S. (2023). Revealing patterns in the stressed-strained state of load-bearing structures in special rolling stock to further improve them. *Eastern-European Journal of Enterprise Technologies*, 4 (7 (124)), 30–42. <https://doi.org/10.15587/1729-4061.2023.285894>
2. Muradian, L., Shvets, A., Shvets, A. (2024). Influence of wagon body flexural deformation on the indicators of interaction with the railroad track. *Archive of Applied Mechanics*, 94 (8), 2201–2216. <https://doi.org/10.1007/s00419-024-02633-2>
3. Okorokov, A., Fomin, O., Lovska, A., Vernigora, R., Zhuravel, I., Fomin, V. (2018). Research into a possibility to prolong the time of operation of universal open top wagon bodies that

- have exhausted their standard resource. *Eastern-European Journal of Enterprise Technologies*, 3 (7 (93)), 20–26. <https://doi.org/10.15587/1729-4061.2018.131309>
4. Fomin, O., Kulbovsky, I., Sorochinska, E., Saponova, S., Bambura, O. (2017). Experimental confirmation of the theory of implementation of the coupled design of center girder of the hopper wagons for iron ore pellets. *Eastern-European Journal of Enterprise Technologies*, 5 (1 (89)), 11–18. <https://doi.org/10.15587/1729-4061.2017.109588>
 5. Melnyk, O., Onyshchenko, S., Onishchenko, O., Lohinov, O., Ocheretna, V. (2023). Integral Approach to Vulnerability Assessment of Ship's Critical Equipment and Systems. *Transactions on Maritime Science*, 12 (1). <https://doi.org/10.7225/toms.v12.n01.002>
 6. Sagin, S. V., Sagin, S. S., Fomin, O., Gaichenia, O., Zablotyskiy, Y., Pištěk, V., Kučera, P. (2024). Use of biofuels in marine diesel engines for sustainable and safe maritime transport. *Renewable Energy*, 224, 120221. <https://doi.org/10.1016/j.renene.2024.120221>
 7. Melnyk, O., Onishchenko, O., Onyshchenko, S., Golikov, V., Sapiha, V., Shcherbina, O., Andrievska, V. (2022). Study of Environmental Efficiency of Ship Operation in Terms of Freight Transportation Effectiveness Provision. *TransNav, the International Journal on Marine Navigation and Safety of Sea Transportation*, 16 (4), 723–729. doi.org/10.12716/1001.16.04.14
 8. Fomin, O., Lovska, A., Kulbovskyi, I., Holub, H., Kozarchuk, I., Kharuta, V. (2019). Determining the dynamic loading on a semi-wagon when fixing it with a viscous coupling to a ferry deck. *Eastern-European Journal of Enterprise Technologies*, 2 (7 (98)), 6–12. <https://doi.org/10.15587/1729-4061.2019.160456>
 9. Melnyk, O., Onyshchenko, S., Onishchenko, O., Shumylo, O., Voloshyn, A., Koskina, Y., Volianska, Y. (2022). Review of Ship Information Security Risks and Safety of Maritime Transportation Issues. *TransNav, the International Journal on Marine Navigation and Safety of Sea Transportation*, 16 (4), 717–722. <https://doi.org/10.12716/1001.16.04.13>
 10. Sokolov, V., Porkuian, O., Krol, O., Stepanova, O. (2021). Design Calculation of Automatic Rotary Motion Electrohydraulic Drive for Technological Equipment. *Advances in Design, Simulation and Manufacturing IV*. Cham: Springer, 133–142. https://doi.org/10.1007/978-3-030-77719-7_14
 11. Krol, O., Sokolov, V. (2020). Modeling of Spindle Node Dynamics Using the Spectral Analysis Method. *Advances in Design, Simulation and Manufacturing III*. Cham: Springer, 35–44. https://doi.org/10.1007/978-3-030-50794-7_4
 12. Kondratiev, A., Gaidachuk, V., Nabokina, T., Kovalenko, V. (2019). Determination of the influence of deflections in the thickness of a composite material on its physical and mechanical properties with a local damage to its wholeness. *Eastern-European Journal of Enterprise Technologies*, 4 (1 (100)), 6–13. <https://doi.org/10.15587/1729-4061.2019.174025>
 13. Krol, O., Sokolov, V. (2020). Research of toothed belt transmission with arched teeth. *Diagnostyka*, 21 (4), 15–22. <https://doi.org/10.29354/diag/127193>
-

14. Gubarevych, O., Goolak, S., Daki, E., Tryshyn, V. (2021). Investigation of Turn-To-Turn Closures of Stator Windings to Improve the Diagnostics System for Induction Motors. *Problems of the Regional Energetics*, 2 (50), 10–24. <https://doi.org/10.52254/1857-0070.2021.2-50.02>
15. Gubarevych, O., Goolak, S., Melkonova, I., Yurchenko, M. (2022). Structural diagram of the built-in diagnostic system for electric drives of vehicles. *Diagnostyka*, 23 (4), 1–13. <https://doi.org/10.29354/diag/156382>
16. Kondratiev, A., Slivinsky, M. (2018). Method for determining the thickness of a binder layer at its non-uniform mass transfer inside the channel of a honeycomb filler made from polymeric paper. *Eastern-European Journal of Enterprise Technologies*, 6 (5 (96)), 42–48. <https://doi.org/10.15587/1729-4061.2018.150387>
17. Fomin, O., Lovska, A. (2021). Determination of dynamic loading of bearing structures of freight wagons with actual dimensions. *Eastern-European Journal of Enterprise Technologies*, 2 (7 (110)), 6–14. <https://doi.org/10.15587/1729-4061.2021.220534>
18. Tkachenko, V., Saponova, S., Kulbovskiy, I., Fomin, O. (2017). Research into resistance to the motion of railroad undercarriages related to directing the wheelsets by a rail track. *Eastern-European Journal of Enterprise Technologies*, 5 (7 (89)), 65–72. <https://doi.org/10.15587/1729-4061.2017.109791>
19. Kondratiev, A. (2019). Improving the mass efficiency of a composite launch vehicle head fairing with a sandwich structure. *Eastern-European Journal of Enterprise Technologies*, 6 (7 (102)), 6–18. <https://doi.org/10.15587/1729-4061.2019.184551>
20. Fomin, O., Gerlici, J., Lovska, A., Kravchenko, K., Prokopenko, P., Fomina, A., Hauser, V. (2019). Durability Determination of the Bearing Structure of an Open Freight Wagon Body Made of Round Pipes during its Transportation on the Railway Ferry. *Communications – Scientific Letters of the University of Zilina*, 21 (1), 28–34. <https://doi.org/10.26552/com.c.2019.1.28-34>
21. Fomin, O., Lovska, A., Pištěk, V., Kučera, P. (2019). Dynamic load computational modelling of containers placed on a flat wagon at railroad ferry transportation. *Vibroengineering Procedia*, 29, 118–123. <https://doi.org/10.21595/vp.2019.21132>
22. Fomin, O., Lovska, A., Radkevych, V., Horban, A., Skliarenko, I., Gurenkova, O. (2019). The dynamic loading analysis of containers placed on a flat wagon during shunting collisions. *ARNP Journal of Engineering and Applied Sciences*, 14 (21), 3747–3752. Available at: http://www.arnpjournals.org/jeas/research_papers/rp_2019/jeas_1119_7989.pdf
23. Sagin, S., Kuropyatnyk, O., Sagin, A., Tkachenko, I., Fomin, O., Pištěk, V., Kučera, P. (2022). Ensuring the Environmental Friendliness of Drillships during Their Operation in Special Ecological Regions of Northern Europe. *Journal of Marine Science and Engineering*, 10 (9), 1331. <https://doi.org/10.3390/jmse10091331>
24. Gorobchenko, O., Fomin, O., Gritsuk, I., Saravas, V., Grytsuk, Y., Bulgakov, M. et al. (2018). Intelligent Locomotive Decision Support System Structure Development and Operation

- Quality Assessment. 2018 IEEE 3rd International Conference on Intelligent Energy and Power Systems (IEPS). Kharkiv, 239–243. <https://doi.org/10.1109/ieps.2018.8559487>
25. Sulym, A. O., Fomin, O. V., Khozia, P. O., Mastepan, A. G. (2018). Theoretical and practical determination of parameters of on-board capacitive energy storage of the rolling stock. *Naukovyi Visnyk Natsionalnoho Hirnychoho Universytetu*, 5, 79–87. <https://doi.org/10.29202/nvngu/2018-5/8>
26. Fomin, O., Sulym, A., Kulbovskiy, I., Khozia, P., Ishchenko, V. (2018). Determining rational parameters of the capacitive energy storage system for the underground railway rolling stock. *Eastern-European Journal of Enterprise Technologies*, 2 (1 (92)), 63–71. <https://doi.org/10.15587/1729-4061.2018.126080>

Edited by
Oleksij Fomin

ASSESSMENT OF TECHNICAL CONDITION: MEANS OF MEASUREMENT, SAFETY, RISKS

Oleksij Fomin, Gregori Boyko, Andrii Lytvynenko, Vladyslav Bezlutsky, Pavlo Prokopenko,
Mariia Miroshnykova, Andriy Klymash, Stanislav Sidnei, Mykola Pelypenko, Mykola Grygorian,
Mykhailo Kropyva, Ihor Taran, Serhii Holovchenko, Ievgen Medvediev, Tetiana Sotnikova,
Tetiana Yarkho, Tatyana Emelyanova, Dmytro Legeyda

Collective monograph

Technical editor I. Prudius
Desktop publishing T. Serhiienko
Cover photo Copyright © 2024 Canva

TECHNOLOGY CENTER PC®
Published in December 2024
Enlisting the subject of publishing No. 4452 – 10.12.2012
Address: Shatylova dacha str., 4, Kharkiv, Ukraine, 61165
